UNIVERSITÀ DEGLI STUDI DI MILANO

PhD degree in Systems Medicine

Dept. Of Oncology and Emato-Oncology

Novel Mono-, Bi- and Tri-specific Immunomodulatory Antibodies for Cancer Therapy and Tools for Other Therapeutic and Diagnostic Applications

BIOS-07/A

Student: Rosa Rapuano Lembo
Matr. R13498
ORCID n. 0009-0007-4810-8255

Tutor: Claudia De Lorenzo

DIEGO PASINI

A.A. 2024-2025

TABLE OF CONTENTS

LIST OF ABBREVIATIONS

ADCC	Antibody-Dependent Cellular Cytotoxicity
ADCP	Antibody-Dependent Cellular Phagocytosis
AE(s)	Adverse Event(s)
ALL	Acute Lymphoblastic Leukemia
APC	Antigen-Presenting Cell / Activated Protein C
aPTT	Activated Partial Thromboplastin Time
BLI	Bio-Layer Interferometry
BiTE	Bispecific T-cell Engager
BsAb	Bispecific Antibody
CDC	Complement-Dependent Cytotoxicity
CHO	Chinese Hamster Ovary
CRC	Colorectal Cancer
CTLA-4	Cytotoxic T-Lymphocyte Antigen 4
DOAC	Direct Oral Anticoagulant
ECM	Extracellular Matrix
EGFR	Epidermal Growth Factor Receptor
ELISA	Enzyme-Linked Immunosorbent Assay
EpCAM	Epithelial Cell Adhesion Molecule
Fab	Fragment Antigen-Binding
Fc	Fragment crystallizable region
FcγR	Fc gamma Receptor
FoxP3	Forkhead Box P3
FV / FVa	Factor V / activated Factor V
Gal-3	Galectin-3
HAMA	Human Anti-Mouse Antibody
HCC	Hepatocellular Carcinoma
HEK293	Human Embryonic Kidney 293 cells
HNSCC	Head and Neck Squamous Cell Carcinoma
HRP	Horseradish Peroxidase

hPBMCs	Human Peripheral Blood Mononuclear Cells
ICI(s)	Immune Checkpoint Inhibitor(s)
IC(s)	Immune Checkpoint(s)
IFNγ	Interferon gamma
IgG	Immunoglobulin G
IL-2	Interleukin-2
IMAC	Immobilized Metal ion Affinity Chromatography
IPTG	Isopropyl β-D-1-thiogalactopyranoside
K_D	Dissociation Constant
LAG-3	Lymphocyte Activation Gene 3
LDH	Lactate Dehydrogenase
LMWH	Low Molecular Weight Heparin
mAb(s)	Monoclonal Antibody(ies)
MHC	Major Histocompatibility Complex
NGS	Next-Generation Sequencing
NFAT	Nuclear Factor of Activated T cells
NF-κB	Nuclear Factor kappa-light-chain-enhancer of activated B cells
NK	Natural Killer cells
NSCLC	Non-Small Cell Lung Cancer
OX40 / OX40L	CD134 receptor / Ligand
PD-1	Programmed Death-1
PD-L1	Programmed Death-Ligand 1
PI3K	Phosphoinositide 3-kinase
RT	Room Temperature
RCC	Renal Cell Carcinoma
scFv	Single Chain Variable Fragment
SEC	Size-Exclusion Chromatography
SDS-PAGE	Sodium Dodecyl Sulfate Polyacrylamide Gel Electrophoresis
TAA	Tumor-Associated Antigen
TCE	T-cell Engager

TCR	T Cell Receptor
TGF-β	Transforming Growth Factor beta
TIL	Tumor-Infiltrating Lymphocyte
TKI	Tyrosine Kinase Inhibitor
TME	Tumor Microenvironment
TNBC	Triple-Negative Breast Cancer
TNF-α	Tumor Necrosis Factor alpha
TsAb	Trispecific Antibody
UFH	Unfractionated Heparin
VH / VL	Variable Heavy / Variable Light chain
VKA	Vitamin K Antagonist
WB	Western Blot

FIGURES INDEX

ABSTRACT

Cancer represents one of the leading causes of death worldwide, and the development of novel immunotherapeutic strategies, such as that of immune checkpoint inhibitors (ICIs), has generated long-lasting responses in multiple malignancies. Even though safer than chemotherapies, some adverse events, including rare cases of cardiotoxicity, have also been reported for ICIs, especially when used in combination.

In this context, the aim of my research project was to identify combinations of novel human immunomodulatory monoclonal antibodies targeting different ICs, with improved efficacy and safety profiles. Some novel ICIs were previously isolated in our laboratory and characterized for their biological properties. Here, they were tested in combinations to identify those with stronger anti-tumor effects and reduced cardiotoxic side effects on cardiomyocytes, compared to combinatorial treatments with clinically validated monoclonal antibodies (mAbs). Interestingly, the combination of novel human PD-L1_1 (anti-PD-L1 mAb) and ID-1 (anti-CTLA-4 mAb) induced efficient lysis of triple-negative breast cancer cells and lower cytotoxicity on cardiomyocytes, when co-cultured with lymphocytes, compared to the treatments with Ipilimumab, Atezolizumab or their combination. We further evaluated the pro-inflammatory effects of FDA-approved combinatorial treatments of ICIs, and we found that these combinations, especially regimens including the anti-LAG-3 antibody Relatlimab, promoted an important increase of pro-inflammatory cytokines secretion, such as IL-6, IL-1β, TNF-α, IFNγ and granzyme B.

Since combinations of novel mAbs showed a better profile, we decided to fuse the binding moieties derived from LAG-3_1 with those of PD-L1_1 and PD-1_1, generating four novel bi-specific immunomodulatory tribodies. The novel compounds showed binding affinities for their targets comparable to those of validated mAbs (Atezolizumab, Pembrolizumab or Relatlimab) and, more interestingly, an increased ability to induce lymphocyte activation and stronger *in vitro* tumor cytotoxicity compared to the combination of clinically validated mAbs.

In parallel, with the aim of recruiting T cells against cancer cells, we also generated novel tri-specific T-cell engager (TCE) tribodies, able to simultaneously recognize the oncofetal antigen 5T4 on tumor cells, CD3 on T cells, and an IC (PD-L1, PD-1 or LAG-3) by including the scFvs derived from the mentioned novel mAbs. We found that the novel TCEs enhanced cytokine release from hPBMCs, with a strong secretion of IL-2 and IFNγ and showed more potent antitumor effects than the

combination of the parental bispecific compound and clinically validated mAbs targeting the same ICs. Notably, the TCE including the anti-PD-L1 moiety induced complete tumor regression in a mouse model.

To increase the collection of mAbs specific for ICs, human anti-OX-40 scFvs were identified by phage display selections on hPBMCs and purified receptor and used to generate four novel fully human mAbs targeting this immunostimulatory receptor expressed on immune cells. The novel mAbs were tested for their biological effects on human lymphocytes alone or in co-cultures with tumor cells and enhanced both T cell activation and tumor cell killing, displaying additive effects when combined with Atezolizumab.

Finally, a novel human antibody targeting the coagulation cascade, and in particular Factor V, was also generated by using phage display. The novel mAb, called D9, was found able to efficiently bind to Factor V in both its native and activated forms, with nanomolar K_D values and to slow down the coagulation by prolonging the activated partial thromboplastin time (aPTT). These features could make this mAb a potential tool for both diagnostic and therapeutic applications.

Overall, these findings highlight the potential of the newly generated bi- and tri-specific antibodies to overcome the limitations of conventional IC inhibitors, paving the way for next-generation anti-tumor immunotherapeutics with improved safety and efficacy and show the possibility to enlarge the combinatorial strategies including novel immunostimulatory mAbs. Furthermore, novel antibody-based approach has been used also for facing cardiovascular disorders.

1. INTRODUCTION

1.1 Cancer Immunotherapy

1.1.1 Tumor Microenvironment and Cancer Immunotherapy

According to the World Health Organization, cancer represents one of the leading causes of mortality worldwide, responsible for about 10 million deaths every year [**1**]. Cancer is a disease based on abnormal proliferation caused by mutations affecting proteins involved in the control of normal cell growth. It is an evolutionary process that involves dynamic and reciprocal interactions between tumor cells and the surrounding environment, commonly known as the tumor microenvironment (TME).

The TME is a heterogeneous entity comprising many cellular components, including fibroblasts, endothelial cells, adipocytes, adaptive and innate immune cells, as well as non-cellular components, including the extracellular matrix (ECM) and soluble products, such as chemokines, cytokines and growth factors. The TME actively contributes to cancer progression, angiogenesis, invasion, and evasion of immune responses and resistance to treatments [**2**].

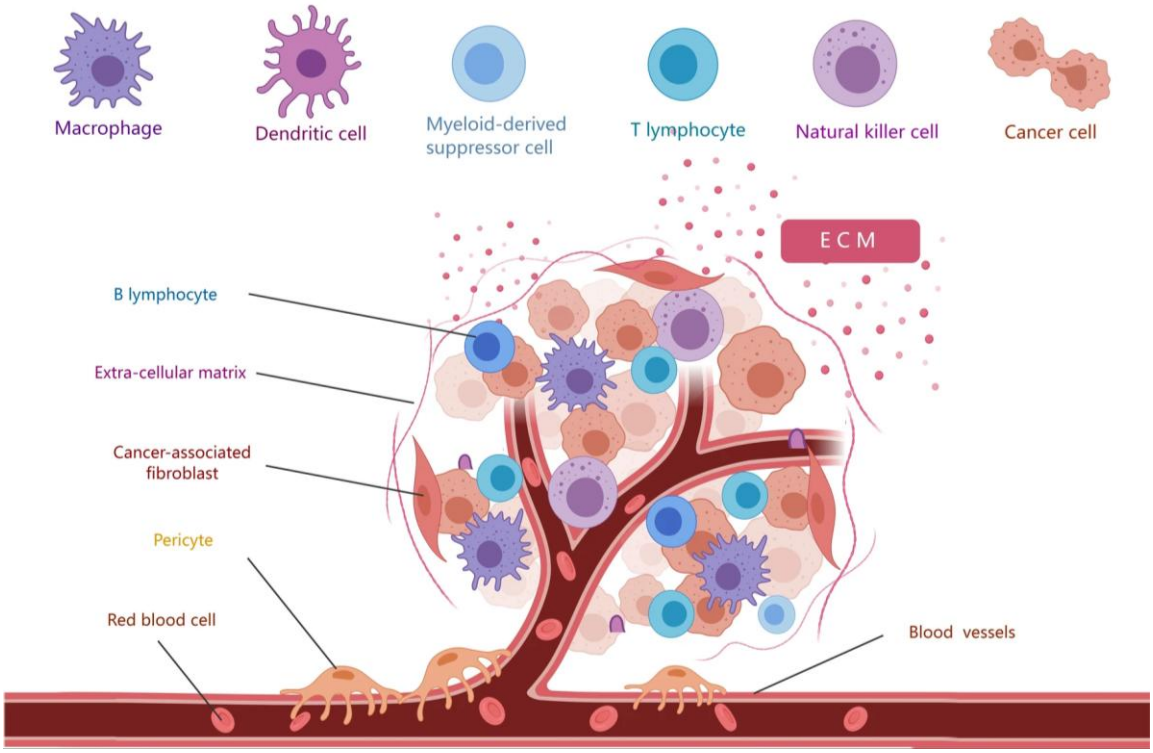

Figure 1. Schematical Representation of the Tumor Microenvironment. The TME comprises tumor cells, immune cells, and supporting cells (such as fibroblasts, stromal cells, and endothelial cells), where secretion of molecules like cytokines and chemokines occurs and plays an important role [**2**].

The complex nature of tumor biology, characterized by heterogeneity, genetic instability, survival to apoptosis and immune evasion mechanisms and resistance to drugs underlie the persistent challenges in cancer treatment. The biological characteristics acquired during the development of tumors were described by Hanahan and Weinberg in 2000 and 2010 as hallmarks of cancer [**3**].

The landscape of cancer treatment has evolved significantly over the last two decades, from conventional treatments such as surgery, chemotherapy and radiotherapy, currently used in oncology practice, to more selective targeted therapies and biological agents. While cytotoxic chemotherapy remains a milestone in many treatment regimens, its lack of specificity for tumor cells often causing systemic toxicity in healthy tissues with high cellular turnover, such as hematopoietic cells, gastrointestinal cells, represents still a limit. Similarly, radiotherapy, although effective for localized effects, is limited by its impact on surrounding healthy tissues and by potential secondary malignancies induced by radiation treatment [**4, 5**].

Advances in molecular cancer biology paved the way for the development of Tyrosine Kinase Inhibitors (TKI) targeting oncogenic gene alterations or their associated signalling pathways. For instance, Imatinib (Gleevec), a first generation TKI targeting BCR-ABL1, is a reversible small inhibitor approved by the FDA (Food and Drug Administration) in 2001 for chronic myeloid leukemia treatment [**6**]. Since then, many others such as Erlotinib and Gefitinib, but also second generation TKI such as Afatinib and third generation Osimertinib, which target mutations in the epidermal growth factor receptor (EGFR), have been approved for non–small cell lung cancer (NSCLC) therapy [**7-9**]. However, their efficacy is often limited by lack of selectivity and the emergence of resistance through secondary mutations or activation of alternative pathways. This has shifted interest towards alternative approaches aimed at achieving more durable tumor control.

Over the past two decades, researchers turned their attention to the immune system's potential role in controlling cancer, and immunotherapy has emerged as an alternative safe strategy in cancer treatment. Cancer immunotherapy relies on the ability of immune cells to specifically detect mutated proteins expressed only on malignant cells, called Tumor-Specific Antigens (TSA) or Tumor-Associated Antigens (TAA), which are proteins over-expressed on tumor cells but expressed at very low levels on healthy cells [**10**].

The use of monoclonal antibodies has emerged as a novel approach against cancer that should avoid off-target effects due to their selective and specific recognition of targets. The mechanisms of action of mAbs which can promote the death of tumor cells are several: first, they can inhibit oncogenic receptors by blocking essential survival signalling pathways; second, they can kill tumor cells by antibody-dependent cellular cytotoxicity (ADCC), as the antibody binds to tumor cells and recruits immune effector cells by Fc; third, they can also induce antibody-dependent cellular phagocytosis (ADCP), mediated by Fc recruitment of FcγRI receptors expressed on macrophages and neutrophils; and finally, they can activate complement-dependent cytotoxicity (CDC) [**11, 12**].

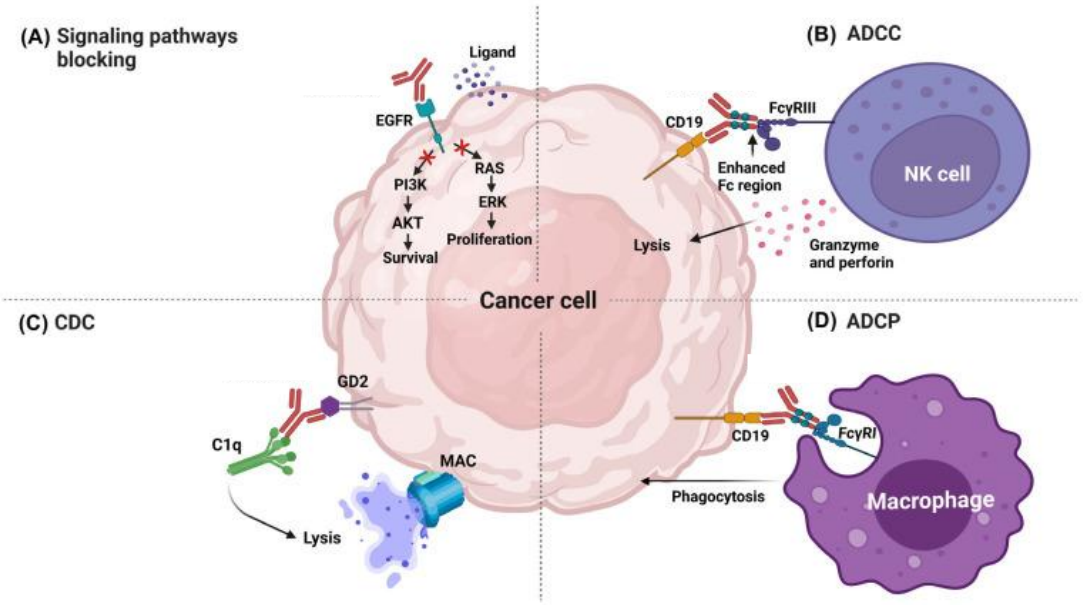

Figure 2. Mechanisms of action of monoclonal antibodies in cancer treatment. (**A**) Interference with tumor growth signalling, (**B**) ADCC-mediated tumor cell elimination (**C**) Complement system activation, (**D**) Fc receptor-mediated phagocytosis by ADCP. [**11**]

The first generation of monoclonal antibodies used for cancer therapy comprises those targeting tumor-associated antigens, designed to directly recognize and bind antigens specifically expressed on tumor cells, such as Human Epidermal Growth Factor Receptor 2 (HER2) in breast cancer, CD20 in B-cell lymphomas, or EGFR in lung, colorectal, and head and neck cancers [**4**]. These antibodies act primarily through ADCC, complement activation, and inhibition of receptor signalling [**13**]. Among the most successful FDA approved anti-TAA mAbs, we can mention Trastuzumab, a humanized monoclonal antibody that specifically targets the extra-cellular domain of HER2 receptor and was approved by the FDA in 1998 for the treatment of HER2+ metastatic breast

cancer [**14**] and Rituximab, a chimeric human/mouse anti-CD20 monoclonal antibody which was approved by the FDA in 1997 and revolutionized the treatment of B-cell malignancies [**15**, **16**].

Even though successful, some side effects emerged for these mAbs. Indeed, Trastuzumab has been associated with cardiotoxicity [**14, 17**], Rituximab treatment with infusion-related reactions, severe dermatologic and mucosal adverse events, as well as cardiac arrhythmias [**18**]. Moreover, first-generation anti-TAA therapies often failed to generate durable responses in solid tumors due to limited T-cell infiltration and activation, antigen loss or heterogeneity [**11, 19**]. Thus, the increasing understanding of tumor-induced immune suppression paved the way for the development of second generation of antibodies acting as immune checkpoint inhibitors (ICIs).

These novel mAbs can modulate immunological pathways by targeting immune checkpoints expressed on T cells and essential for immune surveillance, providing either stimulatory or inhibitory signals to regulate T cell responses.

Immune checkpoints are regulatory surface proteins that function as molecular switches controlling T cell activation and exhaustion. They include either co-stimulatory receptors (such as CD28, ICOS, 4-1BB, OX40, CD27) that enhance immune responses by inducing T cell proliferation and cytokines secretion or inhibitory ones (such as CTLA-4, PD-1, LAG-3, TIGIT, TIM-3) that have opposite effects [**20**, **21**]. While this regulatory system in physiological conditions prevents autoimmunity, tumors can exploit these inhibitory pathways to evade immune detection and suppress anti-tumor responses by expressing their ligands.

On the basis of these considerations, the surface expression of immune checkpoints makes them attractive targets for monoclonal antibodies to inhibit in the interactions of ICs and their ligands and release the brake of anti-tumor immunity. Over the past decade, research has focused on developing agonistic antibodies to enhance co-stimulatory signals or antagonistic antibodies to block inhibitory pathways [**22, 23**]. This strategy has yielded several FDA-approved ICI therapies with efficacy and long-lasting responses in several types of cancer, particularly for melanoma, breast, non-small cell lung cancer (NSCLC) and head and neck cancers [**12, 23**].

1.1.2 The Role of Immune Checkpoints in Anticancer Immune Response

The anticancer immune response involves a series of sequential steps that have the potential to be self-reinforcing during the course of response [**24-26**]. As shown in **Figure 3**, during an inflammatory response, tumor cell death leads to the release of neoantigens and enables antigen-presenting cells (APCs) to capture and process them. During the priming phase, APCs present the associated peptides/neoantigens via major histocompatibility complex II (MHC II) molecules to naïve T cells in tumor-draining lymph nodes, resulting in the activation of effector T cells against cancer cells. The activated T cells then migrate to and infiltrate the tumor, where they specifically recognize and bind to cancer cells through their specific interaction between T cell receptor (TCR) and peptide antigens displayed on MHC class I, leading to activation of T cells, secretion of perforin and other cytokines and cancer cell killing [**25, 26**].

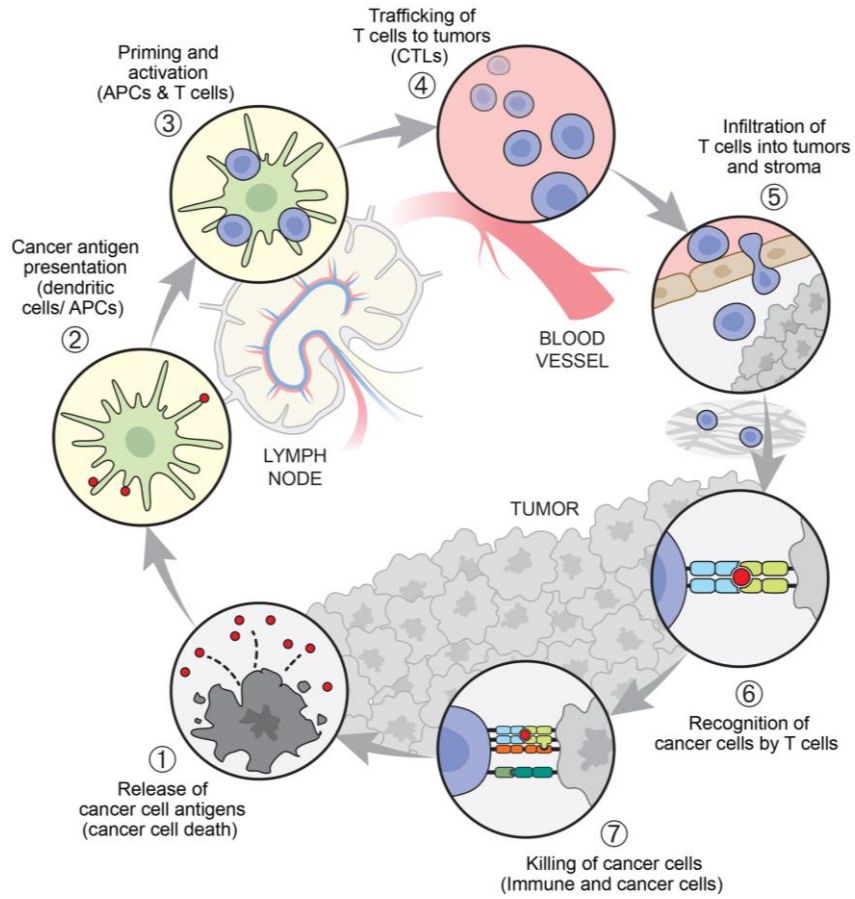

Figure 3. The cancer-immunity cycle. Schematical representation of the sequential steps involved in the anti-tumor immune response. Tumor antigen release (1); neoantigen presentation by APCs (2); priming and activation of naïve T cell in lymph nodes (3); trafficking (4), and tumor infiltration (5) of activated effector T cells; recognition (6) and killing (7) of cancer cells by effector T cells [**24, 25**].

However, antigen-MHC recognition alone is not sufficient to fully activate naïve T cells and may instead induce anergy in the absence of appropriate co-stimulatory signals. Full T-cell activation requires the interaction between CD28, a receptor constitutively expressed on both CD4+ and CD8+ T cells, and its ligands B7-1 (CD80) or B7-2 (CD86) expressed on APCs. This CD28-B7 binding stimulates downstream signalling cascades that promote clonal expansion, survival, and differentiation of T cells through autocrine production of interleukin-2 (IL-2) [**20**].

This activation process triggers a negative feedback loop aimed at limiting excessive responses: Cytotoxic T-Lymphocyte Antigen 4 (CTLA-4), a receptor of the immunoglobulin family, usually sequestered in intracellular compartments of T cells, is rapidly transported to the immunological synapse. There, CTLA-4 competes with CD28 for binding to B7 molecules, for which it shows higher affinity and effectively inhibits activation signals and T cell responses [**20**]. Moreover, other studies showed that CTLA-4 can also sequester B7.1 and B7.2 from the surface of APCs through trans-endocytosis, inducing their degradation [**27**]. This results in a substantial reduction of T cell proliferation and IL-2 secretion through inhibition of key transcription factors, including the Nuclear Factor of Activated T cells (NFAT) or the Activator Protein 1 (AP-1). Additionally, CTLA-4 promotes the anti-inflammatory cytokine release by Treg cells, which further reduces the activation and proliferation of effector T cells [**28, 29**]. In the tumor microenvironment CTLA-4 exerts its role by using additional mechanisms, such as promoting Treg differentiation and T cell apoptosis, which enables tumor cell proliferation [**28, 29**].

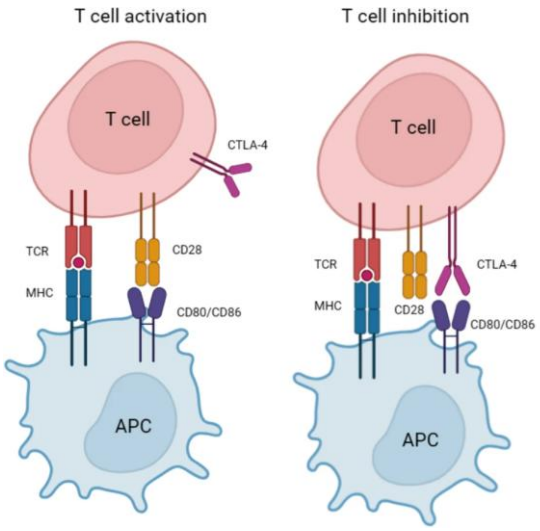

Figure 4. Role of CTLA-4 in T cell inhibition. T cell activation requires co-stimulatory signalling through CD28 binding to its ligand

B7 on APCs. CTLA-4, a high-affinity inhibitory receptor, competes with CD28 for B7 binding, suppressing T cell activation by blocking co-stimulation [**28**].

While CTLA-4 regulates the priming phase of T-cell activation in lymphoid tissues, the other inhibitory receptor programmed cell death protein 1 (PD-1) and its ligand PD-L1 exert their effects in peripheral tissues to prevent excessive lymphocyte activation and regulate immune tolerance to self-antigens [**30**]. PD-1 is an inhibitory receptor, member of the immunoglobulin (Ig) superfamily, expressed during the immune reaction phase on activated T cells, B cells, and NK cells. PD-L1 is a type I transmembrane glycoprotein, expressed in several cell types and organs, including hematopoietic cells (T-cells, B cells, macrophages, dendritic cells, and neutrophils), non-hematopoietic cells and APCs. Moreover, tumor cells also express PD-L1 to evade immune response [**31**]. PD-1/PD-L1 interaction transduces a negative intracellular signal that suppresses TCR signalling by activation of SHP-2 phosphatase, which dephosphorylates ZAP70 and, in turn, inhibits the RAS-MEK-ERK and PI3K-Akt pathways (**Figure 5**). This leads to a reduction in proliferation, cytokine production, and induces a state of T-cell exhaustion [**30, 31**].

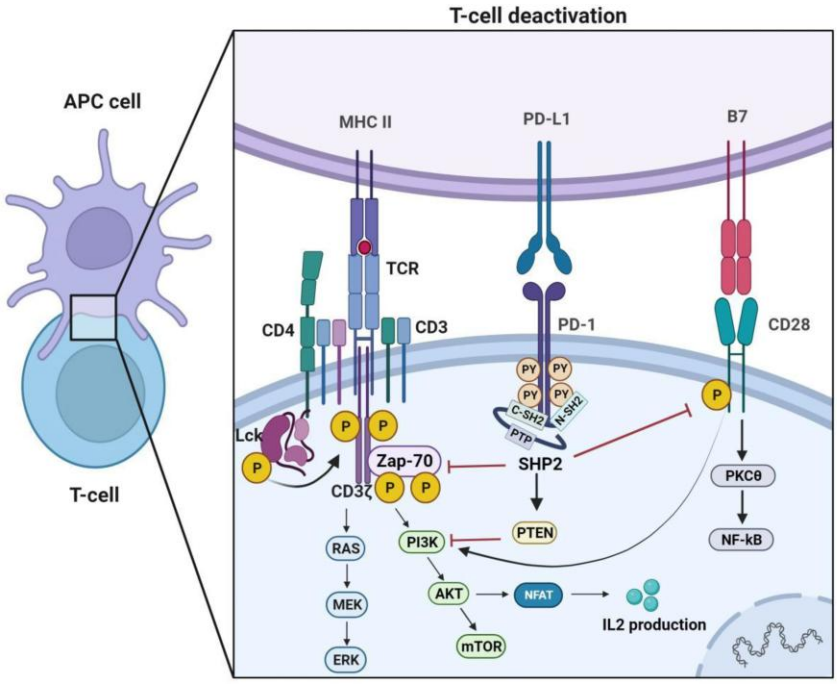

Figure 5. Inhibitory pathway of PD-1/PD-L1. Upon PD-L1 engagement, PD-1 recruits SHP-2 phosphatase, which dephosphorylates TCR signalling molecules, suppressing IL-2 secretion and other effector functions. This results in T-cell exhaustion and tumor immune evasion. [**30**]

High levels of PD-L1 expression have been reported in several types of malignancies, such as lung, breast, and brain cancers, as well as melanoma. Within the TME, the interaction of PD-L1 and PD-1 on activated T lymphocytes leads to impaired T-cell activation and proliferation, decrease in the secretion of cytokines, including IL-2, interferon-gamma (IFNγ), and tumor necrosis factor (TNF)-α. Consequently, these T-cells lose their efficacy in eradicating cancerous cells [**31**].

Another key inhibitory receptor involved in peripheral tolerance is Lymphocyte Activation Gene 3 (LAG-3), a type I transmembrane protein belonging to the immunoglobulin superfamily. LAG-3 is expressed by T cells, Natural Killer (NK) cells and B cells upon T cell activation [**33**]. LAG-3 primarily binds to MHC-II present on APCs by competing with CD4 and therefore delivering inhibitory signals that suppress T cell expansion and cytokines production [**34**]. However, this receptor can bind also to other ligands such as fibrinogen-like protein 1 (FGL-1) and Galectin-3 (Gal-3) which are expressed on different cell types such as dendritic cells, monocytes, stromal, liver, and cancer cells [**35**]. To date, the mechanisms of action of LAG-3 upon ligand engagement leading to T cell inhibition remain poorly understood [**33**]. Some studies showed that LAG-3 contains two domains implicated in inhibitory function: a membrane proximal FXXL motif and a KIEELE motif in the cytoplasmic tail [**36**]. Interestingly, some studies demonstrated that LAG-3 and PD-1 were frequently co-expressed in tumor-infiltrating lymphocytes (TILs) and synergized to drive T cell exhaustion and promote tumoral immune escape [**37**, **38**].

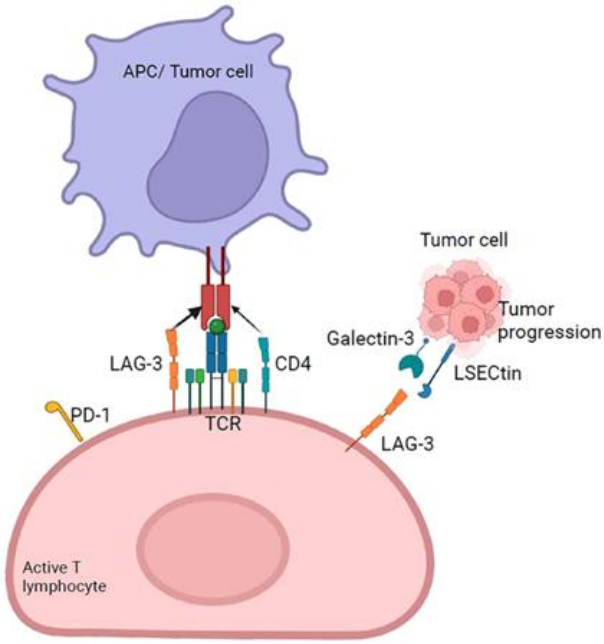

Figure 6. Schematical representation of the role of LAG-3 in immune system. LAG-3 is expressed on activated T cells and binds to MHC-II with higher affinity than CD4. This interaction generates the overexpression and secretion of immunoregulatory cytokines, such as IL-10 and TGF-β, which suppress T cells. In addition to MHC-II, other ligands have been discovered: FGL-1, galectin-3, LSECtin which contribute to tumor progression and immune suppression [**39**].

In contrast to these inhibitory checkpoints, OX40 (CD134) is a co-stimulatory receptor, member of the TNF receptor superfamily. This immune checkpoint is transiently expressed on activated CD4+ and CD8+ T cells following initial stimulation [**40**]. Upon binding to its ligand OX40L, which is expressed on APCs, OX40 promotes T cell proliferation, survival, generation of immunological memory, and cytokine production. The ligand induces formation of trimeric receptor–ligand complexes that cluster the cytoplasmic domain of OX40, creating docking sites for TRAF adaptor protein, thus allowing the activation of multiple downstream signalling cascades. These effects are mediated through the regulation of key transcriptional pathways, including PI3K–Akt, NF-κB and, specifically for Treg cells, the Forkhead box P3 (FoxP3) [**41, 42**]. OX40 co-stimulation induces also NK cell activation and cytokine production, enhancing their cytotoxicity against cancer cells [**43**]. Activation of the OX40 downstream pathway can prevent the effects of T cell exhaustion and improve immune persistence within the tumor microenvironment. It has been reported in literature that anti-OX40 mAbs can be involved in the depletion of tumor-infiltrating Treg cells, which constitutively express high levels of OX40, by suppressing FoxP3 expression or by inducing ADCC and are able to enhance anti-tumor activity against several malignancies such as MCA303 sarcoma, CT26 colon carcinoma or SM1 breast cancer [**44**]. Moreover, high levels of OX40 expression on

tumour infiltrating lymphocytes (TILs) is associated with a better prognosis for several types of cancer. [**43**, **44**]

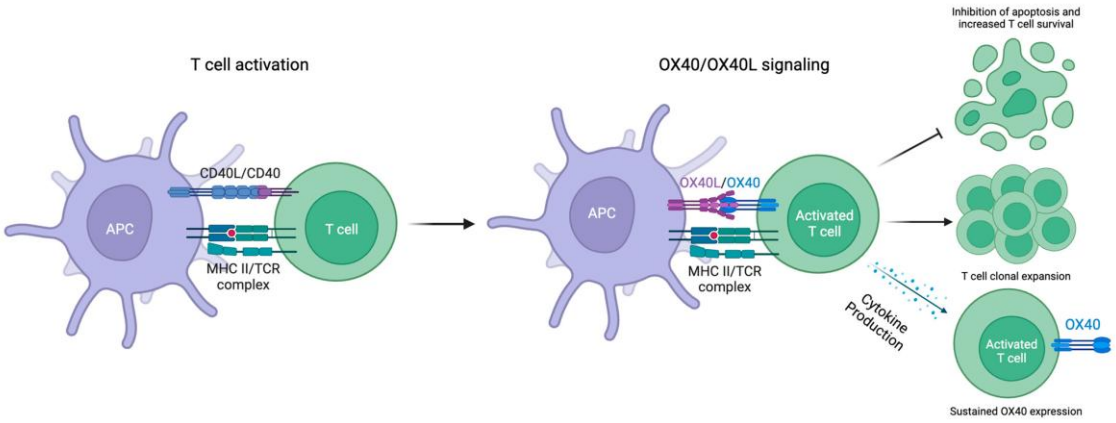

Figure 7. OX40/OX40L signalling in T-cell activation. Following antigen recognition, OX40 is upregulated on activated $CD4^+$ and $CD8^+$ T lymphocytes, while its ligand OX40L is expressed on APCs. OX40-OX40L interaction promotes the clonal expansion of effector CD4+ and CD8+ T cell populations, enhances the secretion of proinflammatory cytokines, and promotes the survival of T cells [**45**].

1.1.3 Second Generation of mAbs Targeting Immune Checkpoints in Cancer Therapy: Indications and Side Effects

Ipilimumab, a human anti-CTLA-4 IgG1, was the first checkpoint inhibitor approved by the FDA in 2011, after a phase III randomized clinical trial for metastatic melanoma which improved overall survival. Ipilimumab is now used for therapy of several cancer types, such as lung and renal cell carcinoma (RCC), often in combination regimens [**46**]. For instance, the combination of Ipilimumab with the anti-PD-1 Nivolumab has received the FDA approval in first-line therapy for unresectable melanoma, RCC and microsatellite-high colorectal cancer, and as a first-line option in metastatic NSCLC and malignant pleural mesothelioma [**47**-**49**]. A second anti-CTLA-4 antibody, named Tremelimumab (IgG2), has been approved more recently in 2022 in combination with Durvalumab (anti-PD-L1); this therapeutic regimen demonstrated significant survival benefits for unresectable hepatocellular carcinoma (HCC) in the HIMALAYA trial [**50**].

However, treatments with anti-CTLA-4 mAbs have shown some side effects, such as colitis, hypophysitis, rash, and hepatitis. Other affected organs could include eyes, nervous system, lungs, heart, kidneys, and joints. The breadth of immune-related adverse

events (irAEs) is consistent with the biological role of CTLA-4 in early T-cell priming [**29**, **51**].

Among the first anti-PD-1 monoclonal antibodies developed, Pembrolizumab (Keytruda) and Nivolumab (Opdivo) were approved in 2014 by the FDA for the following indications: melanoma, NSCLC, RCC, head and neck squamous cell carcinoma (HNSCC), Hodgkin lymphoma, urothelial carcinoma, hepatocellular carcinoma (second-line), esophageal squamous cell carcinoma, gastric cancer, cervical cancer, and others [**46**]. Combinatorial strategies of anti-PD-1 and anti-CTLA-4 mAbs were then tested and recent trials of Nivolumab plus Ipilimumab showed an overall survival after 10 years in patients with advanced melanoma and 5 years in patients affected by NSCLC [**52, 53**].

Pembrolizumab used in monotherapy has shown strong efficacy in PD-L1^{high} metastatic NSCLC, prolonging median overall survival [**54**]. In 2021, its combination with chemotherapy was approved for early-stage triple-negative breast cancer (TNBC) [**55**]. Despite their efficacy, immune-related adverse events emerged also in anti-PD-1 treatments even though milder than those observed with anti-CTLA-4 mAbs. Pembrolizumab commonly caused fever, fatigue, cough, and gastrointestinal disorders [**56**], while Nivolumab was often associated with nausea, digestive disorders, oral ulcerations, dermatologic manifestations, hormone dysfunction and liver disorders [**57**].

The PD-1 ligand (PD-L1) was also chosen as a target for three mAbs that entered the clinic between 2016 and 2017: Atezolizumab (Tecentriq), Durvalumab (Imfinzi), and Avelumab (Bavencio) [**46**]. Atezolizumab has been approved by FDA for multiple cancer types: first-line treatment of PD-L1^{high} NSCLC in combination with chemotherapy (IMpower130 trial [**58**]), small cell lung cancer in combination with carboplatin/etoposide (IMpower133 [**59**]), advanced PD-L1^{+} triple-negative breast cancer in combination with nab-paclitaxel [**60**]. Durvalumab was indicated in Stage III NSCLC [**61**], limited-stage small cell lung cancer [**62**] and, more recently, in March 2025, for invasive bladder cancer [**63**]. Avelumab was initially approved for Merkel cell carcinoma, and later as maintenance therapy in metastatic urothelial carcinoma, and consolidation therapy in bladder cancer after chemotherapy regimen [**64**]. These anti-PD-L1 mAbs share the same spectrum of immune-mediated toxicities of anti-PD-1 mAbs, including dermatologic reactions, endocrinopathies, hepatitis and pneumonitis, diarrhea/colitis, even though less severe and less frequent compared to Ipilimumab [**51**].

The first FDA and EMA-approved LAG-3 inhibitor, in March 2022, was Relatlimab, a human anti-LAG-3 mAb, used in a fixed-dose combination with nivolumab under the brand name of Opdualag [**65**]. The indication of this novel drug is first-line unresectable or metastatic melanoma. Beyond melanoma, subsequent studies focused on Opdualag administration in multiple other treatments including those of advanced/recurrent NSCLC (RELATIVITY-104), advanced gastric/gastroesophageal junction carcinoma (RELATIVITY-060), third-line microsatellite stable (MSS) colorectal cancer (CRC) (RELATIVITY-123). Neoadjuvant treatments in multiple indications are also being tested [**66**]. Opdualag showed an intermediate toxicity profile with the most common AEs, such as fatigue, rash, pruritus, diarrhea/colitis, and endocrinopathies (especially hypothyroidism and thyroiditis). Treatment discontinuations were mainly due to myocarditis (1.7%) and pneumonitis (1.4%) [**65**, **66**].

A few monoclonal antibodies targeting OX40 have already been generated and are currently being tested. Among them, Telazorlimab and Rocatinlimab are under evaluation in clinical trials to treat atopic dermatitis [**67**]. However, clinical results of fully human anti-OX40 mAbs have been modest in monotherapies therefore, combinatorial treatments have been considered in ongoing clinical trials, especially with anti PD-1 and anti-PD-L1 mAbs to overcome this limit [**68**]. Examples are represented by the phase I clinical study of GSK3174998, a novel humanized anti-OX40 IgG1 monoclonal antibody tested alone or in combination with the anti-PD-1 Pembrolizumab in patients with advanced solid tumors, including renal cell carcinoma, TNBC, NSCLC, melanoma, sarcoma, and colorectal carcinoma (NCT02528357), and the phase I/II trial of INBRX-106, another OX40 agonistic antibody, tested in combination with Pembrolizumab (NCT04198766) [**69**].

Despite their rarity, cardiac adverse events associated with ICIs, especially in combination treatments, can have severe consequences in oncology patients [**70**]. The most severe include inflammatory conditions affecting myocardium, blood vessels, and endothelium, that can lead to fatal events [**70**, **71**]. Non-viral inflammatory myocarditis represents the predominant cardiotoxic event, however the incidence remains extremely low (<1%) [**72**]. Severe myocarditis with potentially fatal consequences has been reported in patients receiving Pembrolizumab or Ipilimumab. Notably, the risk of myocarditis was significantly higher with combined ICI regimens: combinations of mAbs targeting CTLA-4 and PD-1 showed an increase in myocarditis events compared to monotherapies [**73**]. Indeed, Ipilimumab in combination with Nivolumab, when used as a first-line

treatment for NSCLC (CHECKMATE-227), was an example of increased cardiotoxic risk [**74**].

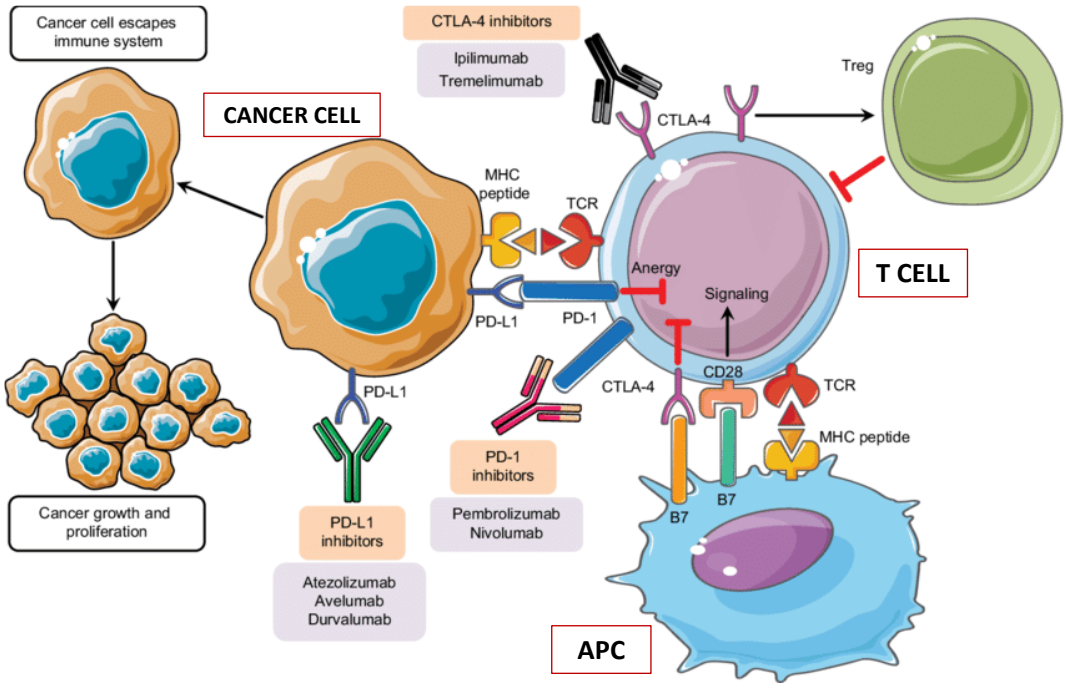

Figure 8. Immune checkpoints and therapeutic blockade with monoclonal antibodies. Immune checkpoints can inhibit T-cell activity, enabling tumor immune evasion. Monoclonal antibodies targeting CTLA-4 (Ipilimumab, Tremelimumab), PD-1 (Nivolumab, Pembrolizumab), or PD-L1 (Atezolizumab, Avelumab, Durvalumab) can revert these inhibitory pathways, by restoring T-cell function and allowing cancer cell elimination [**75**].

1.1.4 Innovative Strategies: Bispecific and Trispecific Antibodies

Emerging immunotherapeutic strategies for cancer therapy include bispecific and trispecific antibodies. These compounds are engineered to simultaneously engage multiple immune targets at once, achieving additive or synergistic anti-tumor effects, thus overcoming the limits of single agent or even combinatorial treatments. These constructs allow to expand their use in a wide range of clinical applications and improve therapeutic outcomes for patients with tumors resistant to monotherapy. Indeed, bispecific compounds can either recognize two TAAs or two ICs simultaneously or behave as T cell engagers by targeting a TAA on cancer cells and CD3 receptor on lymphocytes, physically creating an immune synapse and directly inducing tumor cell lysis [**76, 77**].

The first bispecific antibody (BsAb) was developed in the early 1960s by using mild reoxidation of binding fragments obtained from two distinct polyclonal sera [**78**]. Later, quadroma technology, derived from hybridoma strategy, allowed the generation of bispecifics by fusing two different hybridoma cells;

however, this approach was limited by the frequent generation of bsAbs with mismatched binding regions [**79**]. Nowadays, following the development of recombinant technologies, more than 200 bsAbs are currently in clinical development and 14 received approval by FDA for cancer treatment. In particular, 11 new bispecifics were approved in the last 3 years, of which 7 for hematological malignancies and 4 for solid tumors [**80**].

BsAbs can be classified based on their structural composition: those containing crystallizable fragment (Fc) domains and those lacking Fc regions. BsAbs with Fc regions enable immune activation also through direct engagement of Fc receptors on immune effector cells. While bispecifics without Fc region lack the effector functions mentioned above, they show better biodistribution in the tumor tissues and reduced immune-related toxicity [**76, 77, 81**].

The first bsAb approved in the European Union in 2009 was Catumaxomab, a bsAb targeting epithelial cellular adhesion molecule (EpCAM) on tumor cells and CD3ε on T cells. Its indication was for treatment of malignant ovarian ascites but was withdrawn from the market due to severe infusion reactions and a high incidence of immunogenicity [**81, 82**].

More recently, several bi-specific antibodies lacking Fc have reached clinical practice thanks to their lower immunogenicity and toxicity. Blinatumomab is a bispecific T cell engager (BiTE) targeting CD3 and CD19, the first approved by FDA in 2014 for the treatment of acute lymphoblastic leukemia (ALL). In recurrent ALL, Blinatumomab led to complete responses in 70% of patients and minimal residual disease in 88%, thus confirming its efficacy even at much lower doses (μg) than conventional mAbs [**83**]. However, its low molecular weight (55 kDa) was responsible for its reduced half-life and continuous infusions needed [**81**].

Considering the frequent emergence of resistance to IC inhibitors in the tumor microenvironment due to the compensatory expression of other ICs [**84**], the development of compounds combining two different binding moieties against distinct ICs has been proposed as an interesting strategy to overcome resistance in patients. Indeed, another additional type of bi-specific recently approved in China is Cadonilimab**,** which

simultaneously binds to two ICs, PD-1 and CTLA-4, with increased avidity due to tetravalency even though it lacks Fc. Encouraging results in clinical studies across multiple advanced solid tumors with a favourable safety profile led to its approval in 2022 for patients with refractory metastatic cervical cancer [**85**].

On the basis of this rationale, during my PhD project, we generated four novel different bispecific immunomodulatory tribodies by fusing the Fab portion of one anti-IC antibody with two scFv domains of a different immune checkpoint inhibitor [**86**]. The novel bispecific compounds (named TR0102, TR0304, TR0506, TR0708) combine the biological properties of two different antibodies (an anti-PD-1 with anti-LAG-3 mAb or an anti-PD-L1 with an anti-LAG-3 mAb) into one single molecule. Moreover, these novel bispecific tribodies show some advantages such as a higher molecular weight of 100 kDa, in comparison with BiTEs, and an Fc-free format to reduce unwanted toxicity.

Many other bsAbs have reached FDA or EMA approval in the last 4 years, 8 of them are T cell engager (TCE) specific for multiple myeloma, B cell lymphoma and small-cell lung cancer. For instance, Mosunetuzumab, a TCE targeting CD20 and CD3, was approved in 2022 for the treatment of relapsed/refractory follicular lymphoma, while Tarlatamab became the first-in-class TCE approved for lung cancer in 2024 [**80, 87**].

Among non-T cell engagers bi-specific antibodies approved in recent years, which simultaneously target two TAAs, Amivantamab, binding to two tyrosine kinase receptors on tumor cells (EGFR and cMet), was approved by FDA in 2021 for advanced or metastatic NSCLC [**88**]. More recently, Zanidatamab, a bispecific targeting two distinct epitopes of HER2, was approved both by FDA (in 2024) and EMA (in 2025) for HER2-positive cancer [**89**].

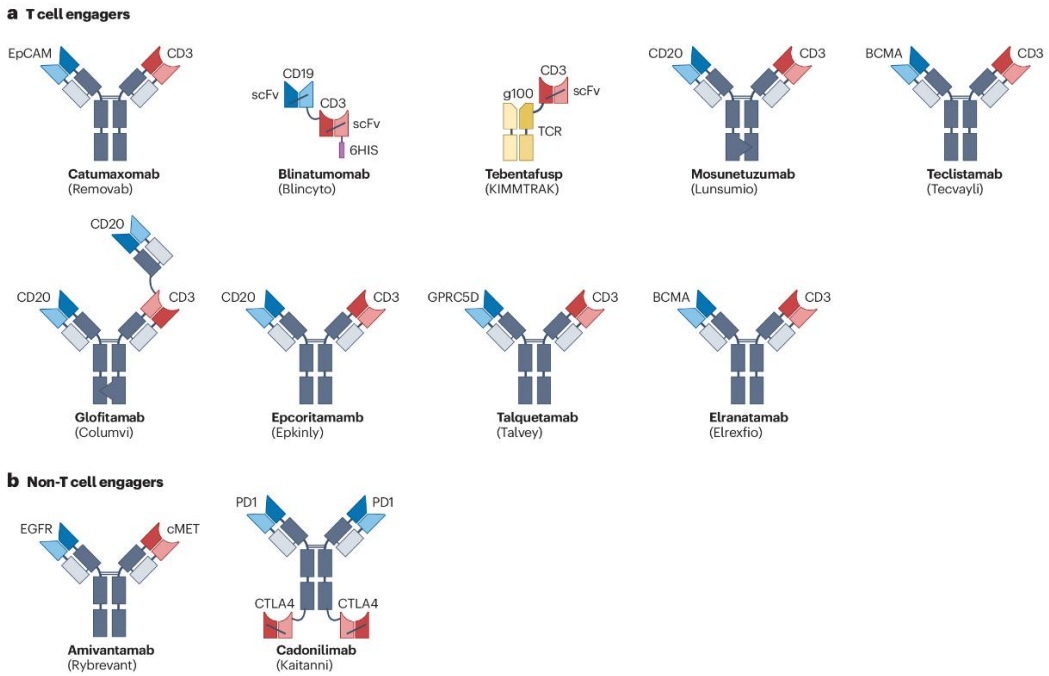

Figure 9. Schematical representation of different bispecific formats. (a) Bispecific T cell engagers, (b) bispecific antibodies non-T cell engagers. 6 out of 11 approved bsAbs have an IgG-like structure made up of 2 heavy chains and 2 light chains. The other bsAbs are Fc-free made up of two fused scFv or a scFv fragment fused to an IgG [**81**].

Despite the clinical success of bispecific antibodies, significant limitations in treating solid tumors remain due to resistance mechanisms and immunosuppressive tumor environment. To overcome these limitations, trispecific compounds were designed to target three different antigens, thus prolonging T-cell activation [**90, 91**].

Early clinical studies of trispecific constructs, such as CD38/CD28/CD3 in multiple myeloma and CD19/CD22/CD3 compounds in B-cell malignancies, have generated strong proof-of-concept findings [**92, 93**]. Other trispecific constructs were designed as NK-engagers (CD16 × NKp46 × TAA such as CD20) to simultaneously bind to TAA and engage FcγRIII (CD16) and an activating NK receptor (NKp46) [**94**, **95**]. However, the inclusion of an anti-CD28 binding domain is associated with the risk of severe side effects due to excessive cytokine release [**96, 97**].

Another example of trispecifics can be generated by using tribodies. Tribodies harness the natural heterodimerization between heavy and light chains within Fab fragments to generate a scaffold that can be used to incorporate two or three binding domains, such as scFvs [**98**]. Therefore, tribodies are made up of a Fab genetically fused to two scFvs, with a molecular weight of 100 kDa, which allows for a longer half-life in circulation, compared to BiTEs.

In recent years, we have focused on Tb535H, a bi-specific tribody which inhibited tumor growth in xenograft mouse models and is currently being tested in phase I clinical trial (NCT07016997) [**99**]. Tb535H is made up of a Fab and an scFv domain both targeting 5T4, which is an oncofetal antigen expressed on many types of tumor cells [**100, 101**], and another scFv targeting CD3. With the aim of potentiating its antitumor activity, five novel tri-specific and multifunctional tribodies, called 53X tribodies were generated in our laboratory in collaboration with the Japanese company, Chiome Inc. The trispecifics are composed of a Fab arm binding to 5T4, an scFv binding CD3, but differently from the parental Tb535H, for the first time they include an additional scFv derived from an antibody specific for an immune checkpoint, such as PD-1, PD-L1 or LAG-3 [**102**]. The immunomodulatory scFv was inserted by replacing the scFv recognizing 5T4 in the parental tribody to increase T cell activation and overcome the immunosuppressive environment of solid tumors.

Although the promising advances in cancer treatment, challenges remain: the potent immunostimulatory activity of bi-specific or tri-specific compounds should be carefully monitored to avoid cytokine release syndrome, which nevertheless occurred in a low percentage (less than 3%) of patients treated with Blinatumomab [**83**].

1.2 Generation Of Monoclonal Antibodies As Tools For Other Therapeutic And Diagnostic Applications

1.2.1 Phage display technology: principle and applications

The earliest and most widely used method for monoclonal antibody production was the hybridoma technique, developed by Köhler and Milstein in 1975 [**103**]. This innovative method represented a turning point for both therapeutic and diagnostic applications, and the two scientists were awarded by a Nobel Prize in Medicine in 1984 [**104**]. The strategy consists in mice immunization with an antigen, followed by isolation of splenocytes to be fused with immortal myeloma cells. These fusion cells, called hybridoma, can grow in culture for unlimited time and produce monoclonal antibodies. However, this approach is limited by immunogenicity of murine antibodies and the laborious process of generation. To overcome these limits, the generation of chimeric, humanized, and fully human antibodies was obtained by implementing molecular biology techniques [**11**].

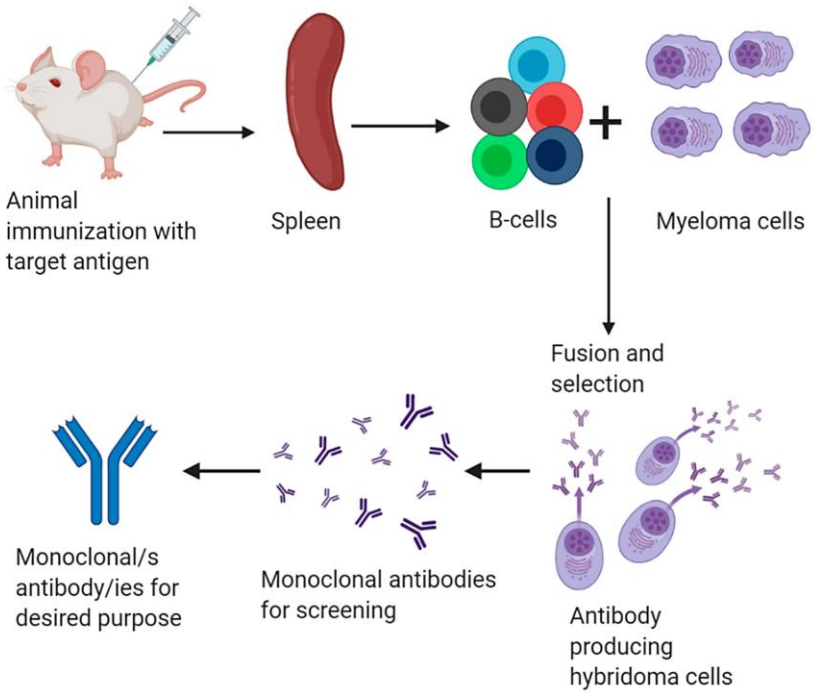

Figure 10. Representation of steps of hybridoma technique. After mouse immunization, isolated splenocytes are fused with myeloma cells to create hybridomas, which are selected and expanded to obtain monoclonal antibodies [**105**].

As an alternative to conventional hybridoma technology, phage display provides a reliable and potent technology for production of fully human mAbs with no risks of

generating Human Anti-Mouse Antibody (HAMA) responses in therapeutic applications [**106**]. Phage display was introduced for the first time by George P. Smith in 1985, who was later awarded the Nobel Prize in Chemistry in 2018 [**107**]. This method is based on the display of peptides or antibody fragments (such as scFvs or Fab fragments) on the surface of filamentous bacteriophages, typically *M13* phages. The gene encoding the antibody fragment is inserted into the phage or phagemid genome, resulting in the expression of the antibody fragment fused to a phage coat protein, displayed on the viral surface, thus allowing for direct association of the DNA sequence (genotype) and phenotype. This platform enables the creation of extremely large libraries, often including more than 10^{10} distinct antibody variants, which can be selected through affinity techniques on antigens, including purified proteins, cell-surface receptors, or even whole cells [**108**].

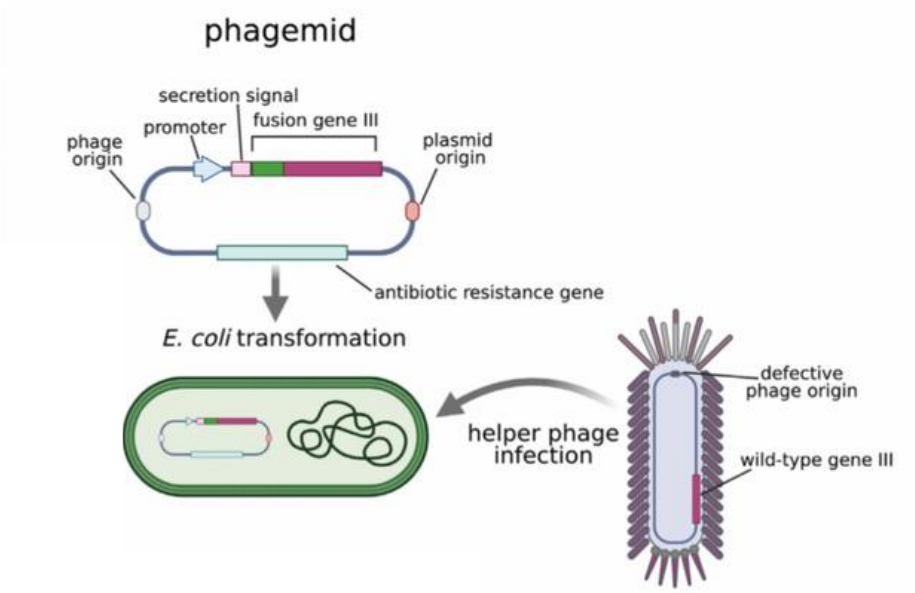

Figure 11. Graphical representation of phagemid vector. The phagemid vector carries the elements required for antibody gene insertion and packing into viral particles. After transformation into *E. coli*, infection with a helper phage enables the assembly of functional phage particles, each displaying a single copy of the encoded peptide [**109**]. (Image adapted from Jaroszewicz W. et al, *FEMS Microbiology Reviews,* 2022).

Library design represents the fundamental step for successful phage display selection, as its size affects the probability of selecting binders. Usually, they can contain millions of DNA clones encoding peptides or antibody fragments derived from the genes of human B cells or synthetic DNA. These resulting libraries can be also cloned into phagemid vectors and transferred into *E. coli* to be infected with helper phage to generate phage

particles which are submitted to 3-4 cycles of "biopanning" on the chosen target, so that high affinity binders can be enriched, amplified, and characterized, as indicated in **Figure 12**.

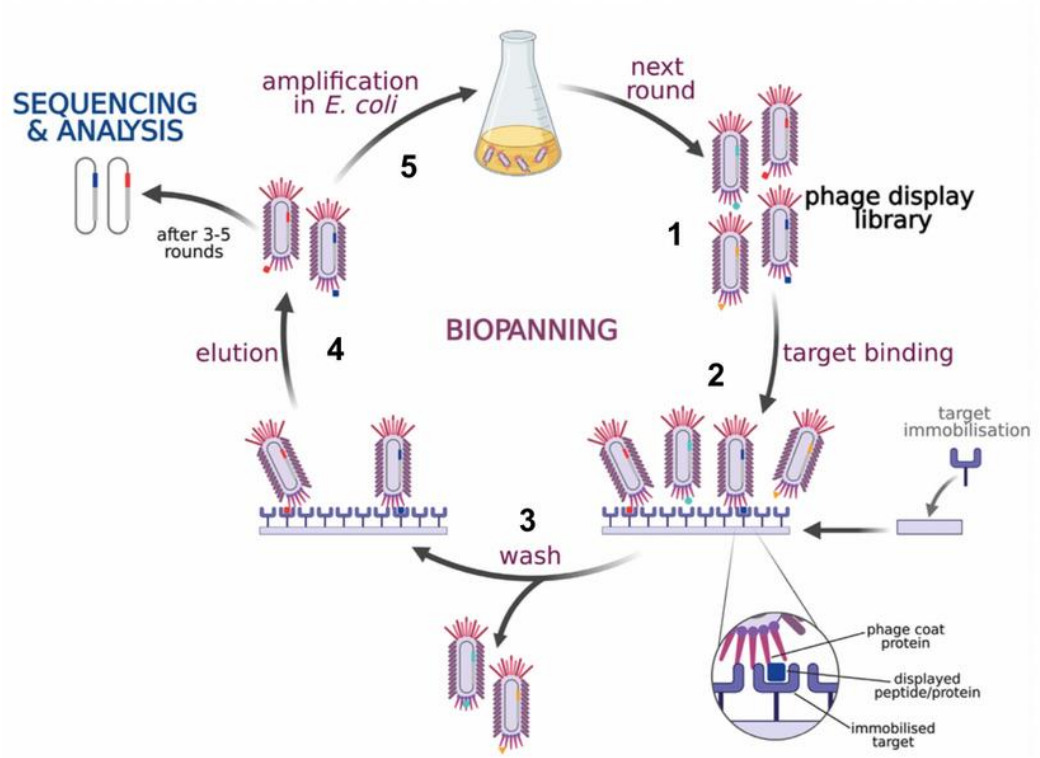

Figure 12. Phage display: selection steps. (1) After library preparation, (2) affinity selection is performed by panning the library on immobilized target molecule. (3) The washing step is required to remove unbound phages. (4) After washes, the bound phages are eluted by lowering pH (pH ≤ 2) and amplified in *E. coli* (5) to produce an enriched pool to use for the next rounds. After 3-4 rounds of biopanning, the obtained clones are functionally analysed [**109**]. (Image adapted from Jaroszewicz W. et al, *FEMS Microbiology Reviews,* 2022)

After collection of the eluted phages and confirmation of target specificity by ELISA assays, both VH and VL fragments are isolated and can be cloned into appropriate expression vectors for mammalian cell transfection in order to generate a fully human antibody. The selection of appropriate vectors enables the production of different isotypes of immunoglobulin according to the following applications [**110**].

Phage display technology has been successfully applied in our laboratory over the years to generate immunoagents against several viral or tumor-associated antigens, such as ErbB2 or nucleolin for breast cancer therapies [**111, 112**]. Among antiviral

applications, an anti-claudin 1 mAb that inhibits hepatitis C virus infection was generated and tested [**113**].

More recently, during the coronavirus pandemic in 2020, the same approach was employed to isolate an antibody against the SARS-CoV-2 spike protein, named D3. This antibody efficiently inhibited viral entry by neutralizing SARS-CoV-2 in cell cultures and was used to quantitatively detect pseudoviral particles expressing Spike protein in cell cultures, as a proof of concept for testing it as a diagnostic tool for measuring viral load in biological samples [**114-116**].

High-Throughput Phage Display for Fully Human Anti-Immune Checkpoint Antibodies

In order to generate repertoires of specific binders for multiple ICs, a massive parallel screening was performed for the first time in our laboratory on activated human peripheral blood mononuclear cells (hPBMCs). The pool of phages recovered from the first selection cycle potentially constitutes a large collection of binders against several different immune checkpoint targets, designated as the 'Immunome Library'. Subsequently, a panel of 10 human recombinant proteins (such as PD-1, PD-L1, LAG-3, OX40) was used to perform further selection pannings to increase the specificity of the binders. Phage clones selected through this methodology were identified by massive parallel sequencing and the most enriched scFv sequences were chosen for further characterization and converted into fully human IgG4 [**110, 116**]. The resulting novel mAbs specific for PD-1, PD-L1 and LAG-3 demonstrated to be able to recognize the ICs either expressed on activated lymphocytes or as purified recombinant proteins with binding affinities in the low nanomolar range (0.1–0.4 nM). Additionally, *in vitro* functional studies showed that these novel mAbs efficiently stimulate T cell proliferation, promoting secretion of IL-2 and IFNγ and T cell activation in co-cultures with TNBC cells [**117-119**].

Another strategy useful for obtaining cross-reactive mAbs specific for ICs and suitable for *in vivo* studies in mouse models consisted in parallel selections on human and mouse recombinant proteins, as previous\sly described [**120**]. In particular, these selections were performed on CTLA-4 by using human and mouse proteins in parallel and by identifying the common sequences enriched in both the selections. The newly-generated anti-CTLA-4 mAbs exhibited high-affinity for both purified proteins and ICs expressed on

lymphocytes from both species, and were able to activate human and mouse PBMCs, with significant increase of IL-2 and IFNγ secretion [**119, 120**].

This approach proved to be efficient in order to obtain a repertoire of novel antibodies for therapeutic and diagnostic applications: for instance, antibodies against immune checkpoints such as PD-1 and PD-L1 are already employed not only for therapy but also for diagnostic purposes to evaluate the expression of these proteins in tumor tissues, to predict eventual therapeutic responses to immunotherapy [**121**].

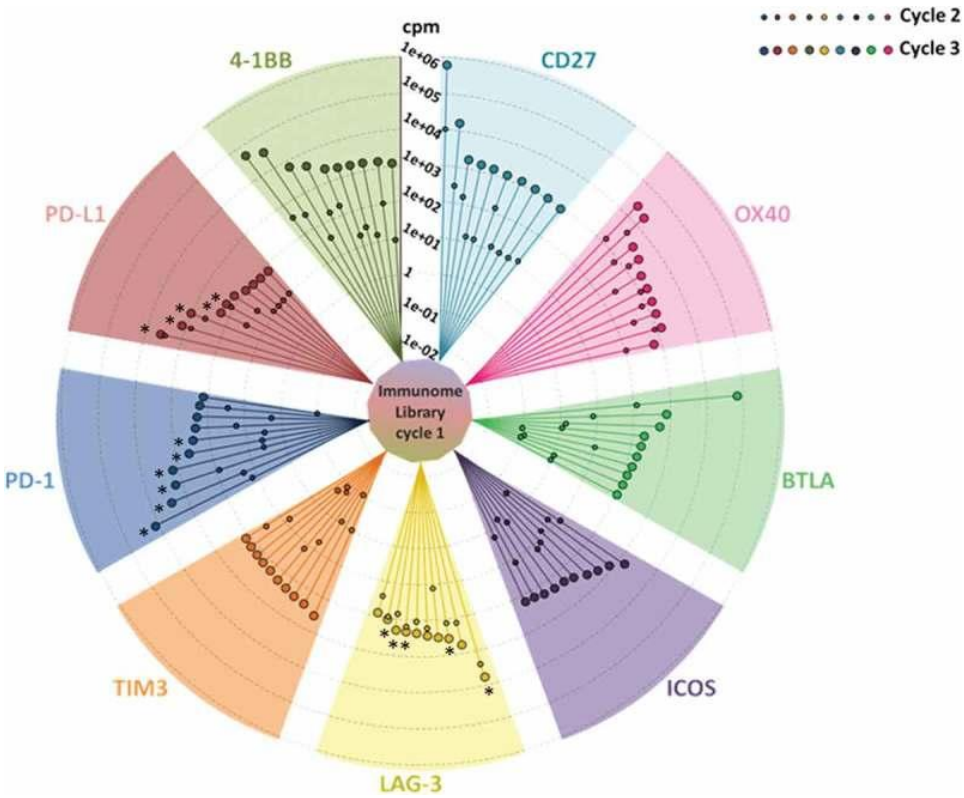

Figure 13. Immunome screening. Enrichment of the top 10 scFv clones for each immune checkpoint after selection on activated hPBMCs (cycle 1) and recombinant proteins (cycles 2 and 3) [**103**].

In order to expand the repertoire of immune checkpoint inhibitors, in this project we generated novel fully human anti-OX40 monoclonal antibodies from the most enriched scFv sequences and characterized their biological properties.

1.2.2 Antibodies Targeting the Coagulation Cascade

The Coagulation System and Anticoagulant Therapeutic Approaches

Cardiovascular pathologies represent the primary cause of global mortality, with one-third of all registered annual deaths worldwide. There is a wide spectrum of etiological factors, both genetic and environmental, which ultimately lead to a shared downstream clinic manifestation: the development of thrombotic events [**122, 123**]. Thrombosis is a medical condition in which the dysregulated formation of blood clots (thrombus) causes the occlusion of blood vessels.

The equilibrium of the haemostatic system is based on a fine balance between procoagulant and anticoagulant factors, enabling effective response to bleeding while preventing pathological thrombus formation. Disruptions of this equilibrium lead to either thromboembolic events or haemorrhagic complications, respectively. Several mechanisms can contribute to these clinical outcomes, classified into three fundamental categories referred to as "Virchow's triad": hypercoagulability, stasis of blood flow and endothelial injury [**124**]. Given that blood hypercoagulability significantly contributes to thrombogenesis, understanding and controlling the coagulation cascade is crucial to diagnose and prevent thrombotic events [**125, 126**].

The coagulation process is a complex biochemical cascade comprising intrinsic, extrinsic, and common pathways, involving the activation of different factors, as shown schematically in **Figure 14**.

The intrinsic pathway is triggered by exposed subendothelial collagen and involves Factors XII, XI, IX, VIII, X, and II (prothrombin). The extrinsic pathway instead is activated by tissue factor (Factor III) released at the site of injury, which forms a complex with Factor VIIa to directly activate Factor X. Both pathways converge in the common pathway involving the activation of Factor X to Xa.

In the common pathway, Factor Xa and Factor V, in presence of calcium and phospholipid assemble into a complex, the prothrombinase complex, on platelets surface. Factor V, also called proaccelerin, is a cofactor which significantly accelerates the conversion of prothrombin to thrombin induced by Factor Xa. Thrombin then cleaves fibrinogen (Factor I) into fibrin monomers which polymerize to finally form the fibrin clot [**127**].

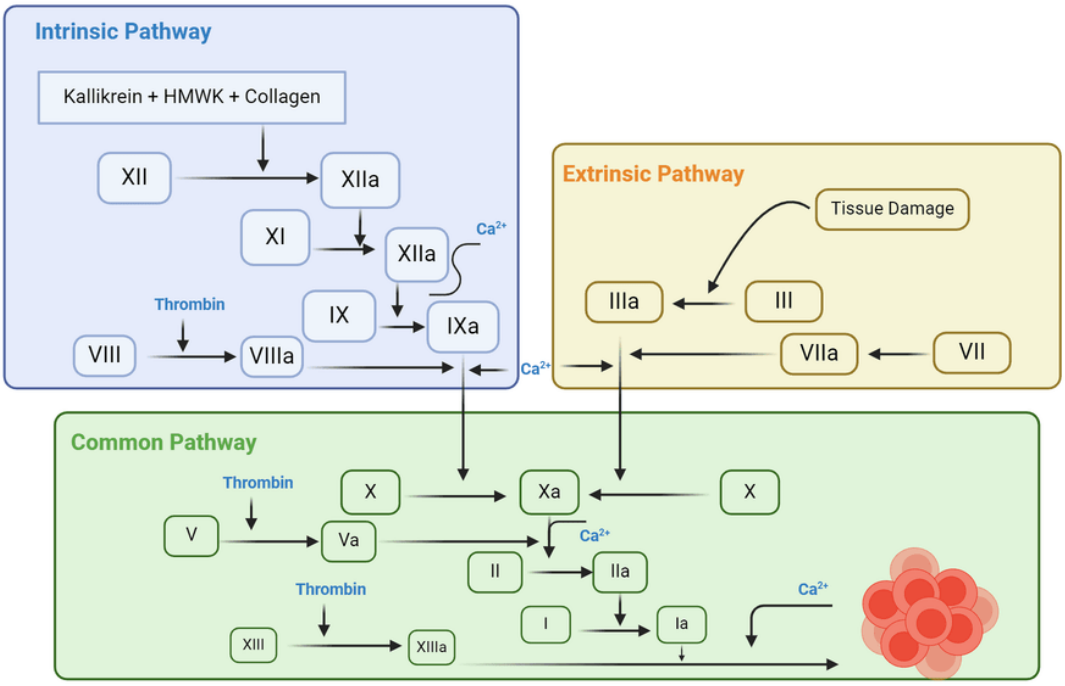

Figure 14. Coagulation cascade. The coagulation process comprises the intrinsic and extrinsic pathways which converge, in the common pathway, on the activation of Factor X, key step that drives the conversion of prothrombin into thrombin. Thrombin, in turn, cleaves fibrinogen to fibrin, ultimately leading to clot stabilization. [Image adapted from *assaygenie.com*]

For decades, the therapeutic landscape of anticoagulants was dominated by unfractionated heparin (UFH) (nowadays replaced by low-molecular-weight heparins) and vitamin K antagonists (VKAs), such as warfarin [**128**]. Despite their efficacy, both classes of drugs present important limitations: UFH exerts its anticoagulant activity by inactivating thrombin and factor Xa, however it is associated with unpredictable pharmacokinetics, and the risk of heparin-induced thrombocytopenia (HIT), an antibody-mediated adverse drug reaction [**129**]. The introduction of low-molecular-weight heparins (LMWHs), such as enoxaparin and dalteparin, improved therapies by offering more predictable pharmacodynamics and a longer half-life, reduced need for monitoring and lower risk of HIT; nevertheless, it still carries risks of HIT and long-term administration remains problematic [**130**].

VKAs, such as warfarin and acenocoumarol, are the most frequently prescribed oral anticoagulants. They inhibit vitamin K epoxide reductase, thus impairing the synthesis of the vitamin K–dependent clotting factors (FII, FVII, FIX, and FX). Limits of VKAs are still represented by delayed onset of action, response variability due to genetic factors, food and drug interactions [**131**].

To overcome these limitations, over the last two decades, attention has shifted towards the development of direct oral anticoagulants (DOACs), which specifically target individual factors in the coagulation cascade and received FDA approval in 2010. For instance, Dabigatran directly inhibits thrombin, Edoxaban and Apixaban exert their action blocking Factor Xa, thus allowing for a much faster anticoagulation effect (within 0.5–4 h) [**131**]. DOACs have a more predictable pharmacokinetic and pharmacodynamic and fewer food and drug interactions. Nonetheless, their use does not lack risks: although lower than VKAs, major bleeding remains the most common adverse effect, particularly in the elderly and in those patients with comorbidities [**132**]. Considering the persistent risk of bleeding, current research is increasingly directed at developing targeted and safer anticoagulant agents.

Aptamers have been investigated as potential anticoagulant agents because they can recognize target proteins with high affinity and specificity lacking immunogenicity. Several candidates directed against coagulation factors reached clinical evaluation with encouraging results. However, none of these aptamers has been approved for clinical use due to limitations related to their short half-life and fast renal clearance [**133, 134**].

The generation of novel human monoclonal antibodies, characterized by a higher MW (~155 kDa), improved stability, and binding specificity, offers the potential to target coagulation factors with minimal or absent off-target effects and cross-reactivity with other proteins in the coagulation cascade, as well as to prolong the half-life of therapeutic agents in circulation.

In recent years, some monoclonal antibodies targeting coagulation factors have been developed and tested in clinical trials. For instance, Abelacimab (MAA868) is a fully human monoclonal antibody which binds to the catalytic domain of Factor XI locking it in a zymogen conformation and preventing its activation by Factor XIIa or thrombin [**135**], Osocimab (BAY 1213790) is another fully human IgG1 that targets Factor XIa, by preventing amplification of thrombin generation through the intrinsic pathway [**136**]. The first has shown promising results in Phase 2 clinical trial, whereas the second was investigated in the FOXTROT phase II trial by Weitz et al., demonstrating efficacy in preventing venous thromboembolism and showing better safety than low-molecular-weight heparins [**135**, **136**].

Factor V as a Potential Therapeutic Target

In this context, attention could be extended to targets within the common pathway, such as Factor V which plays a key role in the prothrombinase complex.

Factor V (FV) is a 330 kDa single-chain plasma glycoprotein produced mainly in the liver as an inactive precursor and is activated to mature Factor Va (FVa) through proteolysis by thrombin. FV structure contains multiple domains (A1, A2, A3, C1, C2) and a large activation peptide (B domain) [**Figure 15**]. The A1 domain (residues 1-316) is linked to the A2 domain (residues 317-709) through a short, basic amino acid segment (residues 304-316). An acidic segment (residues 657-709) connects the A2 domain to the large B domain (residues 710-1545), whose principal role is to maintain Factor V in an inactive form. The B domain is followed by the A3 domain (residues 1546-1877), which in turn is connected to the C1 (residues 1878-2036) and C2 (residues 2037-2196) domains.

Structural analysis, solved by Ruben et al., by using X-ray crystallography reveals a beta-barrel structure with three protruding loops that are thought to contribute to its ability to bind to negatively charged phospholipid membranes [**137, 138**].

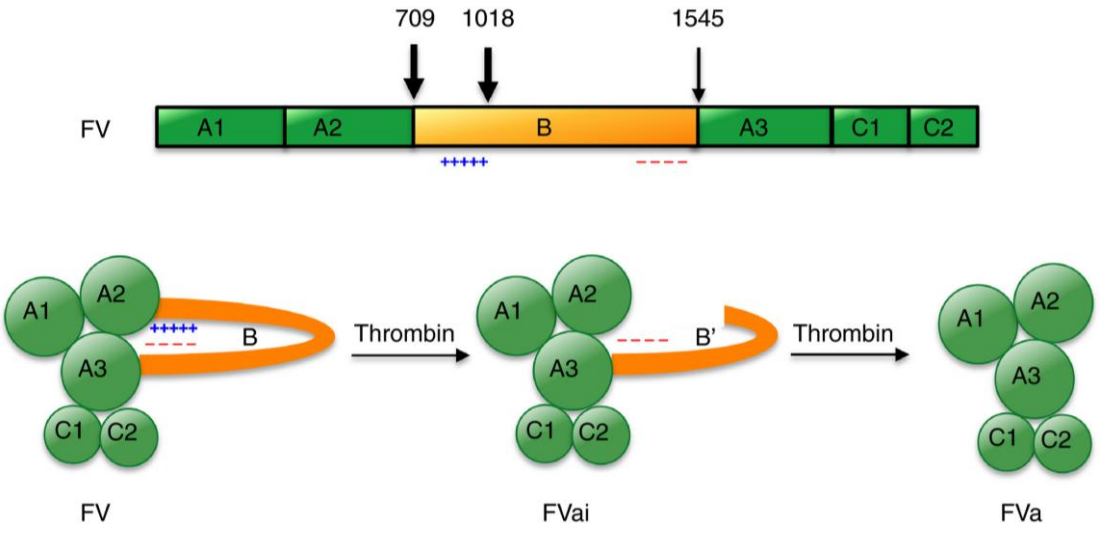

Figure 15. Schematical structure of FV and its activation to FVa. Factor V (FV) circulates as an inactive procofactor. Thrombin cleaves FV at Arg709, Arg1018, and Arg1545, releasing the B domain and generating activated Factor V (FVa). The process occurs in the following steps: cleavage at Arg709 and Arg1018 produces an intermediate (FVai) with partial procoagulant and anticoagulant activity, whereas cleavage at Arg1545 completes activation, yielding full procoagulant FVa [**141**].

FV is converted in FVa by thrombin following cleavage at R709, R1018, and R1545 sites and release of the entire B domain. Complete deletion of the B domain results in separation of the protein into an A1–A2 heavy chain (~105 kDa) and an A3–C1–C2 light chain (~74 kDa), which associate through calcium-dependent noncovalent interactions to form a heterodimer [**138**].

To prevent excessive thrombin formation, Factor Va is downregulated through proteolytic inactivation by Protein C, as negative feedback control. Activated protein C (APC), with protein S as a cofactor, first cleaves at Arg506 in the A2 domain. Complete inactivation is achieved after other cleavages at Arg306 (A1 domain) and Arg679 (C-terminal region of A2). Additionally, Factor V has also an anticoagulant function when partially cleaved by activated Protein C as it accelerates the inactivation of Factor VIIIa, inhibiting thrombin generation. These mechanisms highlight the critical role of FV in maintaining hemostatic balance [**138**-**140**].

The clinical relevance of the Arg506 cleavage site is highlighted by the Factor V Leiden mutation, the most common inherited venous thrombosis risk factor. This G1691A substitution in the F5 gene creates an Arg506Gln mutation that prevents APC cleavage, resulting in increased APC resistance and thrombotic predisposition. [**137, 139**].

To date, only a few molecules specifically targeting Factor V have been developed and are in preclinical stages, such as, HA2 which is an anti-FV monoclonal antibody that binds to the C-terminal end of FV heavy chain and blocks cleavage at Arg709, thus inhibiting FV activation [**141**].

We focused on the development of a novel human anti-FV monoclonal antibody with the aim of obtaining not only an effective anticoagulant drug, with a favorable pharmacokinetics and reduced immunogenicity, but also a diagnostic and research tool to be used for evaluating FV levels in human blood samples to detect its deficit in haemorrhagic patients, or for FV purification by immunoaffinity techniques [**143**].

2. MATERIALS AND METHODS

2.1 Antibodies and recombinant proteins

The following commercial antibodies were used:
anti–PD-L1 mAb (G&P Biosciences, Santa Clara, CA, USA), anti–CTLA-4 and anti–LAG-3 mAbs (R&D Systems, Minneapolis, MN, USA), CD134/OX40 polyclonal antibody (Proteintech, Rosemont, IL, USA), anti–Factor V mAb (Invitrogen, Thermo Fisher Scientific, Rockford, IL, USA), anti–actin antibody (Sigma-Aldrich, Darmstadt, Germany), HRP-conjugated anti–human IgG (H+L) from Promega (Madison, WI, USA), HRP-conjugated anti–human IgG $(Fab')_2$ from Abcam (Cambridge, UK), HRP-conjugated anti–human IgG (Fc-specific) and anti–mouse IgG (Sigma-Aldrich), HRP-conjugated anti–His-tag mAb (Proteintech), HRP-conjugated anti–M13 mAb (Cytiva, Wilmington, DE, USA), HRP-conjugated anti–c-Myc antibody (Miltenyi Biotec, Bergisch Gladbach, Germany), HRP-conjugated goat anti–mouse IgG (Sigma-Aldrich), and goat anti–rabbit IgG (H+L) (Invitrogen, Thermo Fisher Scientific).

ID-1 (anti-CTLA-4), PD-L1_1 (anti-PD-L1) and LAG-3_1 (anti-LAG-3) mAbs were produced and purified as previously described [**117, 118, 120**]. Tb535H tribody was prepared as previously described [**102**].

The clinically validated antibodies used are listed below:
Anti-PD-1 Pembrolizumab (Merck Sharp & Dohme B.V., Haarlem, The Netherlands), anti-LAG-3 Relatlimab (Bristol-Myers Squibb, Princeton, NJ, USA), anti-CTLA-4 Ipilimumab (Bristol-Myers Squibb) and anti-PD-L1 Atezolizumab (InvivoGen, San Diego, CA, USA) mAbs.

The following recombinant proteins were used:
recombinant human LAG-3/Fc, PD-L1/Fc, PD-1/Fc and human IgG1/Fc proteins (all from R&D Systems); recombinant human LAG-3/His-GST and Human HLA class II histocompatibility antigen, DRA (from Cusabio Technology LLC, Houston, TX, USA); recombinant human OX40/TNFRSF4/Fc chimeric protein (Acro Biosystems, Newark, NJ, USA); recombinant human OX40/TNFRSF4 His-tagged protein (R&D Systems); native human coagulation factor V (FV; Creative Biomart, Shirley, NY, USA) and activated factor Va (FVa; Invitrogen, Thermo Fisher Scientific).

2.2 Bacterial strains, culture media and antibiotics

E.Coli TG1 and *E.Coli* SF110 bacterial strains (ATCC) were used for the production of phages and expression of the scFvs as soluble proteins, respectively.

Bacterial cultures were maintained in YT medium (PanReac, AppliChem, Darmstadt, Germany), supplemented with 1% D-(+)-glucose (Sigma-Aldrich). The antibiotics used were Ampicillin (100 μg/ml) and Kanamycin (25 μg/ml) both from AppliChem (Darmstadt, Germany).

2.3 Eukaryotic cell lines and culture conditions

The following eukaryotic cell lines were used:

MDA-MB-231 (human triple negative breast cancer) and HEK293T (human embryonic kidney) cells were maintained in Dulbecco's Modified Eagle's Medium (DMEM; Gibco, Life Technologies, Paisley, UK). BT-549 (human triple negative breast cancer) and Li-7 (human hepatocellular carcinoma) cells were cultured in Roswell Park Memorial Institute 1640 medium (RPMI 1640; Gibco). A-549 (human lung carcinoma) cells were cultured in Kaighn's Modification of Ham's F-12 medium (F-12K; Gibco). HuT-78 (human cutaneous T-cell lymphoma) cells were maintained in Iscove's Modified Dulbecco's Medium (IMDM; HiMedia Laboratories GmbH, Modautal, Germany). Human fetal cardiac (HFC) myocytes were cultured in Cardiac Myocyte Medium (CMM; Innoprot, Derio, Spain).

All cell lines were grown in a humidified incubator at 37 °C with 5% CO_2. Culture media were supplemented with 10% heat-inactivated fetal bovine serum (FBS; Sigma-Aldrich, St. Louis, MO, USA), 2 mM L-glutamine, 50 U/mL penicillin, and 50 μg/mL streptomycin (all from Gibco, Life Technologies).

2.4 Isolation of Human Peripheral Blood Mononuclear Cells

Human peripheral blood mononuclear cells (hPBMCs) were isolated from healthy donor blood by using Greiner Leucosep® tubes (Sigma-Aldrich, St. Louis, MO, USA), following the manufacturer's instructions. Cells were cryopreserved in 90% fetal bovine serum (FBS) and 10% dimethyl sulfoxide (DMSO).

For use, cryopreserved vials were gently thawed out in RPMI 1640 medium supplemented with 1% L-glutamine, 1% CTL Wash™ (Immunospot, Cellular Technology Limited, Cleveland, OH, USA), and 100 U/mL Benzonase (Merck Millipore, Darmstadt, Germany), followed by washing using centrifugation. Recovered hPBMCs were incubated overnight at 37°C in R10 medium, consisting of RPMI 1640 supplemented with 10% heat-inactivated FBS, 1% L-glutamine, 50 U/mL penicillin, 50 μg/mL streptomycin, and 1% HEPES (all from Gibco, Thermo Fisher Scientific).

After overnight resting, hPBMCs were collected, washed in phosphate-buffered saline (PBS), counted using the Muse Cell Analyzer (Merck Millipore, Darmstadt, Germany), and resuspended in the appropriate volume of medium.

2.5 Selection of scFv-phage clones

Phagemid particles were rescued from *E. coli* TG1 cells transformed with the scFvs library through superinfection with M13-K07 helper phage (Invitrogen, Rockford, IL, USA), following previously established protocols [**117**]. Phage particles were subsequently purified by two consecutive rounds of precipitation with ice-cold 20% PEG (Thermo Fisher Scientific) in 2.5 M NaCl, and the resulting phage pellets were resuspended in PBS, centrifuged and stored at 4 °C until further use.

The first round of biopanning was performed by incubating the phages with recombinant human Factor V (20 μg/mL) on Nunc polypropylene tubes for 2 h at 4 °C under gentle rotation. After extensive washes with PBS, bound phages were eluted by using 76 mM citric acid in PBS (pH 2.5) for 5 min and immediately neutralized with 1 M Tris-HCl (pH 8.0). Recovered clones were amplified by infecting *E. coli* TG1 and then subjected to two additional cycles of selection, performed in parallel on immobilized human Factor V and activated Factor Va (20 μg/mL). After the final round, eluted phage pools were collected and stored at 4 °C for downstream use.

2.6 scFv-phages preparation for screening and sequence analysis of positive clones

Eluted phages were used to infect *E. coli* TG1 cells, which were then plated on YT/agar supplemented with 1% glucose and 100 μg/mL ampicillin. Clones colonies were individually picked and transferred in 96-well plates in YT medium supplemented with 1% glucose and ampicillin and cultured for 18 h at 37 °C with gentle shaking. The scFv-phages were produced after superinfection with M13-K07 helper phage for 1 h at 37 °C. Following centrifugation at 1200 rpm for 30 min at 4 °C to pellet the bacteria, 50 μL of supernatants containing phages were collected and screened by ELISA.

Positive clones selected by ELISA were then grown in YT medium containing 1% glucose and 100 μg/mL ampicillin overnight at 37 °C with gentle agitation. Plasmid DNA was purified using the Wizard® Plus SV Minipreps DNA Purification System (Promega, Madison, WI, USA). To confirm the presence of scFv-encoding cDNAs, plasmids were digested with Nco*I* and Not*I* restriction enzymes (from England Biolabs, Ipswich, MA, USA) and analyzed on 1% agarose gel electrophoresis. Sequencing of scFv inserts was performed by the internal facility at CEINGE (Naples, Italy) by using specific PCR

primers, and sequence data were analyzed with the GENtle software (Magnus Manske, University of Cologne, Germany).

2.7 Soluble scFv expression and partial purification

Plasmids encoding the scFv cDNAs were used to transform competent *E. coli* SF110 cells, which were plated on YT/agar supplemented with 1% glucose and 100 μg/mL ampicillin and incubated overnight at 37 °C. Single colonies were picked up and cultured in YT medium containing ampicillin and glucose under the same conditions until reaching an OD_{600} of 0.8. Cells were collected by centrifugation at 3500 rpm for 15 min and resuspended in glucose-free YT medium. Expression of soluble scFvs was induced with 1 mM isopropyl-β-D-thiogalactopyranoside (IPTG; PanReac, AppliChem, Darmstadt, Germany), and SF110 cultures were incubated overnight at 25 °C with gentle shaking.

Bacterial pellets were collected by centrifugation (3500 rpm, 15 min), and periplasmic extracts were obtained by using B-PER Bacterial Protein Extraction Reagent (Thermo Fisher Scientific, Waltham, MA, USA) with protease inhibitor cocktail (Roche Diagnostics GmbH, Mannheim, Germany), following the manufacturer's instructions. Extracted proteins were analyzed by Western blotting (WB), using HRP-conjugated anti–c-Myc-tag antibody for scFv detection.

2.8 Production and Purification of novel immunoagents

Novel human bi- and tri-specific Tribodies

Tribody constructs were generated as previously described [**102**] in collaboration with Chiome Inc. (Tokyo, Japan) by using the Trisoma platform for expression and purification. The sequences encoding the anti-PD-L1 or anti-LAG-3 Fab and the scFv sequences for PD-1 or LAG-3 included in the novel tribodies had been previously reported [**117**]. For the production of the bi-specific tribodies (TR0102, TR0304, TR0506, TR0708), and tri-specifics (53D, 53L10, 53G, 53P), Expi293 cells were co-transfected with plasmids encoding the heavy and light chains of each construct. Secreted proteins were purified from culture supernatants by immobilized metal ion affinity chromatography (IMAC). Endotoxin levels were measured with a LAL-based assay. Purified tribodies were filtered, aliquoted, and tested for stability before and after storage at −80 °C by using SDS–PAGE and size-exclusion chromatography (SEC).

Novel human Anti-OX-40 mAbs

Plasmid vectors encoding each of the five novel anti–OX40 mAbs were transfected into HEK293–EBNA SINEUP cells plated in 150 mm Corning® tissue-culture treated culture dishes. For transfection a mix of Lipofectamine® 2000 (Invitrogen, Thermo Fisher Scientific) and 10 μg of plasmid DNA at a 2:1 ratio was used. Transfections were carried out in serum-free DMEM high glucose/pyruvate (Gibco), and after 5 h the medium was replaced with chemically defined CHO medium (Gibco) supplemented with 50 U/mL penicillin, 50 μg/mL streptomycin, and 2 mM L-glutamine. Cells were cultured for 10 days at 37 °C, and supernatants were collected and clarified by centrifugation at 2000 × g for 20 min. Antibodies were purified from the culture medium by affinity chromatography by using Protein A HP SpinTrap columns (Cytiva), according to the manufacturer's protocol. Purified antibodies were subsequently analyzed by SDS–PAGE and Coomassie staining. Aliquots were stored at either 4 °C or −80 °C. To evaluate stability after one month under these storage conditions, the novel mAbs were analyzed in parallel by Western blotting and by ELISA assays, as described below, at two concentrations (10 and 100 nM) on immobilized OX40/Fc recombinant protein (5 μg/mL).

Novel human Anti-FV mAb

The novel anti-FV mAb, named D9, was generated by cloning the cDNAs encoding the variable regions of the light and heavy chain of the scFv into the Not*I*/Xho*I* sites of the pcDNA3.4 vector (Invitrogen). The variable regions were respectively fused with the regions encoding the constant domain of human λ chain, or human IgG1 heavy chain. Thus, the corresponding light or heavy chain expression plasmids were generated. CHO cells were maintained in DMEM (Gibco) supplemented with 10% FBS, 100 μg/mL penicillin and 100 μg/mL streptomycin, and 1 mM L-glutamine, and transiently transfected by using the calcium phosphate method. Briefly, equal amounts of each plasmid were mixed with calcium chloride and phosphate buffer, and the resulting mixture was added to the cells. After overnight incubation, the medium was replaced with serum-free medium (Opti-MEM, Gibco) and maintained for an additional 48 h. Conditioned medium was then collected, and secreted antibodies were purified by affinity chromatography on protein G–Sepharose FPLC columns.

2.9 Enzyme-Linked Immunosorbent Assays (ELISA)

ELISA assays were performed to evaluate the binding of the immunoagents to recombinant proteins to the targets expressed on the cell surface, or in order to detect ICs expression levels on cell surface.

For protein-based ELISA assays, 96-well Nunc plates were coated for 48 h with the recombinant targets (5 µg/mL) at 4°C. The indicated immunoagents were added in triplicates and incubated for 1h 30 min at room temperature. After washes, bound molecules were detected by using either HRP-conjugated anti-Fab antibody (for mAbs and tribodies) or HRP-conjugated anti-c-Myc antibody (for scFvs), followed by incubation with 3,3',5,5'-tetramethylbenzidine (TMB; Sigma-Aldrich). The reaction was stopped with 1 N HCl, and absorbance was measured at 450 nm with Envision plate reader (PerkinElmer, San Diego, CA, USA).

For cell-based ELISA assays, cells were seeded in triplicate into round-bottom 96-well plates (2×10^5 cells/well), blocked with PBS/BSA 6% for 20 min, and then incubated with immunoagents in PBS/BSA 3% for 1h 30 min at room temperature under gentle agitation. After washing, the appropriate HRP-conjugated secondary antibody was added for 1 h, and detection was carried out with TMB substrate as described above.

To induce the expression of ICs on the cell surface, lymphocytes were pre-activated with either Staphylococcal enterotoxin B (SEB) from Sigma-Aldrich (Darmstadt, Germany) used at the concentration of 50 ng/mL for 24–96 h, or with Dynabeads Human T-Activator CD3/CD28 (Gibco, Life Technologies, Paisley, UK) for 72 h prior to the assay.

Binding data were analyzed by using GraphPad Prism software (GraphPad, San Diego, CA, USA). Binding curves were fitted according to a nonlinear regression model $Y=Bmax \times X/(Kd+X)+NS \times X+Background$, and K_D were derived from the fitted curves.

2.10 Biolayer Interferometry (BLI) Analyses

Binding kinetics of the mAbs and tribodies were performed on the Octet® R4 Protein Analysis System (Sartorius, Fremont, CA, USA) by using Protein A or HIS1K biosensors. Prior to use, biosensor tips were hydrated for 15 min in 200 µL of kinetic buffer (PBS 1X with 0.1% BSA and 0.02% Tween-20). Assay steps were programmed with Octet® BLI Discovery Software 13.0. Sensors were first loaded with Fc-tagged or His-tagged recombinant human immune checkpoint proteins (2 µg/mL) for up to 500 s, followed by a washing step. Association kinetics were then tested by exposing the loaded

sensors to serial dilutions of analytes (novel or clinically validated mAbs and tribodies, as specified in the Results) for 600 s, while dissociation was performed in kinetic buffer for 200 s.

Epitope binning assays were performed by BLI in tandem assays. After ligand immobilization and washing, sensors were saturated with Atezolizumab, Pembrolizumab, or Relatlimab at a concentration of 200 nM for 600 s. Subsequently, TR0304 or TR0506 tribodies were added at increasing concentrations (50, 100, and 200 nM) for 600 s. At the end of the assays, biosensors were regenerated according to the manufacturer's guidelines. Data acquisition and analyses were carried out using Octet® Analysis Studio Software 13.0.

2.11 Cytotoxicity Assays by LDH Detection

To test the cytotoxic activity of the indicated immunoagents, tumor cells were plated in 96-well flat-bottom plates: MDA-MB-231 (1×10^4), BT-549, A-549 and Li-7 (1.5×10^4) and HFC (2×10^4) cells/well. Effector immune cells were then added at effector:target ratios of 3:1 or 5:1, and co-cultures were treated with the indicated immunoagents, either alone or in combination, as specified in the Results section. Co-cultures were incubated for 48 h at 37 °C, after which supernatants were collected. In parallel assays untreated cells or those incubated with an unrelated isotype antibody were used as negative controls. Cell lysis was quantified by measuring lactate dehydrogenase (LDH) release using a commercial LDH detection kit (Thermo Fisher Scientific, Rockford, IL, USA), according to the manufacturer's instructions. The percentage of specific lysis was calculated relative to maximal lysis (positive control) obtained by incubating the cells with 10% Triton X-100.

2.12 Cell Viability by MTT Assays

To test the effects of novel immunomodulatory mAbs on cell viability, cancer cells were plated in 96-well flat-bottom plates (5×10^3 cells/well) and then, incubated for 72 h with anti-IC mAbs or their combinations. Untreated cells or those treated with an unrelated IgG were used as negative controls. Following treatment, the medium was replaced with fresh medium containing MTT substrate at a final concentration of 0.5 mg/mL and incubated for 4 h at 37 °C, until intracellular purple formazan crystals became evident. The medium was then discarded, and crystals were solubilized with DMSO for

30 min with the same incubation conditions. Absorbance was measured at 570 nm, and cell viability was expressed as the percentage of viable cells relative to untreated controls.

2.13 Cytokine Secretion Assays

To evaluate the effects of the immunoagents on immune cell activation, hPBMCs were seeded at a density of 1×10^6 in 96-well plates, after stimulation with SEB (Sigma-Aldrich, St. Louis, MO, USA) for 66 h. In case of co-cultures of hPBMCs with tumor or cardiac cells, lymphocytes were added at a specific density, on the base of the E:T ratio indicated above, in the absence or presence of the immunoagents or an unrelated antibody used as a negative control. After incubation, supernatants were collected and analyzed for measuring the secretion of cytokines. The levels of IL-2, IFNγ, granzyme B (with R&D Systems kit), IL-1β, IL-6, TNF-α, IL-4, IL-23, IL-17a, IL-12, IL-18 (with Sigma Aldrich kit) were quantified by using ELISA assays, according to the manufacturer's instructions. Concentrations were calculated from standard curves generated with corresponding human recombinant cytokines provided by the kits, and the results were expressed as pg/mL, or pg/L, reported as the mean of at least three independent determinations.

For the detection of NLRP-3 (inflammasome), after the indicated treatments, HFC cells were collected and lysed in a buffer containing 1 mM EDTA, 20 mM NaF, 3 mM Na_3VO_4, 100 mM NaCl, 1 mM PMSF, 50 mM Tris-HCl, and a protease inhibitor. Lysates were clarified by centrifugation, and supernatants were analyzed by using an NLRP3 ELISA kit (Aviva Systems Biology, San Diego, CA, USA) according to the manufacturer's instructions.

2.14 *In vivo* anti-tumor efficacy in a mouse model bearing A-549 xenograft

The *in vivo* anti-tumor activity of the novel tribody 53L10 was evaluated in a A-549 xenograft mouse model in collaboration with the Japanese research group of Chiome Bioscience Inc. Human PBMCs were pre-activated for 4 days with Dynabeads Human T-Activator CD3/CD28 (Gibco) before transplantation. On Day 0, A-549 cells were injected subcutaneously into immunodeficient NOD/SCID mice together with an equal number of activated PBMCs. No randomization procedures were applied. From the day of transplantation, animals received intravenous administrations into the tail vein as follows: vehicle control (PBS), 53P (20 μg/mouse), or 53L10 (20 μg/mouse) every other day for six times (Days 0, 2, 4, 6, 8, and 10). In parallel, a separate group received Atezolizumab (200 μg/mouse) three times (Days 0, 4, and 8), either alone or in combination with the bi-

specific control 53P. Tumor volume was measured starting from Day 3 post-transplantation and subsequently measured twice weekly for up to 42 days.

2.15 Western blotting analyses of cell extracts

Tumor cells were plated at an appropriate density and incubated under the indicated culture conditions. Cells were collected and centrifuged at 1200 rpm, pellets were lysed in a buffer containing Tris-HCl (pH 7.4), 0.5% Nonidet-P-40, 150 mM NaCl, 1 mM sodium orthovanadate (Sigma-Aldrich), and a proteases inhibitors cocktail (Roche). After incubation on ice for 20 min, the cell extracts were clarified by centrifugation at 12'000 rpm for 15 min at 4°C. Proteins concentration was determined by a colorimetric Bradford assay by using a Bovine Serum Albumin (BSA) standard curve, to normalize the loading on SDS-PAGE. After the electroblotting, the nitrocellulose membranes were incubated overnight at 4°C with primary antibodies specific for the proteins of interest, followed by the appropriate HRP-conjugated secondary antibodies. Signals were detected by using ChemiDoc Imaging Systems (BioRad) and the intensity of the bands was normalized to vinculin by using Image Lab software 6.0.1.

2.16 Docking Analysis

For the docking analyses, performed in collaboration with the group of Prof. Merlino of Department of Biology, a 1:1 stoichiometry was considered. The crystallographic structure of FV was retrieved from the Protein Data Bank (PDB ID: 7KVE), while the D9 scFv model was generated with SwissModel using the anti-Mcl-1 scFv (PDB ID: 6QB9, 72% sequence identity; doi.org/10.1107/S2059798319014116) as a structural template. Docking simulations were carried out with the pyDockWEB server. Notably, eight of the first ten predictions positioned the D9 scFv in interaction with the A2 domain of FV, particularly with the acidic segment (residues 657–679). The resulting FV/D9 interaction models were then compared with the known structure of the FVa/FXa complex bound to prothrombin. All structural figures were prepared using PyMOL 1.8.

2.17 Effects of D9 on Blood Coagulation

Plasma samples (0.5 mL) were pre-incubated with D9 mAb at increasing concentrations (100 nM–2 μM) for 1 h at room temperature. Clotting function was then evaluated, in collaboration with Dr. Miele of Laboratory of Medicine of Hematology and Hemostasis, from by routine assays, such as activated partial thromboplastin time (aPTT) and prothrombin time (PT), together with extended coagulation tests for individual factors (FII, FV, FVIII, FIX, FX), by using an automated ACL Top 550 coagulometer

(Instrumentation Laboratory Company, Bedford, MA, USA). Factor activities were determined through a modified PTT-based method: the plasma analyzed was diluted and mixed with factor-deficient plasma, and the degree of clotting time correction reflected the relative activity (%) of the factor under analysis. Quantification was obtained by interpolation from calibration curves generated with plasmas of known factor concentrations, prepared using deficient plasma, calibrator plasma, PT- or aPTT-based reagents, calcium chloride, and appropriate buffers.

2.18 Statistical Analyses

All assays were performed in at least three independent experiments, each carried out in triplicates. Data are presented as mean ± SD. For assays involving lymphocytes, hPBMCs from at least three independent donors were used.

Normality of data distribution was evaluated with the Shapiro–Wilk test. Statistical significance between two variables was determined by using Student's *t*-test, while multiple comparisons were analyzed by the Kruskal–Wallis test.
For *in vivo* studies, variation within each group was estimated to be <10%, and statistical significance of tumor size differences was determined by Tukey's multiple comparison test (MEPHAS software, Osaka University, http://www.gen-info.osaka-u.ac.jp/MEPHAS/tukey-e.html).

Statistical significance was defined as follows: $p \leq 0.001$***; $p < 0.01$**; and $p < 0.05$*.

3. RESULTS

3.1 *Comparative analysis of antitumor and cardiotoxic side effects of combinations of novel and clinically validated ICIs*

3.1.1 Analysis of the effects on human lymphocytes of novel immunomodulatory mAbs and their combinations compared to those of clinically validated ICIs

In our laboratory, a panel of fully human monoclonal antibodies was isolated by phage display selection on human lymphocytes to target several immune checkpoints, such as PD-1, PD-L1, CTLA-4, and LAG-3, with the aim of enhancing T cell activation against tumor cells [**117, 118, 120**]. The novel anti-IC antibodies, named PD-1_1 (anti-PD-1), PD-L1_1 (anti-PD-L1), ID-1 (anti-CTLA-4) and LAG-3_1 (anti-LAG-3), already showed in previous studies high binding affinity for their targets and the ability to interfere in the interaction between their targets and their respective natural ligands. Moreover, they showed efficient activation of the immune cells, and stronger anti-tumor effects in co-culture assays of immune cells with tumor cells when compared to their corresponding clinically validated mAbs targeting the same ICs [**117, 118-120**].

On the basis of these promising results, during my PhD project, I further evaluated their therapeutic potential, by testing them in combinations to identify those with stronger anti-tumor effects and lower cardiotoxic side effects on cardiomyocytes compared to combinatorial treatments with clinically validated mAbs. To this aim, we firstly tested the novel antibodies PD-L1_1, ID-1, LAG-3_1, for their effects on the activation and proliferation of human lymphocytes in comparison with the commercial Atezolizumab (anti-PD-L1) or Ipilimumab (anti-CTLA-4) mAb at the concentration of 100 nM, by using them as single agents or in combinations. Briefly, hPBMCs were previously stimulated with SEB and after 66h of treatments with the mAbs, the supernatants were collected for measuring the levels of IL-2 and IFNγ secreted by ELISA. Lymphocytes untreated, stimulated with SEB or treated with an unrelated monoclonal antibody were used as negative controls.

As shown in **Figure 16**, the novel anti-CTLA-4 and anti-PD-L1 mAbs, either alone or in combination, induced a stronger activation of hPBMCs compared to the clinically approved counterparts. In particular, the combinations of ID-1 and PD-L1_1 showed increased levels of IFNγ with respect to Ipilimumab and higher IL-2 secretion than the combination of Ipilimumab and Atezolizumab, reaching levels of about 23,000 pg/mL.

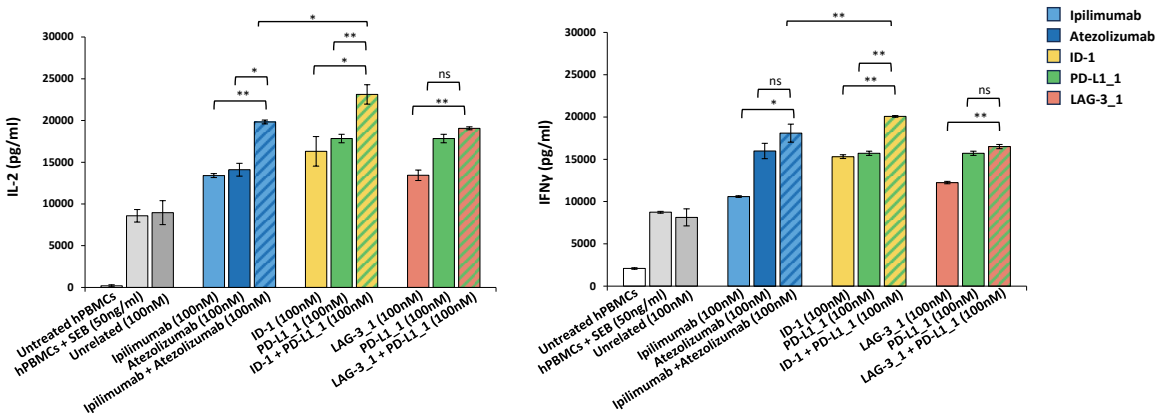

Figure 16. Effects of novel mAbs and their combinations on the activation of stimulated lymphocytes. hPBMCs were stimulated for 66 h with SEB in the absence or presence of anti-CTLA-4, anti-PDL1 or anti-LAG-3 mAbs used alone or in combinations. The levels of IL-2 and IFNγ secreted were measured by ELISA (solid bars indicate single-agent treatments and striped bars the combinations). Untreated hPBMCs or those treated with an unrelated IgG were used as negative controls (white and grey bars, respectively). The values were reported as the mean ± SD of at least three determinations obtained from three independent experiments. Error bars indicate SD. *p*-values were obtained by using the two-tailed Student's *t*-test, and statistical significance is indicated as follows: ns (not significant), ** $p < 0.01$; * $p < 0.05$.

3.1.2 Parallel cytotoxicity assays of the novel ICI combinations on co-cultures of tumor cells or cardiomyocytes with human lymphocytes

In order to evaluate the anti-tumor efficacy of the novel monoclonal antibodies, we tested them, in comparison with clinically validated mAbs, in co-cultures of immune cells with triple negative breast cancer cells, to mimic *in vitro* the *in vivo* tumor microenvironment. Thus, MDA-MB-231 and BT-549 cancer cells were co-cultured with hPBMCs at an effector-to-target ratio of 5:1, and treated for 48 h with either novel or clinically approved anti-CTLA-4 and anti-PD-L1 monoclonal antibodies, used as single agents or in combination. After the treatments, the supernatants were collected and the levels of LDH release were measured, as marker of cytotoxicity. As shown in **Figure 17**, we observed that the novel ID-1 and PD-L1_1 mAbs are able to induce stronger tumor cell lysis than Ipilimumab and Atezolizumab or their combination. In particular, MDA-MB-231 cells, when treated with the novel anti-CTLA-4 (ID-1 mAb) and the novel anti-PD-L1 (PD-L1_1 mAb), showed 91% and 68% of cell lysis, respectively. Notably, the combination of the novel mAbs led to complete tumor cell lysis, reaching 100% compared to 80% observed for the combination of Ipilimumab and Atezolizumab.

To investigate whether the observed tumor cell lysis positively correlated with increased immune cell activation, we also evaluated the levels of IFNγ in the supernatants, by using ELISA assays. The cytokine secretion assays confirmed this hypothesis, showing the highest secretion of IFNγ, marker of T cell activation, following the treatment of ID-1 with PD-L1_1, especially on MDA-MB-231 cells.

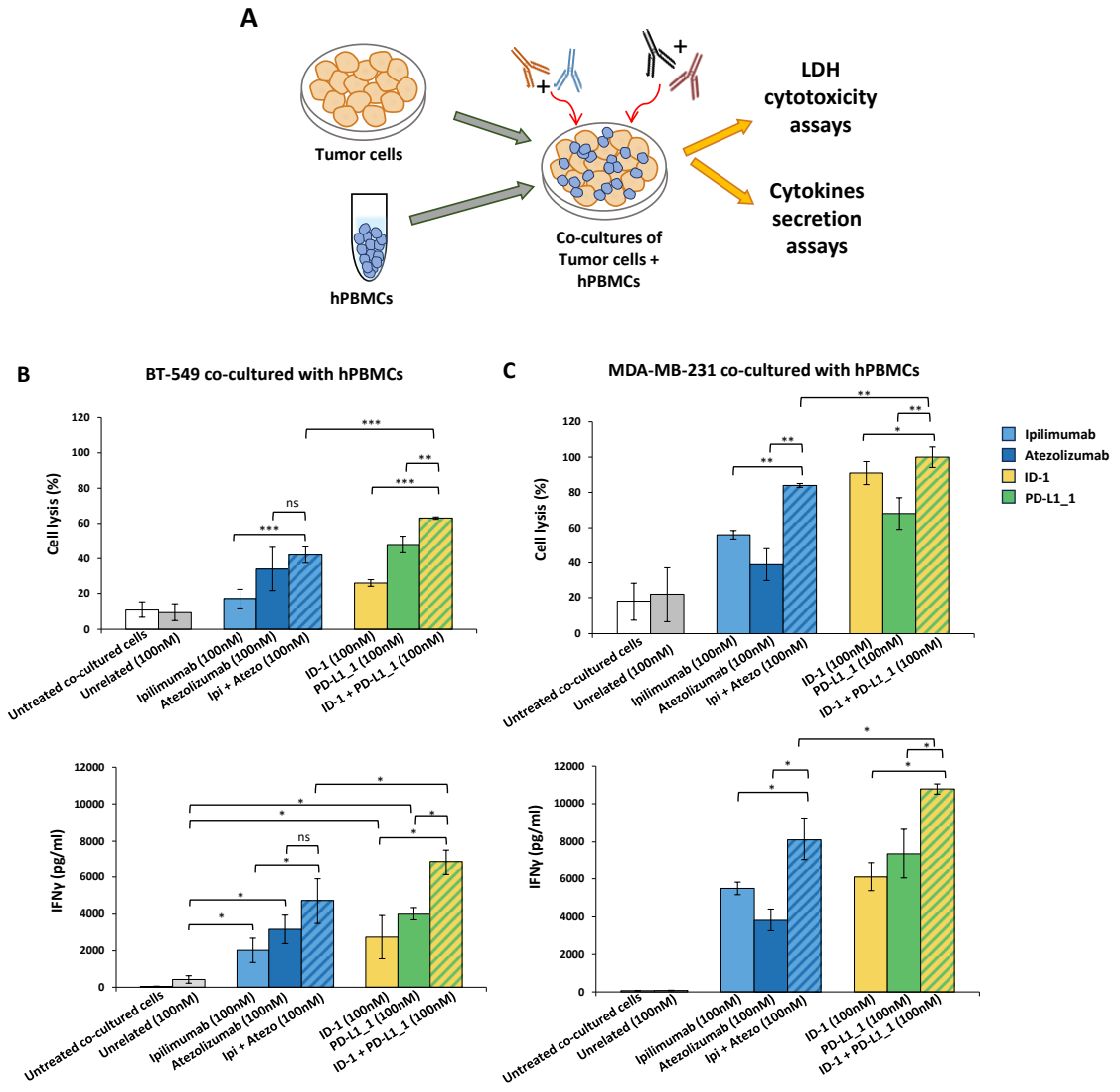

Figure 17. Cytotoxic effects of novel immunomodulatory mAbs on tumor cells co-cultured with hPBMCs. (**A**) Schematical illustration of co-cultures of tumor cells and hPBMCs for early screening of potent combinatorial treatments. BT-549 (**B**) or MDA-MB-231 (**C**) tumor cells were co-cultured with hPBMCs (Effector:Target cells ratio 5:1) and treated for 48 h with anti-CTLA-4 and anti-PD-L1 mAbs or their combination (striped bars) at the indicated concentrations. Co-cultured cells untreated or treated with an unrelated IgG were used as negative controls (white and grey bars, respectively). Cell lysis was measured by detecting LDH release, as described in Materials and Methods. The values were reported as the mean ± SD of at least three determinations obtained from three independent

experiments. Error bars indicate SD. *p*-values were obtained by using the two-tailed Student's *t*-test, and statistical significance is indicated as follows: ns (not significant), ***p <0.001; **p < 0.01; *p < 0.05

Despite the advantages of selectivity and limited side effects of immunomodulatory antibodies in cancer treatment, some cases of myocarditis and pericarditis have been reported, especially in patients undergoing combinatorial treatments with anti-ICs mAbs [**70-74, 143, 144**]. In order to evaluate the eventual cardiotoxic side effects of the novel anti-CTLA-4 and anti-PD-L1 mAbs, we tested them, in a parallel assay, in co-cultures of human cardiomyocytes and immune cells (Effector:Target ratio 5:1) either as single agents or in combination, and compared them to Ipilimumab and Atezolizumab used at the same concentration (100 nM). Untreated co-cultures and those treated with an unrelated antibody were used as negative controls. After 24 h, supernatants were collected and cell lysis was assessed as described in Materials and Methods section, by using LDH Cytotoxicity Assay Kit.

As shown in **Figure 18B**, treatments with PD-L1_1 or ID-1 mAbs, alone or in combination, induced significantly lower cardiac cell lysis (with a maximum of about 50% in the combination) compared to Ipilimumab or Atezolizumab or their combination, which led to 80% of cell lysis. Similar results were observed for IL-6 levels (**Figure 18C**), a proinflammatory cytokine frequently associated with cardiac injury [**144**]. The combination of the novel mAbs showed lower levels of secreted IL-6 compared to those induced by clinically approved ICIs. Moreover, we also evaluated the secretion of granzyme B, a cytokine released by either cytotoxic CD8+ T cells or by Natural Killer cells, by using ELISA assay on the supernatants of the co-cultures. Very low levels were observed in treatments with ID-1, PD-L1_1 or their combination (about 3000 pg/mL of secreted granzyme B) in contrast with the much higher levels (~14.400 pg/mL) detected following treatment with the combination of FDA-approved mAbs (Ipilimumab plus Atezolizumab).

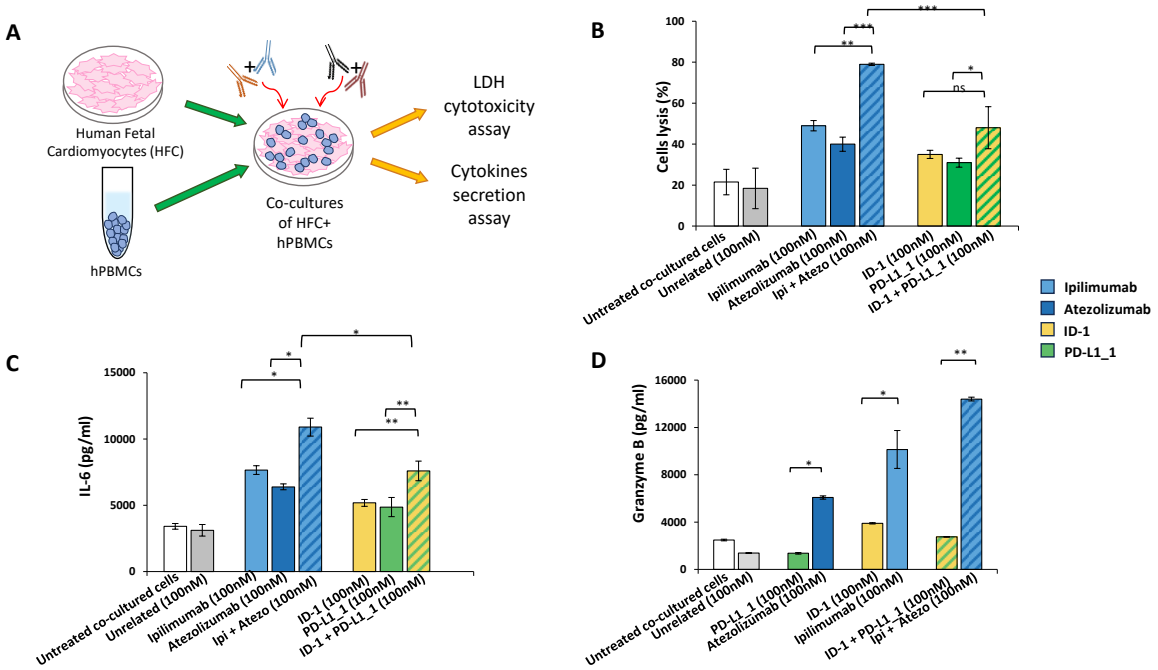

Figure 18. Cardiotoxic and pro-inflammatory effects induced by immunomodulatory mAbs or their combination on human cardiomyocytes. (**A**) Schematical illustration of co-cultures of HFC with hPBMCs, used as a new *in vitro* model for early screening of ICIs-mediated cardiotoxicity. (**B**) Cardiotoxic effects of novel immunomodulatory mAbs were analyzed by evaluating HFC cell lysis in the absence or presence of single mAbs or their combinations (striped bars) for 24 h. (**C**) The pro-inflammatory effects of the indicated mAbs were analyzed by evaluating the secretion of IL-6 in the supernatant of the co-cultures treated with anti-CTLA-4, anti-PD-L1 mAbs, or their combination (striped bars). IL-6 levels are expressed as pg/mL. (**D**) The release of granzyme B was evaluated by detecting its levels in the supernatants of co-cultures treated as mentioned above. As negative controls, cells untreated or treated with an unrelated IgG were used (white and grey bars, respectively). The values were reported as the mean of at least three determinations obtained from three independent experiments. Error bars depict means ± SD. *p*-values were obtained by two-tailed Student's *t*-test, and statistical significance is indicated as: ns (not significant), *** $p \leq 0.001$; ** $p < 0.01$; * $p < 0.05$.

In order to widen the evaluation of the combinations of ICIs by including LAG-3_1, we firstly determined the expression levels of LAG-3 on a panel of different tumor cell lines, including MDA-MB-231, BT-549 (triple-negative breast cancer), A-549 (non-small lung cancer) and HUT-78 (cutaneous T cell lymphoma). As shown in **Figure 19A**, the HUT-78 cell line showed the highest levels of LAG-3 as confirmed by both ELISA and Western Blotting, whereas CTLA-4 and PD-L1 were expressed at higher levels on TNBC cell lines.

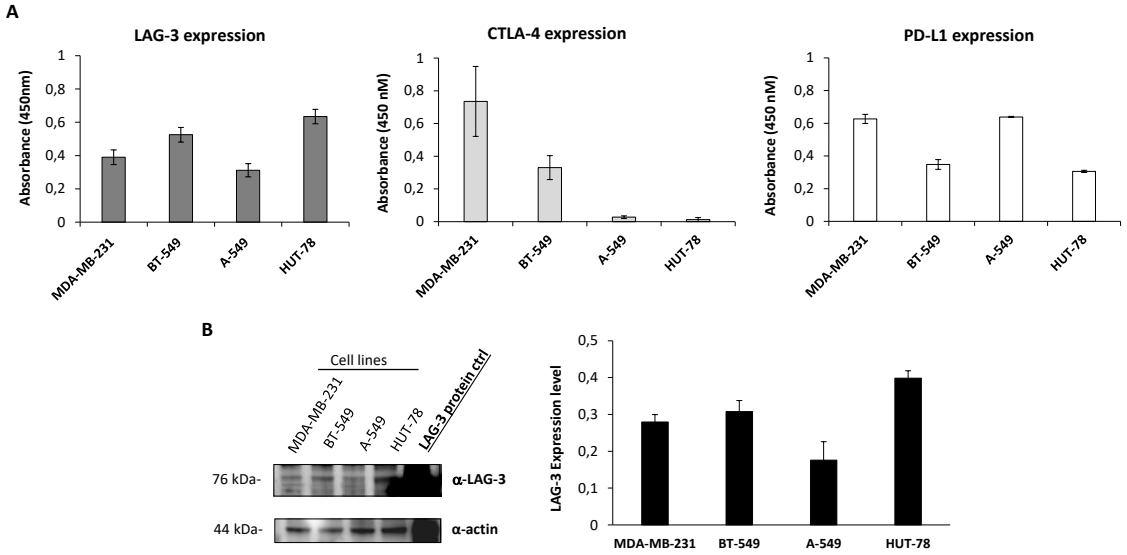

Figure 19. **Expression of PD-L1, PD-1, CTLA-4, and LAG-3 ICs on a panel of cancer cells.** (**A**) Cell ELISA assays were performed on MDA-MB-231, BT-549, A-549, or HuT-78 tumor cells to measure the cell surface expression of the indicated ICs with commercial anti-PD-L1, anti-CTLA-4, or anti-LAG-3 mAbs. Binding values were reported as the mean of at least three determinations obtained in three independent experiments. (**B**) Western blotting analyses of extracts, from MDA-MB-231, BT-549, A-549, and HuT-78 tumor cells, for detecting LAG-3 expression levels were obtained by using the commercial anti-LAG-3 mAb. The intensity of the bands corresponding to ICs was normalized to actin. Error bars depict means ± SD.

Thus, we tested the effects of the novel anti-LAG-3 or anti-PD-L1 mAbs, alone or in combination on the viability of HuT-78 cell line treated for 72h with 100 nM of each drug. MTT assays, carried out to test cell viability, showed that the treatment with LAG-3_1 significantly reduced cell growth, and, more interestingly, its combination with PD-L1_1 induced additive effects reaching about 50% of tumor growth inhibition (**Figure 20A** and **20B)**, compared to the negative controls (untreated cells or treated with an unrelated mAb).

Furthermore, we also investigated on the effects of these two mAbs on co-cultures of HuT-78 and lymphocytes, by evaluating both cell lysis and T cell activation as described above. Tumor cells were plated with hPBMCs at an effector-to-target ratio of 5:1 and treated for 48 h with Atezolizumab, PD-L1_1, LAG-3_1, or their combinations. We found that the combination of LAG-3_1 with the novel PD-L1_1 mAb showed higher efficacy, reaching 48% of cell lysis, compared to that of 38% obtained with combination of LAG-3_1 and Atezolizumab (**Figure 20C**). Accordingly, as indicated by the results of the cytokines assays (**Figure 20D**), the combination involving the novel mAbs also led to higher IFNγ secretion by lymphocytes in the treated co-cultures compared to the

combination including Atezolizumab. Altogether these results show the potential as effective therapeutic tools of the novel human mAbs endowed with improved functional activity compared to currently approved ICIs.

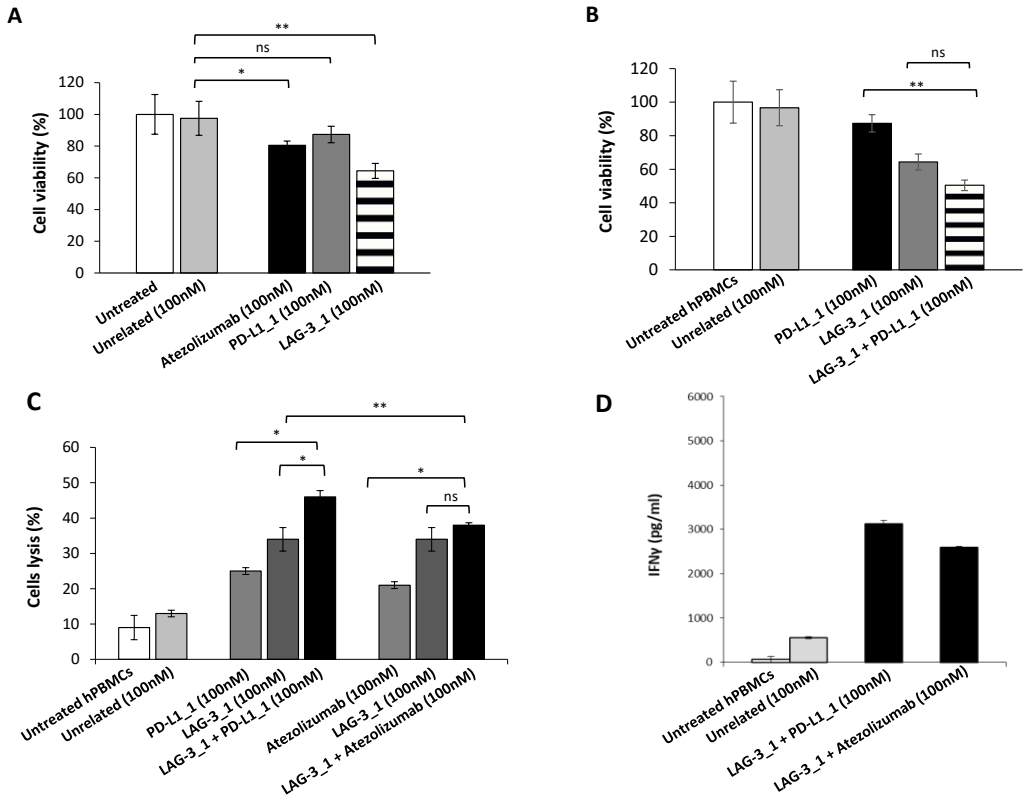

Figure 20. **Effects of novel immunomodulatory mAbs on HUT-78 tumor cells in the absence or in presence of lymphocytes.** (**A, B**) MTT assays were performed on the supernatant of HuT-78 tumor cells, treated for 72 h with anti-PD-L1 or anti-LAG-3 mAbs, used as single agents or in combinatorial treatments. Cell viability is expressed as percentage of viable cells with respect to control untreated ones. Error bars depict means ± SD ** $p < 0.01$; * $p < 0.05$. (**C**) LDH levels were detected in the supernatant of HuT-78 tumor cells co-cultured with hPBMCs (Effector:Target cells ratio 5:1), treated for 48 h with anti-PD-L1 or anti-LAG-3 mAbs, or their combination, at the indicated concentrations. (**D**) Levels of IFNγ secreted by hPBMCs co-cultured with HUT-78 and treated for 48 h with the combination of anti-LAG-3 and anti-PD-L1 mAbs at the indicated concentration. Cells untreated or treated with an unrelated IgG were used as negative controls. The values were reported as the mean of at least three determinations obtained from three independent experiments. Error bars depict means ± SD. *p*-values for the indicated compounds, calculated by using two-tailed Student's *t*-test, are: ** $p < 0.01$; * $p < 0.05$.

3.1.3 *In vitro* full evaluation of cardiotoxic side effects of combinations of clinically validated immune checkpoint inhibitors

During my PhD project, in collaboration with Dr. Maurea's group (Pascale Foundation), we decided to further investigate on the cardiotoxicity of the novel FDA

approved ICIs based on the previous observations [**145-146**]. Indeed, a novel anti-LAG-3 mAb (Relatlimab) has been recently approved (March 2022) by FDA in combination with Nivolumab for melanoma therapy and used in several randomized clinical trials [**65**].

Firstly, we treated co-cultures of HFC and human lymphocytes in the absence or presence of the anti-LAG-3 mAb (Relatlimab), anti-PD-1 (Nivolumab), anti-PD-L1 (Atezolizumab), anti-CTLA-4 (Ipilimumab), each at the concentration of 100 nM, or their combinations as used in clinical trials or approved by FDA. After treatments of 48 h at 37°C, cardiac cell lysis was evaluated by measuring LDH release in the supernatants. As shown in **Figure 21A**, the combinations of Relatlimab plus Nivolumab and that of Atezolizumab plus Ipilimumab resulted in a higher cardiac cell lysis (59% and 43%, respectively) compared to single-agent treatments. To determine whether this increased cytotoxicity was associated with enhanced activation of immune effector cells, we measured granzyme B levels in the supernatants. We found that both combinatorial treatments induced significantly higher secretion of this T-cell activation marker, reaching approximately 10,000 –12,000 pg/mL, compared to single-agent treatments (about 4,000–5,000 pg/mL) for almost all antibodies with the exception of Ipilimumab (**Figure 21B**).

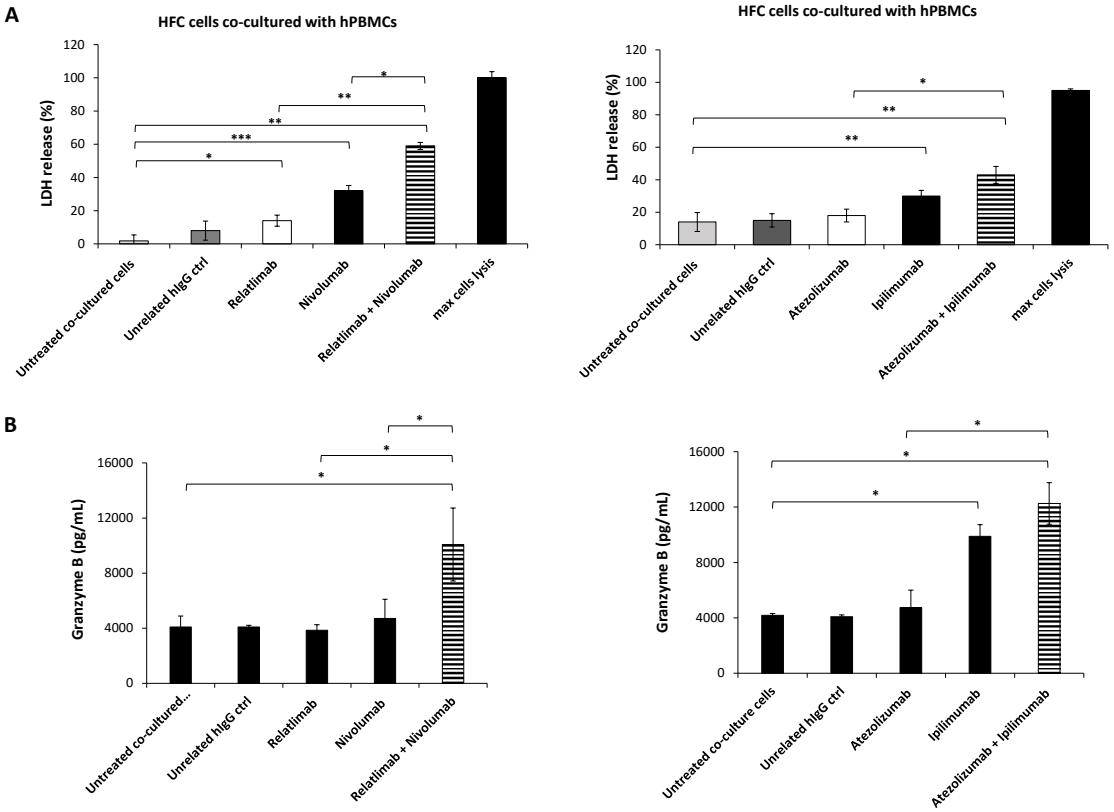

Figure 21. Analysis of cardiac cell lysis and granzyme levels in HFC/hPBMC co-cultures treated with ICIs and their combinations. Co-cultures were treated for 48 h with Relatlimab or Nivolumab (left panels) and with Atezolizumab or Ipilimumab

(right panels), either as single agents or in combination, at a concentration of 100 nM. (**A**) The cytotoxic effects of the mAbs on HFC cells were evaluated by measuring the levels of LDH release in the supernatants. (**B**) The levels of granzyme B were measured in the supernatants of co-cultures by using the ELISA kit from R&D. A human unrelated IgG was used as a negative control. Data represent the mean ± SD of three independent experiments. Statistical significance was calculated by comparing each treatment to untreated co-cultured cells or by comparing combined treatments to single-agent treatments, indicated as ***p <0.001; **p < 0.01; *p < 0.05, by using two-tailed Student's *t*-test.

Since NLRP-3 is a key mediator of inflammatory responses, driving cytokines storm, and implicated in cardiac injury [**145, 147**], we analysed its expression in lysates of human cardiomyocytes co-cultured with hPBMCs and treated as described above. As shown in **Figure 22**, we found that NLRP3 levels were increased in cell lysates following treatment with Atezolizumab, Ipilimumab, especially when they were used in combination (16.6 pg/mL, 17.3 pg/mL and 26.2 pg/mL, respectively). Similar results were obtained with Nivolumab, Relatlimab and their combination (16.4 pg/mL, 17.7 pg/mL, 24.3 pg/mL, respectively).

Furthermore, we evaluated the secretion of a panel of cytokines, including IL-1β, IL-6, TNF-α, IFNγ, L-4, IL-23, IL-17a, IL-12, and IL-18 by using ELISA kits provided by Sigma Aldrich. As reported in **Figure 22**, combinatorial ICIs treatments increased IL-1β, IL-6 levels by approximately ~6–8 fold and TNF-α and IFNγ levels by 5-fold, compared to untreated controls. In addition, other cytokines, including IL-4, IL-23, IL-17a, IL-12, and IL-18, showed a 2–4-fold increase.

Overall, combinatorial treatments of Nivolumab plus Relatlimab or Atezolizumab plus Ipilimumab led to a 1.4 –1.6-fold increase in NLRP-3 expression level and 4 –8-fold increase in pro-inflammatory cytokine release, including IL-1β, IL-6, TNF-α, and IFNγ, when compared to single-agent treatments, highlighting the additive pro-inflammatory potential of combinatorial ICIs regimens.

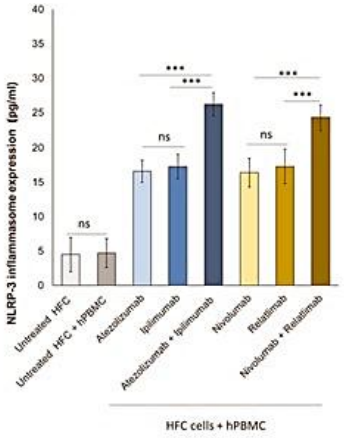
NLRP-3 inflammasome expression (pg/ml)
Untreated HFC
Untreated HFC + hPBMC
Atezolizumab
Ipilimumab
Atezolizumab + Ipilimumab
Nivolumab
Relatlimab
Nivolumab + Relatlimab
HFC cells + hPBMC

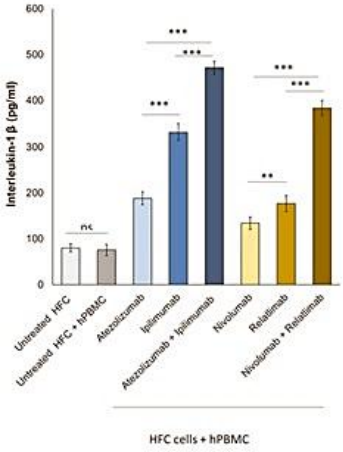
Interleukin-1 β (pg/ml)
HFC cells + hPBMC

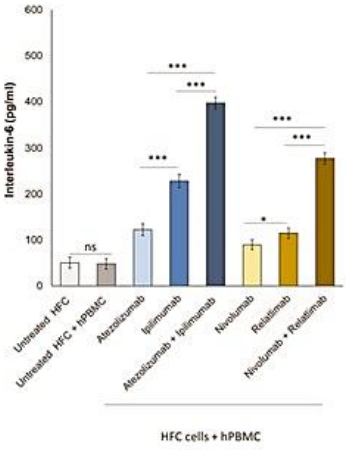
Interleukin-6 (pg/ml)
HFC cells + hPBMC

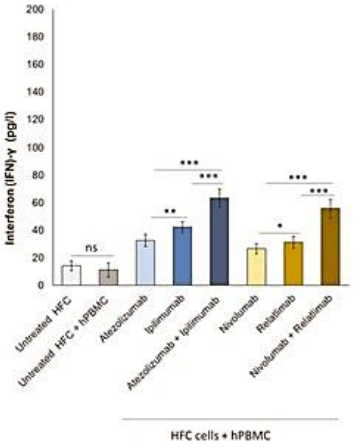
Interferon (IFN)-γ (pg/l)
HFC cells + hPBMC

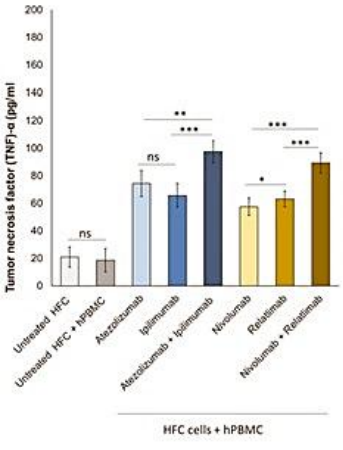
Tumor necrosis factor (TNF)-α (pg/ml
HFC cells + hPBMC

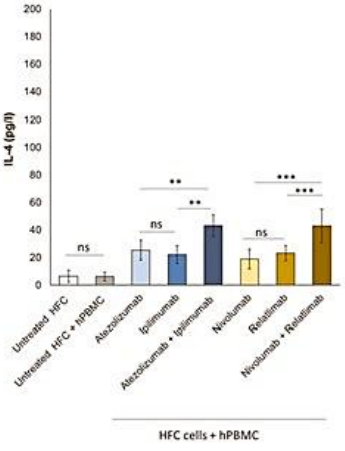
IL-4 (pg/l)
HFC cells + hPBMC

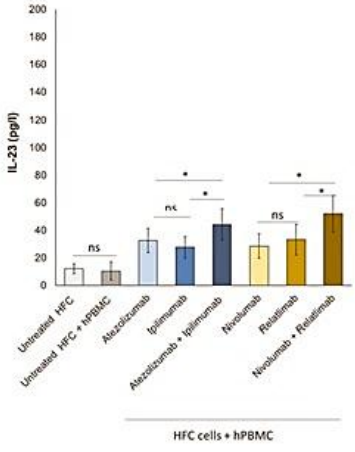
IL-23 (pg/l)
HFC cells + hPBMC

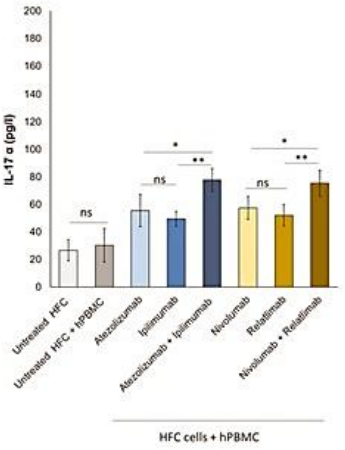
IL-17 α (pg/l)
HFC cells + hPBMC

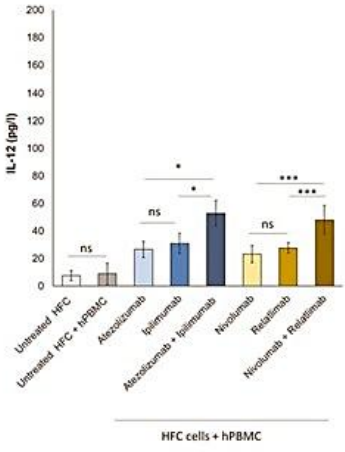
IL-12 (pg/l)
HFC cells + hPBMC

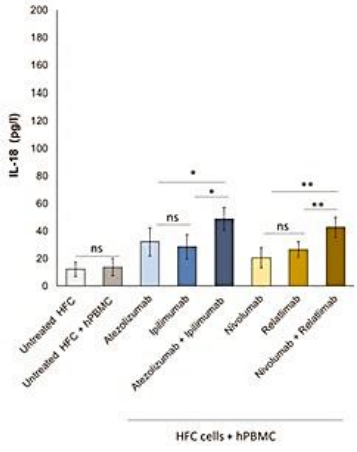
IL-18 (pg/l)
HFC cells + hPBMC

Figure 22. Combinatorial ICIs therapies increase release of several pro-inflammatory cytokines in co-cultures of HFC with hPBMCs. HFC cells were plated with or without hPBMC and treated for 48 h with 100 nM of Atezolizumab, Ipilimumab, Relatlimab or Nivolumab (100nM) and their combinations. NLRP-3 inflammasome expression (in HFC lysate), IL-1β, IL-6, TNF-α, IL-4, IL-23, IL-17a, IL-12, IL-18 and INF-γ release in supernatant (pg/mL) were quantified by using specific ELISA kits, as described in methods. The data represent the mean ±SD of three independent experiments, and significance, calculated by using two-tailed Student's *t*-test, are indicated as ns (not significant), ***$p<0.001$; **$p<0.01$; *$p<0.05$

3.1.4 Identification of effective and safe combinations of anti-LAG-3, anti-PD-1, and anti-PD-L1 antibodies for the generation of multispecific constructs

Based on the previous results, we decided to select the most promising combinations of novel antibodies, generated in our laboratory, endowed with the strongest antitumor activity and the lowest cardiotoxicity. These combinations were tested in parallel on triple-negative breast cancer cells and human fetal cardiomyocytes and compared for their biological effects to corresponding clinical approved monoclonal antibodies and their combinations.

To this aim, co-cultures of MDA-MB-231 or HFC with hPBMCs (effector: target cells ratio 5:1) were treated for 48 h with either newly generated or clinically validated anti-LAG-3, anti-PD-1, and anti-PD-L1 mAbs. In parallel assays we tested also the combinations of the same anti-LAG-3 with the anti-PD-1 or the anti PD-L1 mAbs. After the incubation of 48 h at 37°C, supernatants were collected and LDH release was measured to evaluate cytotoxicity. Untreated co-cultured cells or those treated with an unrelated mAb were used as negative controls, whereas cells treated with the lysis buffer, provided by Cytotoxicity Assay Kit, were used as a positive control. As indicated in **Figure 23A** and **B**, combinations of the newly generated anti-LAG-3 with anti-PD-1 or anti-PD-L1 mAbs achieved 40–45% tumor cell lysis even at a lower dose (66 nM), than that of the combinations of Relatlimab plus Nivolumab or Atezolizumab tested at a concentration of 100 nM. In contrast, the same combinations of novel antibodies, tested at 100 nM induced only 5.6–10% cardiac cell lysis, compared to 59% observed with Relatlimab plus Nivolumab and 76% with Relatlimab plus Atezolizumab, highlighting their improved safety profile while retaining the same or even higher antitumor efficacy (**Figure 23C** and **D**).

These preliminary findings paved the way for the development of multispecific constructs, designed to combine the effects of different anti-ICs monoclonal antibodies into a single molecule, to potentiate their antitumor efficacy and reduce production costs.

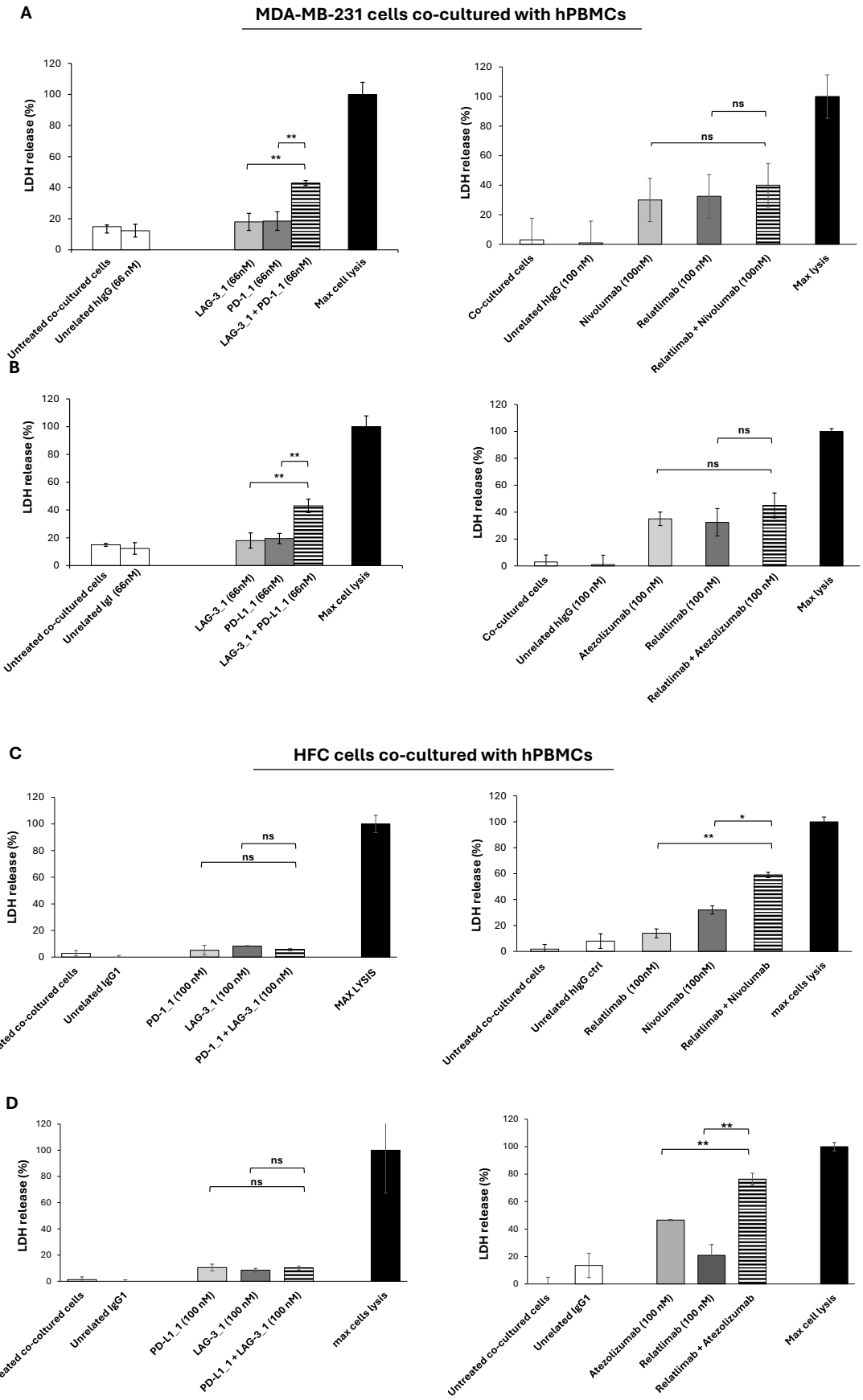

Figure 23. Comparison of cytotoxic effects of novel and clinically validated immunomodulatory mAbs on tumor cells or cardiomyocytes co-cultured with hPBMCs. MDA-MB-231 tumor cells or HFC were co-cultured with hPBMCs

(Effector:Target cells ratio 5:1) and treated for 48 h with either novel or clinically validated anti-PD-L1 or anti-LAG-3 mAb and their combinations (**A**, **C**), with either novel or approved anti-PD-1 or anti-LAG-3 and their combinations (**B**, **D**). Co-cultured cells untreated or treated with an unrelated IgG were used as negative controls (white bars). The values were reported as the mean of at least three determinations obtained in three independent experiments. Error bars mean ± SD. *p*-values were obtained by using two-tailed Student's *t*-test and are indicated as follow: ns (not significant), ** $p < 0.01$; * $p < 0.05$

3.2. *Generation and characterization of novel bi- and tri- specific tribodies*

3.2.1 Construction and purification of novel immunomodulatory bi-specific Tribodies

Considering the promising results of combinatorial treatments based on novel immunomodulatory monoclonal antibodies, we decided to generate four novel different bi-specific immuno-modulatory tribodies in collaboration with the research group of Chiome (Japan) [**86**]. These constructs were engineered by genetically fusing a Fab fragment with two scFv domains derived from different parental anti-LAG-3, anti-PD-1 or anti-PD-L1 antibodies [**117**]. The novel tribodies, with a molecular weight of 100 kDa, called TR0102 and TR0304, were generated by combining binding domains specific for LAG-3 and PD-L1, while those called TR0506 and TR0708 were designed to combine the binding moieties specific for PD-1 and LAG-3 within a single construct (**Figure 24A**).

The novel constructs were expressed by transfecting Expi293 cells with vectors containing the cDNAs encoding heavy and light chains of Fab fused to each scFv sequence, as shown in **Figure 24B**. The tribodies were purified from the conditioned media by IMAC affinity chromatography on Nickel-resin. Their purity was analyzed by SDS-PAGE, and by size-exclusion chromatography (SEC) analyses we evaluated protein aggregation and/or stability after purification and long-term storage (**Figure 24C** and **D**). As shown by both analyses, the constructs were free of contaminants as well as they did not show high molecular weight aggregates.

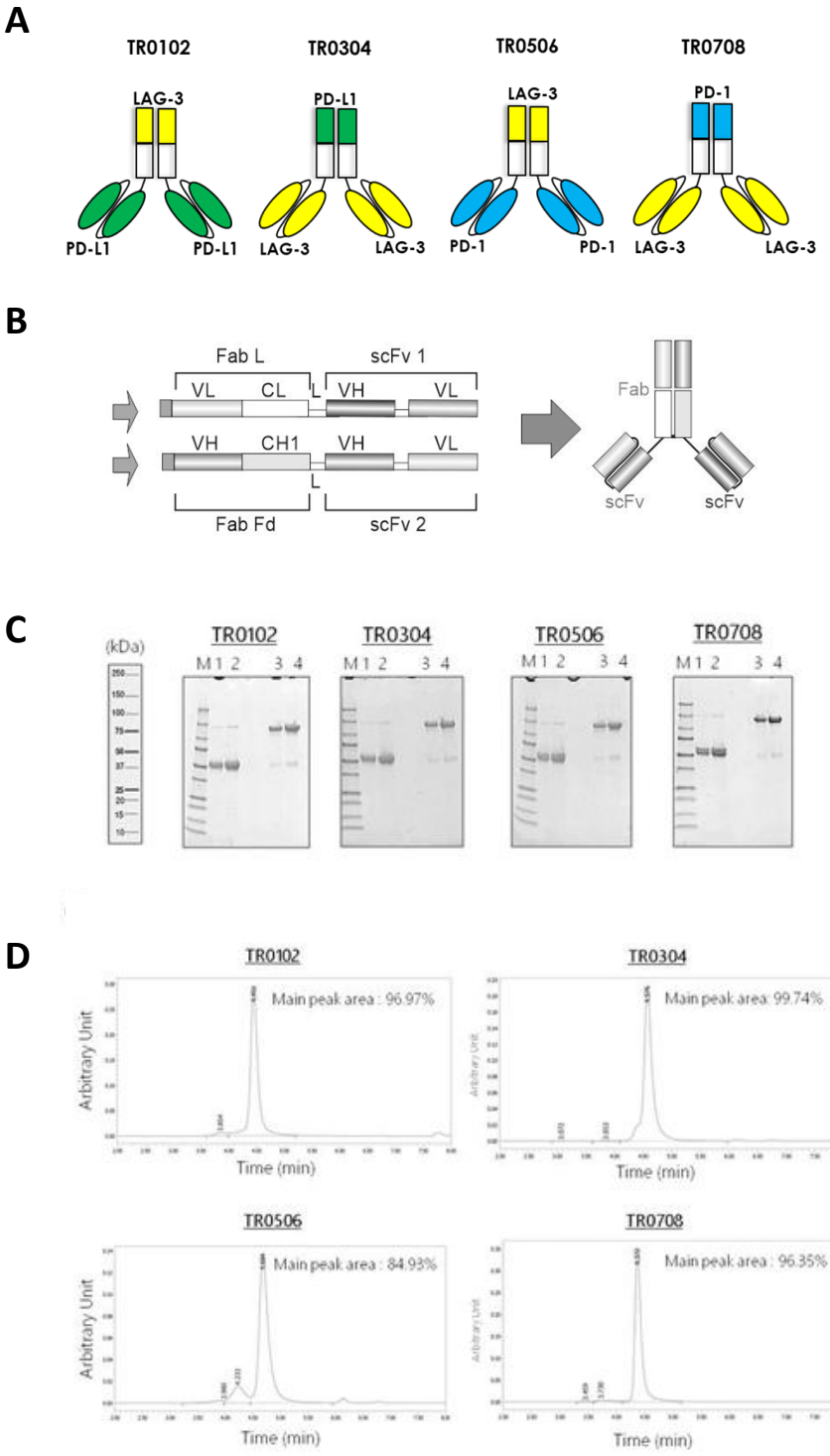

Figure 24. Schematical representation and purification of bi-specific tribodies derived from LAG-3_1, PD-L1_1 and PD-1_1 parental mAbs. (**A**) Structure of the four novel immunomodulatory tribodies TR0304, TR0506, TR0607, TR0708. (**B**) Each TR was obtained by genetically fusing the indicated Fab with two identical scFvs derived from a different anti-IC mAb. (**C**) Analysis of purity of the tribodies by SDS-PAGE of His-tagged Tribodies under reducing (lanes 1 and 2) or non-reducing conditions (lanes 3 and 4) obtained after purification by Ni-affinity chromatography. (**D**) SEC analyses of the final products to confirm the purity.

3.2.2 Binding of the novel bi-specific tribodies to their targets

Once purified, the novel bi-specific tribodies were evaluated for their ability to bind by ELISA assays to recombinant human PD-1/Fc and PD-L1/Fc proteins and to activated lymphocytes expressing immune checkpoints in their native conformation. All the novel tribodies showed high affinity for purified PD-L1 and PD-1 proteins (**Figure 25A** and **B**), with K_D values in the sub-nanomolar range, and efficiently bound to activated lymphocytes with K_D values in the low nanomolar range, as reported in **Figure 25C** and **Table 1** therein.

To verify the LAG-3 binding specificity of the tribodies, we analyzed their binding to HuT78 cells, which expresses high levels of LAG-3, but low or undetectable levels of PD-1 and PD-L1. We tested all the novel tribodies at increasing concentrations (1 – 100 nM), in comparison with the LAG-3_1 parental mAb, by using cell-based ELISA. We found that the tribodies TR0304 and TR0506 bound to the cells with a comparable or even better specificity than LAG-3_1, thus retaining LAG-3 binding even in the tribody format (**Figure 25D**).

Furthermore, to assess the ability of the novel tribodies to interfere in the interactions of immune checkpoints with their natural ligands, competitive ELISA assays were performed. The binding of biotinylated MHCII (HLA-DRA) or PD-L1 ligand to immobilized LAG-3 or PD-1 receptor, respectively, was measured in the absence or presence of a molar excess of tribodies (3:1 M/M excess ratio for anti-LAG-3 and 5:1 M/M for anti-PD-L1 mAbs). Nivolumab, PD-L1_1 and PD-1_1 or LAG-3_1 parental mAbs were used in parallel assays as positive controls for the interference of PD-1/PD-L1 interaction or LAG-3/MHCII (HLA-DRA) interactions, respectively. As indicated in **Figure 25 E** and **F**, both TR0304 and TR0506 inhibited LAG-3/MHCII binding, and all tribodies, TR0102, TR0304, TR0506 and TR0708, efficiently blocked the PD-1/PD-L1 interaction, thus retaining the antagonistic properties of the parental antibodies.

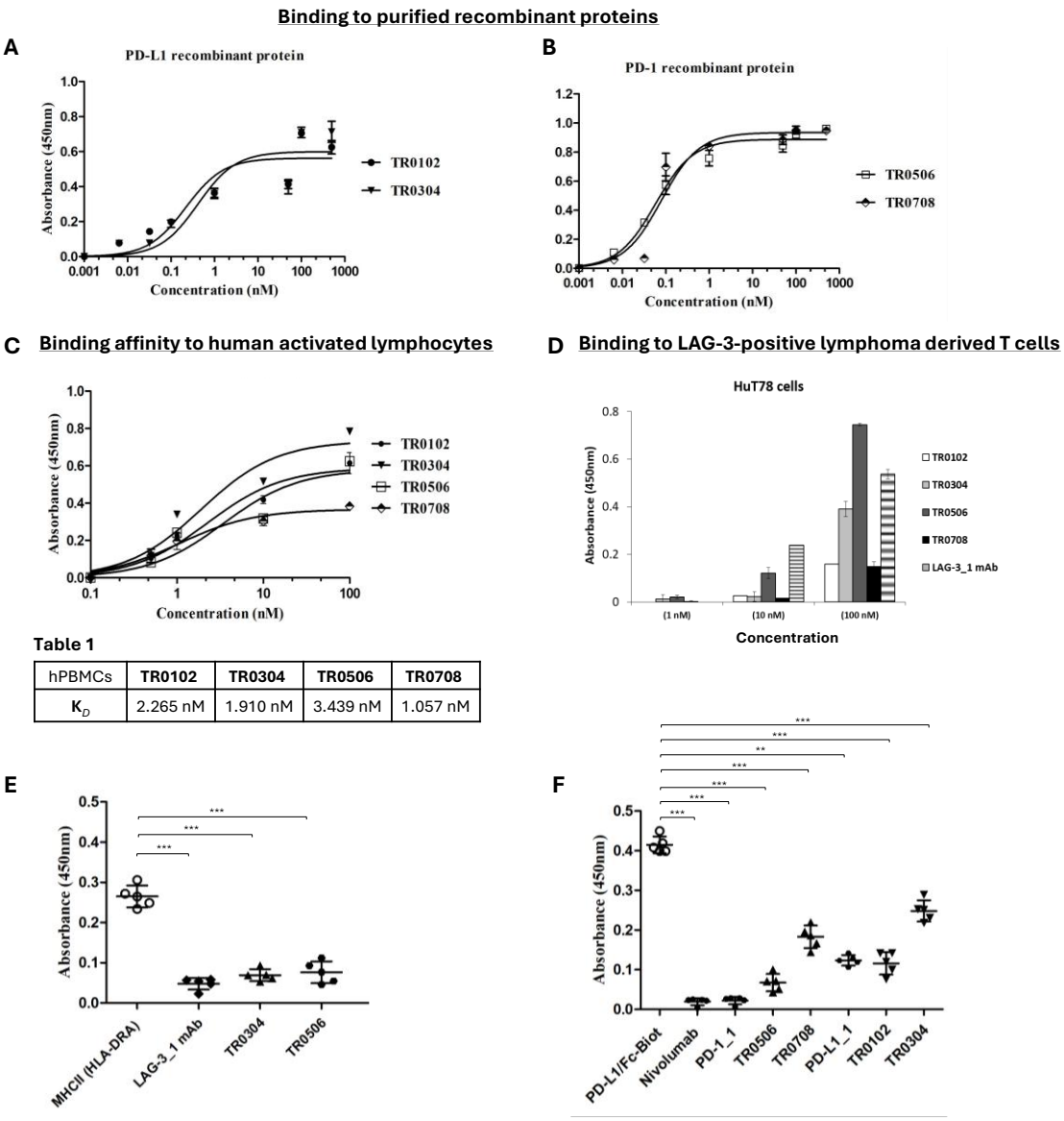

Table 1

hPBMCs	TR0102	TR0304	TR0506	TR0708
K_D	2.265 nM	1.910 nM	3.439 nM	1.057 nM

Figure 25. Binding of newly generated tribodies to their targets and their effects on ligand recognition. (**A**, **B**) Binding curves of the tribodies (0.001–1000 nM) onto immobilized rhPD-L1, rhPD-1 purified proteins. (**C**) Binding affinity of the selected tribodies for activated human PBMCs by using cell ELISA at increasing concentrations (0.1–100 nM). (**D**) Evaluation of binding to HuT78 cells by using cell ELISA. (**E**, **F**) Competitive ELISA assays to assess the ability of the tribodies to interfere in LAG-3/MHCII (HLA-DRA) and PD-1/PD-L1 interactions by measuring the binding of biotinylated MHCII or PD-L1 to immobilized LAG-3 or PD-1, respectively, in the absence or presence of tribodies (3:1 and 5:1 M/M ratios).
Data represent mean absorbance values ± SD from at least three independent experiments performed in triplicate. *p*-values were obtained by using two-tailed Student's *t*-test and are indicated as follow: *** $p < 0.001$; ** $p < 0.01$.
Table 1. Binding affinity values of novel bi-specific tribodies on activated hPBMCs. Binding curves and K_D values were obtained by using GraphPad Prism software.

Based on the higher specificity for LAG-3 observed with TR0304 and TR0506, we selected these two tribodies for further studies and for a comparative analysis with FDA-approved antibodies targeting LAG-3 (Relatlimab), PD-L1 (Atezolizumab), and PD-1 (Pembrolizumab) [**148**].

We first compared the binding to human lymphocytes stimulated with anti-CD-3/CD-28 beads for 72h at 37°C. The tribodies or the mAbs were incubated at increasing concentrations (0.01–100 nM) for 1h at RT and then detected with appropriate secondary mAbs, indicated in the Methods. As reported in **Figure 26**, TR0304 and TR0506 showed binding affinities in a sub- or low nanomolar range, comparable or even better than those of clinically validated mAbs.

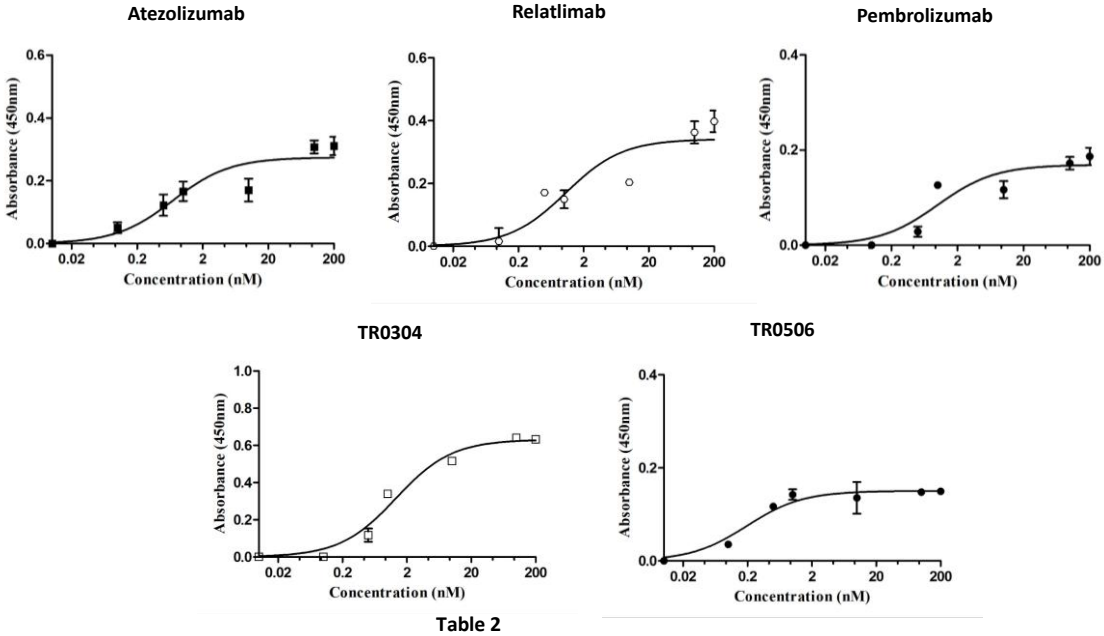

Table 2

mAb	KD (nM)
Atezolizumab	0.7
Relatlimab	1
Pembrolizumab	1
TR0304	1.3
TR0506	0.2

Figure 26. Binding to activated human lymphocytes of bi-specific TR0304 and TR0506, compared to clinically validated monoclonal antibodies. Cell ELISAs to test the binding at increasing concentrations of the indicated TRs, in comparison with validated antibodies, to their targets expressed on lymphocytes activated with anti-CD-3/CD-28 beads. Data are shown as mean of absorbance values ± SD obtained from at least three determinations of three independent experiments.

Table 2. K_D values of novel bi-specific tribodies and FDA-approved mAbs on activated hPBMCs. Binding curves and K_D values were acquired by using GraphPad Prism software.

The binding kinetics of the tribodies TR0304 and TR0506 were further analyzed in comparison with clinically approved monoclonal antibodies by using Biolayer Interferometry (BLI), a label-free method for testing real-time molecular interactions. To this aim, recombinant human LAG-3/Fc, PD-L1/Fc, and PD-1/Fc chimeric proteins were immobilized on Protein A biosensors as ligands for 500s. The tribodies or validated monoclonal antibodies were added as analytes at increasing concentrations (0.2–100 nM) and monitored for their association and dissociation rates. We chose to immobilize the recombinant target proteins on the biosensors, rather than the antibodies, to better mimic *in vivo* conditions, where circulating bivalent antibodies bind to targets displayed on the surface of cells.

Since TR0304 contains a Fab fragment derived from an anti-PD-L1 antibody and two scFvs targeting LAG-3, it was tested on immobilized recombinant immune checkpoints LAG-3 (**Figure 27**) or PD-L1 (**Figure 28**) in comparison with the validated Relatlimab or Atezolizumab, respectively. TR0506, made up of a Fab derived from the same anti-LAG-3 parental mAb and two scFvs derived from an anti-PD-1 mAb, was instead analyzed for binding to immobilized LAG-3 (**Figure 27**) or PD-1 (**Figure 29**) proteins in comparison with Relatlimab or the validated anti-PD-1 Pembrolizumab, respectively.

As indicated in the **Tables A** and **B**, TR0304 was able to bind to both its targets with K_D values comparable to those of the clinically approved mAbs. On the other hand, TR0506 showed high affinity for PD-1 and lower affinity for LAG-3 when compared to Relatlimab (**Tables A** and **C**). This result is consistent with the structural features of the constructs, considering that TR0304 is bivalent, containing two scFvs which recognize LAG-3, whereas TR0506 is monovalent for LAG-3, having only one Fab arm specific for it, compared to the bivalent Relatlimab.

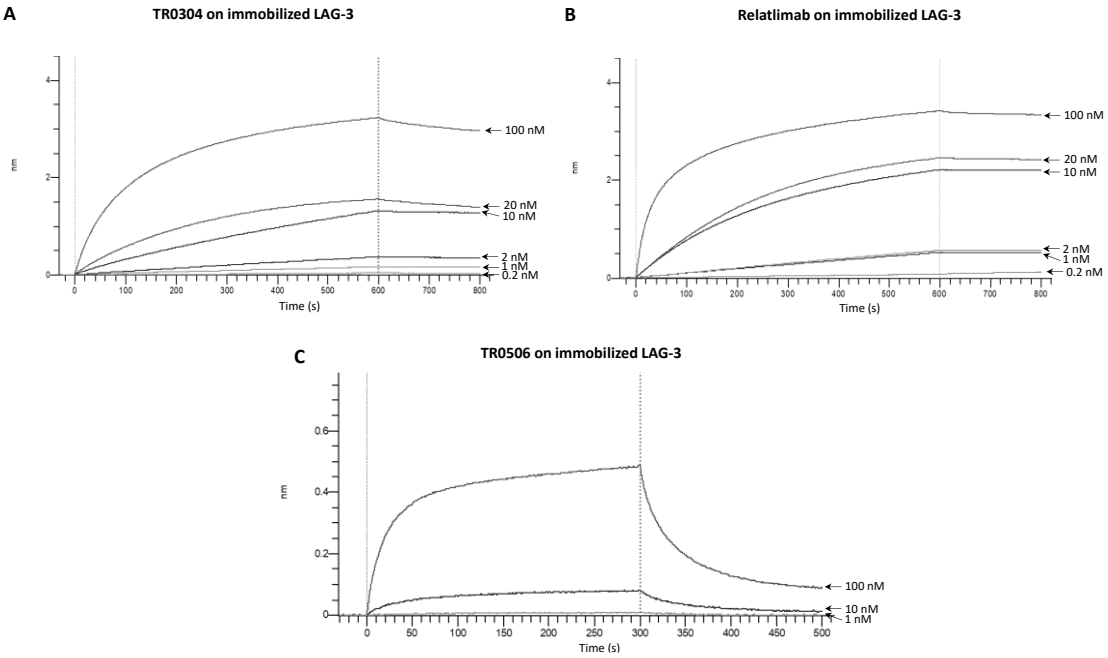

Table A

	KD (M)	ka (1/Ms)	ka Error	kd (1/s)	kd Error
TR0304	4.8×10^{-9}	1.43×10^{5}	8.8×10^{4}	3.35×10^{-4}	1.98×10^{-4}
Relatlimab	1.85×10^{-9}	4.49×10^{4}	2.13×10^{2}	4.25×10^{-2}	3.27×10^{-1}
TR0506	6×10^{-7}	1.9×10^{5}	8.38×10^{4}	9.24×10^{-3}	8.6×10^{-5}

Figure 27. Comparison of the binding kinetics of TR0304 and TR0506 bi-specifics and the anti-LAG-3 Relatlimab. The sensorgrams, obtained by BLI analyses, show the association and dissociation phases of TR0304 (**A**) and TR0506 (**C**), tested at increasing concentrations (0.2–100 nM) and compared with Relatlimab (**B**) on Fc-tagged LAG-3, immobilized on ProA biosensor. In **Table A** are shown K_D, association (ka) and dissociation (kd) rate constants. All the analyses were carried out by using Octet Analysis Studio 13.0 Software.

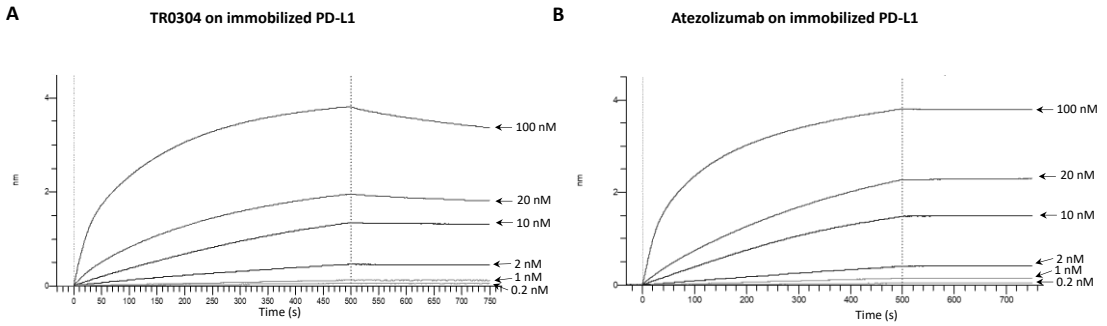

Table B

	KD (M)	ka (1/Ms)	ka Error	kd (1/s)	kd Error
TR0304	9.71×10^{-10}	1.19×10^{6}	1.9×10^{4}	1.75×10^{-4}	4.57×10^{-6}
Atezolizumab	1.24×10^{-10}	7.78×10^{4}	3.7×10^{4}	1.55×10^{-5}	2.31×10^{-7}

Figure 28. Comparison of the binding kinetics of the bi-specific TR0304 and the anti-PD-L1 Atezolizumab. The sensorgrams, obtained by BLI analyses, show the association and dissociation phases of TR0304 (panel **A**), tested at increasing

concentrations (0.2–100 nM) and compared to Atezolizumab (panel **B**), on Fc-tagged PD-L1, immobilized on ProA biosensor. In **Table B** are shown K_D, association (ka) and dissociation (kd) rate constants. All the analyses were carried out by using Octet Analysis Studio 13.0 Software.

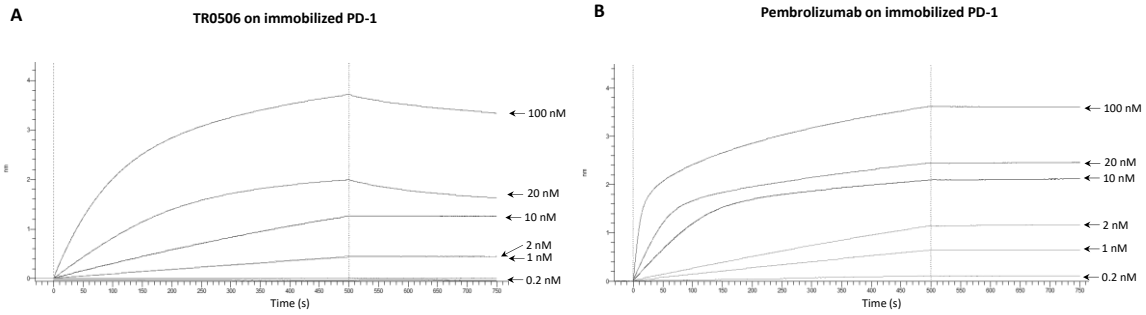

Table C

	KD (M)	ka (1/Ms)	ka Error	kd (1/s)	kd Error
TR0506	2.27×10^{-8}	9.97×10^{4}	1.66×10^{3}	5.35×10^{-4}	1.82×10^{-5}
Pembrolizumab	2.39×10^{-10}	4.82×10^{5}	1.32×10^{6}	8.95×10^{-5}	8.33×10^{-8}

Figure 29. Comparison of the binding kinetics of the bi-specific TR0506 and the anti-PD-1 Pembrolizumab. The sensorgrams, obtained by BLI analyses, show the association and dissociation phases of TR0506 (panel **A**), tested at increasing concentrations (0.2–100 nM) and compared to Pembrolizumab (panel **B**), on Fc-tagged PD-L1, immobilized on ProA biosensor. In **Table C** are shown K_D, association (ka) and dissociation (kd) rate constants. All the analyses were carried out by using Octet Analysis Studio 13.0 Software.

In order to investigate on the epitopes recognized by the novel tribodies and verify whether they differ from those recognized by clinically approved monoclonal antibodies, epitope binning analyses were carried out by using in tandem BLI assays. Recombinant LAG-3 (**Figure 30A**), PD-L1 (**Figure 30B**), and PD-1 (**Figure 30C**) proteins were immobilized on ProA biosensors and saturated with two subsequent incubations of the corresponding validated antibodies (Relatlimab, Atezolizumab, or Pembrolizumab, respectively) at 200 nM. Once plateau was reached, the tribodies (TR0304 for LAG-3 and PD-L1, TR0506 for PD-1) were added at increasing concentrations (50–200 nM). As negative controls, the corresponding clinical antibodies were re-incubated at a concentration of 200 nM to confirm the full saturation of the ligand and absence of further binding signals.

As shown in **Figure 30** by sensorgrams obtained by BLI analyses, the tribodies TR0304 and TR0506 retained the ability to bind to their targets even when the biosensor was

saturated with the validated corresponding mAb specific for the same ICs, suggesting that they recognize distinct, or only partially overlapping epitopes.

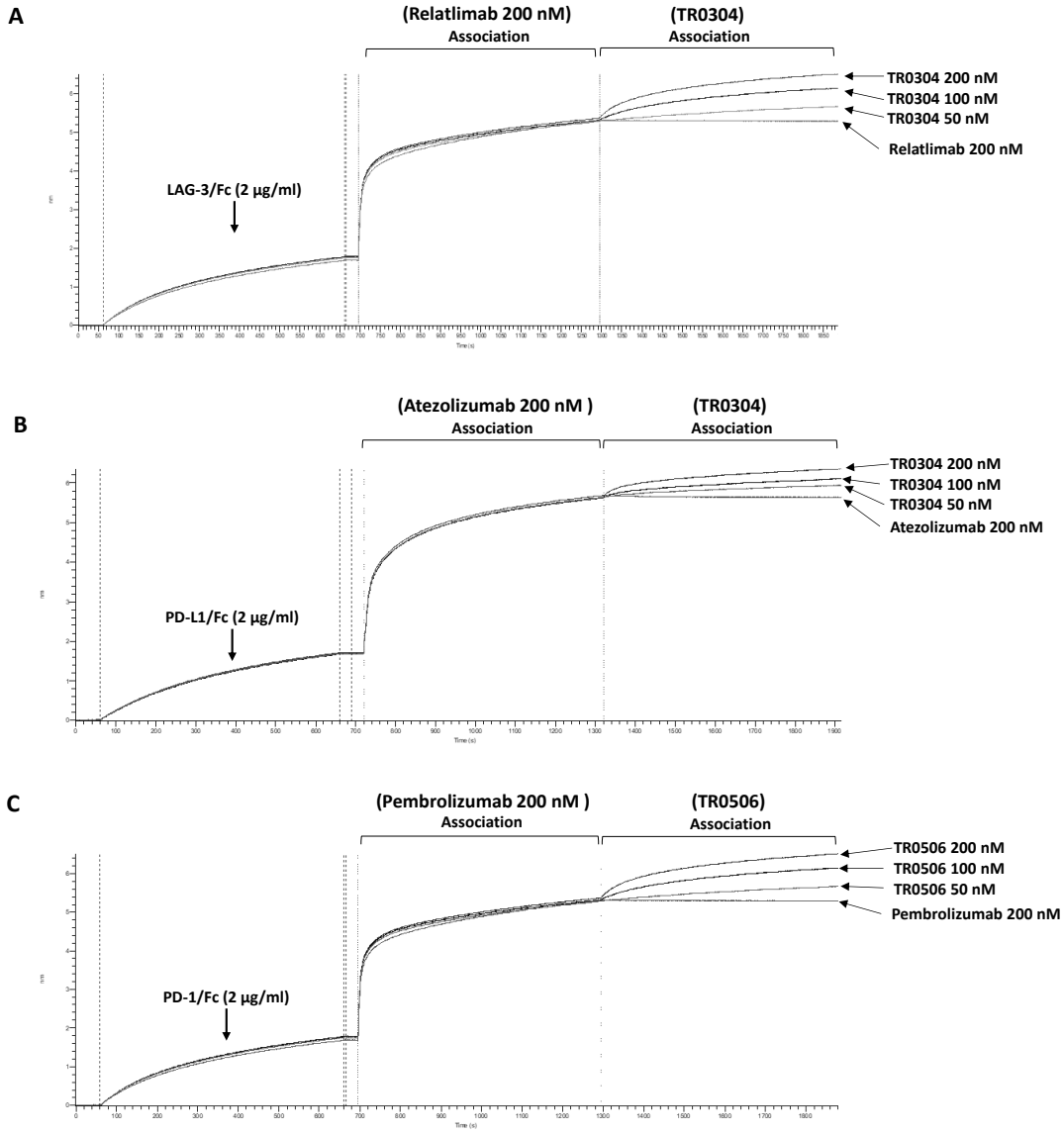

Figure 30. **Epitope binning analyses by using BLI in tandem assays of TR0304 and TR0506 tribodies in comparison with the FDA-approved mAbs recognizing the same targets**. Sensorgram **A** reports the binding of TR0304 to immobilized LAG-3/Fc at increasing concentrations (50, 100 and 200 nM), after saturating the sensor with 200 nM of Relatlimab. Sensorgram **B** shows the binding of TR0304 to PD-L1/Fc at the indicated increasing concentrations, after the saturation with Atezolizumab at the concentration of 200 nM. In panel **C**, the sensorgram shows the binding of TR0506 to PD-1/Fc at increasing concentrations, following saturation with 200 nM of Pembrolizumab. For each sensorgram, the fourth sensor was used as a negative control to confirm the saturation of the target protein after a second incubation with 200 nM of the same clinically validated antibody, used for saturation.

3.2.3 Biological and anti-tumor effects of the novel bi-specific tribodies

Once confirmed the binding specificity and affinity of the novel tribodies, we next evaluated their ability to activate human lymphocytes by measuring IL-2 and IFNγ secretion in the supernatants of treated hPBMCs. To this aim, human PBMCs were stimulated with SEB and treated for 66 hours with the bi-specific compounds TR0304 and TR0506 in comparison with the corresponding parental mAbs at increasing concentrations (1-100 nM). As negative controls, hPBMCs untreated, stimulated with SEB or treated with an unrelated human IgG were used in parallel assays. The results, reported in **Figure 31**, show that TR0304 and TR0506 induced the secretion of cytokines from hPBMCs more efficiently than either the parental mAbs or their respective combinations, thus confirming the advantage of fusing two immunomodulatory moieties into a single tribody to achieve more potent activation of immune cells.

Moreover, we tested TR0304 and TR0506 also in comparison with clinically approved mAbs targeting the same ICs, such as Atezolizumab, Pembrolizumab, and Relatlimab, used either as single agents or in combinations at a concentration of 60 nM. We found that the levels of IL-2 in the supernatants reached 20,775 pg/mL and 24,218 pg/mL following the treatments with TR0304 and TR0506 compared to those (significantly lower) obtained with the combinations of Relatlimab and Atezolizumab or Relatlimab and Pembrolizumab (16,850 pg/mL and 19,500 pg/mL, respectively).
Similarly, IFNγ levels in hPBMCs supernatants reached 12,500 pg/mL and 25,000 pg/mL following treatments with TR0304 and TR0506 compared to the concentration of 8,823.5 pg/mL and 22,580 pg/mL following the combinatorial treatments of Relatlimab plus Atezolizumab or Relatlimab and Pembrolizumab, respectively. Notably, these stronger effects were observed despite the tribodies being tested at a lower concentration (60 nM), corresponding to half of the total concentration used in the combinatorial treatments (60 nM + 60 nM of the two mAbs).

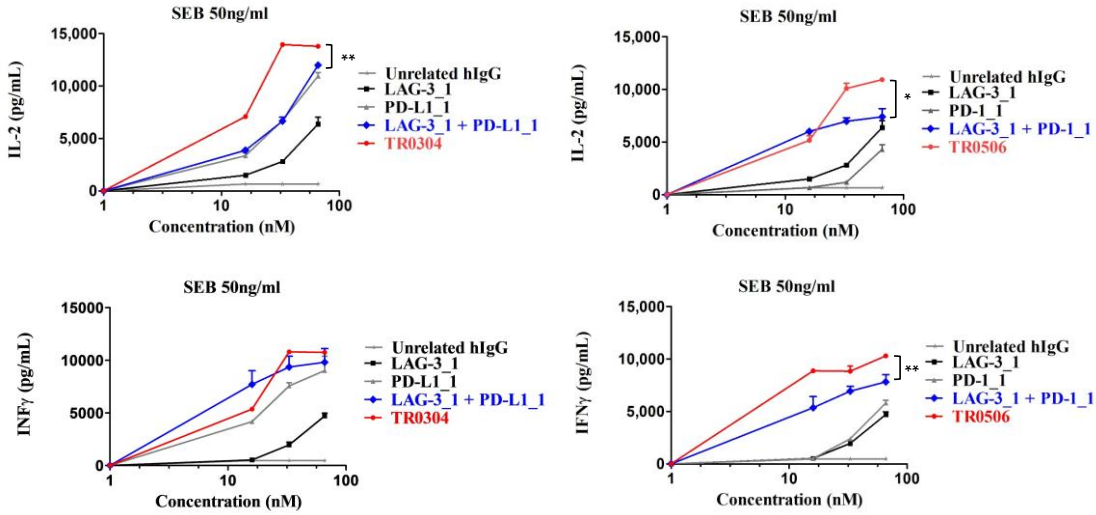

Figure 31. Effects of the bi-specific tribodies on hPBMCs activation. The hPBMCs, stimulated with SEB, were treated with TR0304 and TR0506 or their parental mAbs, used as single agents or in combination, at increasing concentrations. The levels of IL-2 and IFNγ were measured by ELISA assays (R&D kit) and expressed in pg/mL. An unrelated IgG was used as a negative control. The values are reported as the mean of at least three determinations obtained in three independent experiments. Error bars depict means ± SD. *p*-values were calculated using the two-tailed Student's *t*-test, and statistical significance is indicated as follows: ** $p < 0.01$; * $p < 0.05$.

Since the novel tribodies targeting PD-L1, PD-1 and LAG-3 efficiently induced the activation of lymphocytes, we further investigated their antitumor effects on co-cultures of tumor cells and lymphocytes. To this aim, MDA-MB-231 and BT-549 breast cancer cells were co-cultured for 48 h at 37 °C with hPBMCs (3:1 effector:target ratio), in the absence or presence of the TR0304 and TR0506 tribodies or the corresponding parental mAbs at increasing concentrations (16–66 nM). After incubation, cell lysis was measured by evaluating LDH released in the cell supernatants. The tribodies TR0304 and TR0506 induced tumor cell lysis with higher efficacy (56% and 69%, respectively) than the parental mAbs, either as single agents or when used in combinatorial treatments at the same concentrations (43% of cell lysis) (**Figure 32B** and **C**).

In order to further evaluate the potential of the tribodies, we compared their cytotoxic effects on tumor cells in co-culture with immune cells to those of FDA-approved monoclonal antibodies targeting the same ICs. Thus, we treated MDA-MB-231 and BT-549 co-cultured with hPBMCs, in the same conditions described above, with the bi-specific tribodies or with clinically validated mAbs (Relatlimab, Atezolizumab or Pembrolizumab), used as single agents or in combinations, at a concentration of 100 nM. Unrelated IgG1 and IgG4 antibodies were included as negative controls. Following the

treatments for 48 hours at 37°C, tumor cell lysis was evaluated by measuring lactate dehydrogenase release in the supernatants. As shown in **Figure 32D** and **E**, the novel TR0304 and TR0506 induced about 50% tumor cell lysis which is comparable to, or even better, than that observed with the corresponding combinations of mAbs incubated at a total concentration of 200 nM (100 nM + 100 nM of each mAb).

We also analyzed the levels of IL-2 and IFNγ released in the supernatants of the same co-cultures of breast cancer and immune cells. As shown in **Figure 33A** and **B**, we found that the treatment with TR0304 at a concentration of 100 nM led to IL-2 concentration levels of 8,780 pg/mL and 7,230 pg/mL in MDA-MB-231 and BT-549 co-cultures, respectively, about two-fold higher than those observed with the combination of Relatlimab and Atezolizumab (4,830 pg/mL and 2,885 pg/mL, respectively). Interestingly, the treatment with TR0304 led to a secretion of IFNγ 7–8-fold higher in both TNBC co-cultures (29,420 pg/mL and 5,404.5 pg/mL) compared to the combination of Relatlimab and Atezolizumab (3,897.5 and 642.5 pg/mL) in MDA-MB-231 and BT-549 co-cultures, respectively.

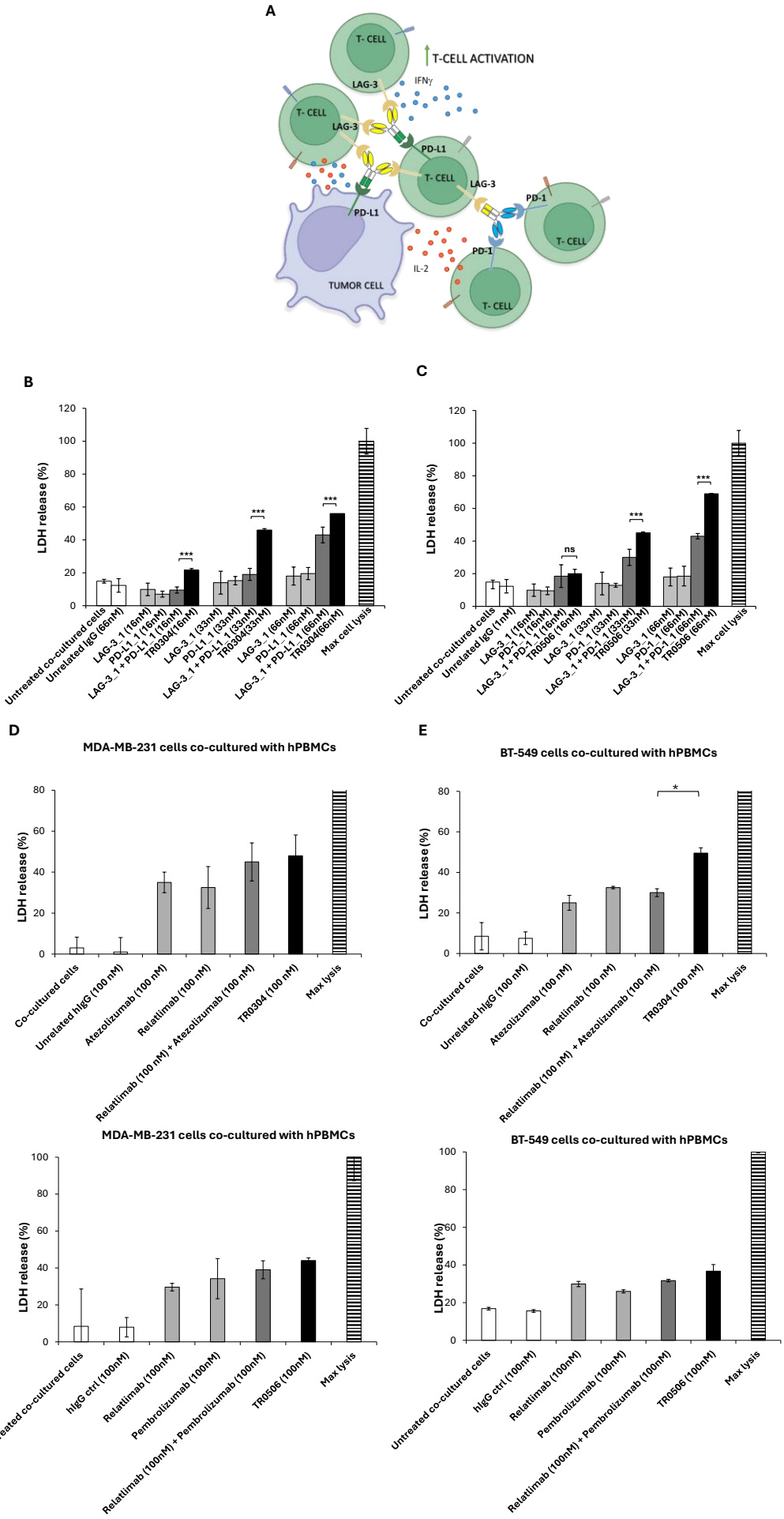
A
T- CELL
T-CELL ACTIVATION
LAG-3
IFNγ
PD-L1
PD-1
IL-2
TUMOR CELL
B
LDH release (%)
Untreated co-cultured cells
Unrelated IgG (66nM)
LAG-3_1 (16nM)
PD-L1_1 (16nM)
LAG-3_1 + PD-L1_1 (16nM)
TR0304(16nM)
LAG-3_1 (33nM)
PD-L1_1 (33nM)
LAG-3_1 + PD-L1_1 (33nM)
TR0304(33nM)
LAG-3_1 (66nM)
PD-L1_1 (66nM)
LAG-3_1 + PD-L1_1 (66nM)
TR0304(66nM)
Max cell lysis
C
LDH release (%)
Untreated co-cultured cells
Unrelated IgG (1nM)
LAG-3_1 (16nM)
PD-1_1 (16nM)
LAG-3_1 + PD-1_1 (16nM)
TR0506 (16nM)
LAG-3_1 (33nM)
PD-1_1 (33nM)
LAG-3_1 + PD-1_1 (33nM)
TR0506 (33nM)
LAG-3_1 (66nM)
PD-1_1 (66nM)
LAG-3_1 + PD-1_1 (66nM)
TR0506 (66nM)
Max cell lysis
D
MDA-MB-231 cells co-cultured with hPBMCs
LDH release (%)
Co-cultured cells
Unrelated hIgG (100 nM)
Atezolizumab (100 nM)
Relatlimab (100 nM)
Relatlimab (100 nM) + Atezolizumab (100 nM)
TR0304 (100 nM)
Max lysis
E
BT-549 cells co-cultured with hPBMCs
LDH release (%)
Co-cultured cells
Unrelated hIgG (100 nM)
Atezolizumab (100 nM)
Relatlimab (100 nM)
Relatlimab (100 nM) + Atezolizumab (100 nM)
TR0304 (100 nM)
Max lysis
MDA-MB-231 cells co-cultured with hPBMCs
LDH release (%)
Untreated co-cultured cells
hIgG ctrl (100nM)
Relatlimab (100nM)
Pembrolizumab (100nM)
Relatlimab (100nM) + Pembrolizumab (100nM)
TR0506 (100nM)
Max lysis
BT-549 cells co-cultured with hPBMCs
LDH release (%)
Untreated co-cultured cells
hIgG ctrl (100nM)
Relatlimab (100nM)
Pembrolizumab (100nM)
Relatlimab (100nM) + Pembrolizumab (100nM)
TR0506 (100nM)
Max lysis

Figure 32. Cytotoxic effects of TR0304 and TR0506 or their parental mAbs on two different breast cancer cell lines co-cultured with hPBMCs. LDH release obtained from supernatants of co-cultures of MDA-MB-231 (**B, D**) or BT-549 (**C**, **E**) tumor cells with hPBMCs (3:1 effector/target cell ratio) after treatments with the novel TR0304 or TR0506 tribodies or anti-PD-L1, anti PD-1, or anti-LAG-3 mAbs (either parental or clinically validated) used as single agents (light gray bars) or in combination (dark gray bars), with respect to the novel TR0304 or TR0506 tribodies (black bars), at the indicated concentrations. Untreated cells or cells treated with an unrelated mAb (IgG1 or IgG4) (white bars) were used as negative controls. The values are reported as the mean ± SD of at least three determinations obtained from three independent experiments. Error bars indicate SD. *p*-values were calculated using the two-tailed Student's *t*-test, and statistical significance is indicated as follows: *p< 0.05, *** p≤ 0.001.

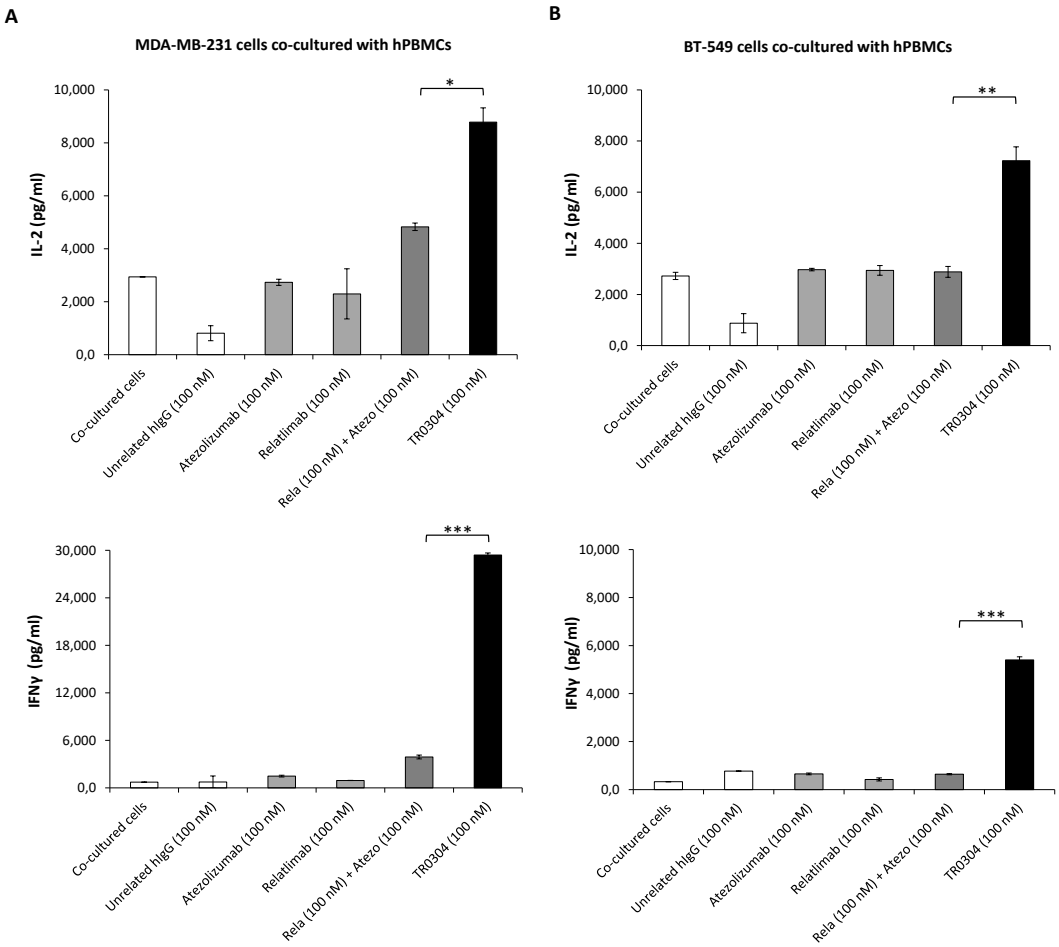

Figure 33. **Cytokines secretion induced by TR0304 in comparison with that of the combination Atezolizumab + Relatlimab**. The effects of the tribody TR0304 on co-cultures of MDA-MB231 (**A**) or BT-459 (**B**) tumor cells with immune cells were evaluated by measuring IL-2 and IFNγ secretion levels by using R&D ELISA kits on supernatants collected after the treatments indicated in the main text. Cells untreated or treated with an unrelated IgG1 or IgG4 were used as negative controls. Data are presented as mean ± SD. *p*-values reported were obtained by performing Student's t-test and are expressed as *** p ≤ 0.001; ** p < 0.01; * p < 0.05.

3.2.4 Evaluation of potential cardiotoxic effects induced by immunomodulatory tribodies

Once assessed their anti-tumor efficacy, we tested the effects of TR0304 and TR0506 also on human cardiomyocytes co-cultured with hPBMCs in order to evaluate their potential side effects. We treated the co-cultures in the absence or presence of bi-specific tribodies or the combinations of the corresponding parental compounds at a concentration of 66 nM. After 24 h, supernatants were collected and LDH release was measured in order to check cardiac cell lysis. As reported in **Figure 34A**, the novel bi-specific compounds induced lower cardiotoxic effects than their respective combination of parental compounds on HFC.

In following assays, we evaluated the potential side effects on human cardiomyocytes of different batches of the novel bi-specific compounds TR0304 and TR0506 also in comparison with the corresponding combinations of clinically validated mAbs (Relatlimab plus Atezolizumab or Relatlimab plus Pembrolizumab, respectively) at a concentration of 100 nM. HFC cells were treated in co-cultures with hPBMCs for 48 h and then the supernatants were collected for LDH evaluation. We found that the combinations of the clinically validated mAbs surprisingly induced stronger cytotoxic effects than the novel tribodies (**Figure 34B**). This result could be likely due to the absence of Fc portion in the tribodies.

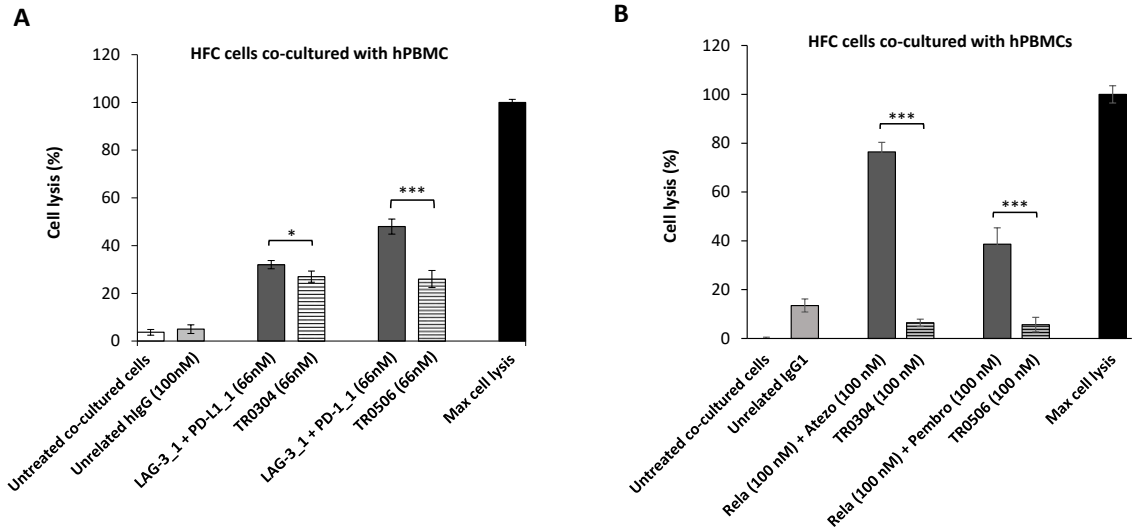

Figure 34. Cardiotoxic effects induced by immunomodulatory tribodies in comparison with the combinations of their respective parental compounds (A) or clinically validated mAbs (B) on human fetal cardiomyocytes. The lysis of HFC cells, co-cultured with hPBMCs in the absence (white bars) or presence of tribodies (striped bars) or the combinations of their respective compounds (grey bars), was analyzed by measuring the release of LDH in the supernatants of cultures. The values are reported as the mean of at least three determinations obtained from three

independent experiments. Error bars depict means ± SD. *p*-value, obtained with the two-tailed Student's *t*-test, are reported as: *** $p \leq 0.001$; * $p < 0.05$.

3.2.5 Construction and purification of novel T cell engagers tri-specific tribodies

Our research group, in collaboration with the Japanese group, also focused attention on a different class of tribodies, called T cell-engagers. These are multispecific constructs with the same scaffold of bi-specific TRs, in which a Fab is fused to two scFvs, but they recognize a target on tumor cells with one arm and the CD3 complex on T cells with the other one, in order to recruit and activate immune cells against cancer cells. In particular the T-cell engager, called Tb535H, binds to the oncofetal antigen 5T4 with a Fab and a scFv domain, and to CD3 on T cells with another humanized scFv. Starting from it, in our lab, novel tri-specific TRs were previously generated by replacing the anti-5T4 scFv with an immunomodulatory scFv derived from parental anti-PD-1, PD-L1 and LAG-3 mAbs, previously generated in our lab [**117**].

All the novel TRs recognize 5T4, expressed on many types of tumor cells (such as breast, lung, ovarian and pancreatic cancer), and CD3 receptor on T cells, but for the first time they include an anti-IC scFv: PD-1 in 53D, PD-L1 in 53L10 and LAG-3 in 53G. As a control, an additional tribody, called 53P, was generated by inserting an unrelated scFv derived from Palivizumab (an antibody targeting respiratory syncytial virus) [**102**].

The five novel T-cell engagers were produced by transfecting Expi293 cells with vectors containing the cDNA cassettes reported in **Figure 35**. After five days, tribodies were purified from the culture supernatants by using His-tag based affinity chromatography followed by gel filtration, and analyzed by SDS-PAGE for purity (data not shown).

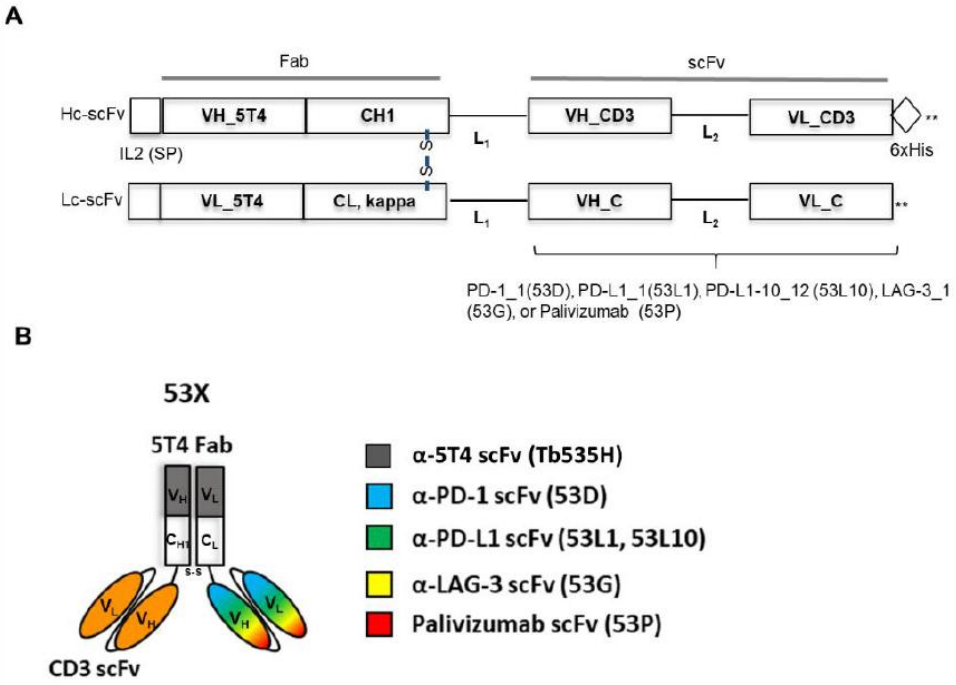

Figure 35. Schematical structure of 53X tribodies. (**A**) Schematical representation of DNA cassettes used for the production of 53X tribodies: VH_5T4 and VL_5T4, represent the variable heavy and light chain sequences derived from Tb535H targeting 5T4; CH1, CL, correspond to the human IgG heavy chain constant region 1 and the kappa light chain constant region, respectively; VH_CD3, VL_CD3, sequences encoding the variable heavy and light chain regions specific for human CD3; VH_C, VL_C, correspond to sequences of the variable heavy and light chain from the parental mAbs PD-1_1, PD-L1_1, 10_12, LAG-3_1. (**B**) Scheme of assembled tribodies for Tb535H [$(5T4)_2 \times CD3$], 53D [5T4 x CD3 x PD-1], 53L1 [5T4 x CD3 x PD-L1], 53L10 [5T4 x CD3 x PD-L1], 53G [5T4 x CD3 x LAG-3] and 53P [5T4 x CD3 x isotype control], respectively.

3.2.6 Characterization of the novel tri-specific tribodies

The newly generated tribodies were previously found able to efficiently activate T cells and induce strong antitumor effects when compared to the parental compounds [**102**].

Here, we further analyzed the binding kinetics of the novel tribodies by using BioLayer Interferometry assays and compared them with antibodies currently in clinical use and targeting the same ICs (Relatlimab, Atezolizumab and Pembrolizumab) [**149**]. Briefly, the recombinant Fc-tagged immune checkpoints (PD-L1, PD-1, or LAG-3) were immobilized on ProA biosensors. Then the tribodies, 53L10, 53D and 53G, or the clinically validated mAbs, used as analytes at increasing concentrations, were incubated for 600 s. As a negative control the tribody 53P was used in parallel assays. As shown in

Figure 36, the tribodies 53L10 (panel **A**), 53D (panel **B**), and 53G (panel **C**) efficiently bound to their respective purified targets with K_D values in the 5–7 nM range, despite their monovalent binding for ICs, as reported in **Table 3**. The clinically approved mAbs demonstrated even lower K_D values, likely due to their bivalent binding. As expected, the negative control, tribody 53P did not show any detectable binding to immobilized PD-L1, PD-1, or LAG-3.

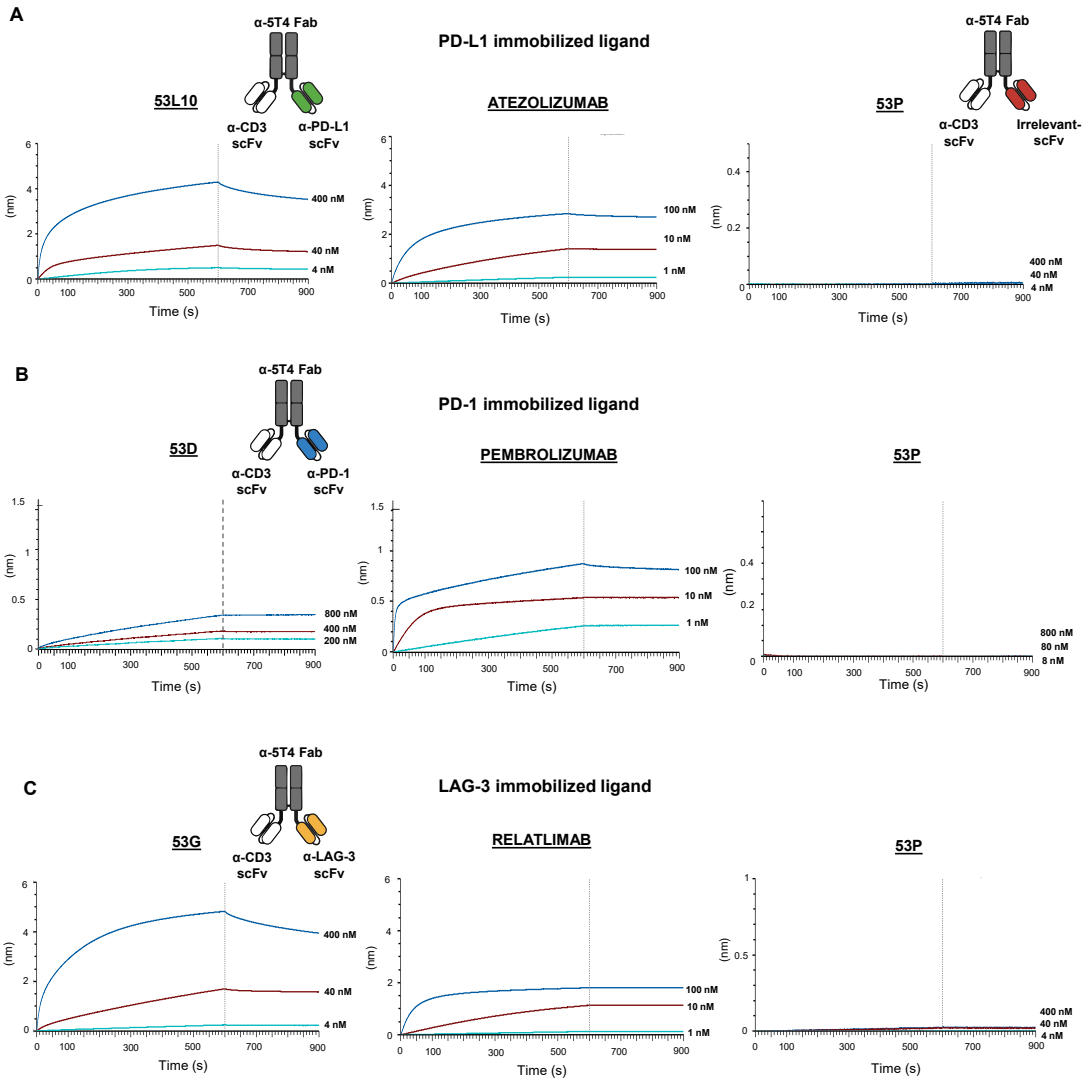

Figure 36. **Binding kinetics of 53X tri-specific tribodies compared to clinically validated mAbs on their corresponding targets**. The sensorgrams reported were obtained by performing BLI analyses: in panel **A** 53L10 is compared to Atezolizumab, in **B** 53D is compared to Pembrolizumab, and in panel **C** 53G to Relatlimab. The recombinant PD-L1/Fc, PD-1/Fc, and LAG-3/Fc were used as ligands, whereas the tri-specific tribodies or corresponding validated mAbs, targeting the same ICs, were used as analytes and tested at increasing concentrations. As a negative control, the tribody 53P was used as analyte in a parallel assay. Schematic representations of the 53X tribodies are shown as insets within each corresponding binding panel.

Table 3

Analyte	K_D (M)	ka (1/Ms)	ka Error	kd (1/s)	kd Error
53L10	6.25×10^{-9}	2.51×10^{5}	1.42×10^{3}	4.93×10^{-4}	8.71×10^{-6}
ATEZOLIZUMAB	1.47×10^{-09}	1.60×10^{5}	1.17×10^{4}	1.63×10^{-4}	1.42×10^{-5}
53D	5.45×10^{-9}	5.60×10^{3}	41.90	4.28×10^{-5}	5.36×10^{-6}
PEMBROLIZUMAB	1.00×10^{-12}	3.63×10^{5}	5.25×10^{4}	1.00×10^{-7}	1.00×10^{-7}
53G	9.64×10^{-9}	1.16×10^{5}	1.17×10^{3}	3.32×10^{-4}	5.77×10^{-6}
RELATLIMAB	1.67×10^{-9}	1.53×10^{5}	5.13×10^{3}	3.53×10^{-4}	1.91×10

Table 3. K_D values and association (ka) and dissociation (kd) constants of the binding of each analyte to its corresponding immobilized ligand on a pro-A biosensor. Analysis was performed using Octet Analysis Studio 13.0 Software (Sartorius, Fremont, CA, USA).

We then evaluated their binding properties to targets expressed on hPBMCs pre-activated with anti-CD3/CD28 beads, by performing parallel cell ELISA assays. As indicated in **Figure 37A**, although 53G and 53L10 bound with lower affinity to the chimeric immune checkpoints compared to Relatlimab and Atezolizumab, they showed comparable or even higher binding affinity for activated immune cells, likely due to the presence of the anti-CD3 scFv within the tribody structure. Indeed, 53L10 and 53G showed apparent affinities in the sub-nanomolar range (0.2–0.9 nM), when tested on hPBMCs; whereas Atezolizumab and Relatlimab exhibited affinities in the nanomolar range (3-10 nM). Only 53D showed a higher EC50 value of 13 nM, consistent with its lower affinity if compared to Pembrolizumab (3 nM), in line with the data on purified proteins shown in previous BLI assays.

To further investigate on the binding of the novel tri-specific tribodies also on tumor cells, we first analyzed the surface expression of 5T4 and PD-L1 on a panel of cell lines, including A-549 (NSCLC), MDA-MB-231 (TNBC), and Li-7 (liver cancer). As shown in **Figure 37B**, 5T4 expression was detected at comparable levels on all tumor cell lines, while PD-L1 was expressed at higher levels on A-549 and MDA-MB-231 cells compared to Li-7 cells.

The tribodies were tested for their ability to bind to the surface of these tumor cells by cell ELISA and showed an affinity in the nanomolar range (**Figure 37C**). In particular, 53L10 showed the lowest K_D value, likely due to its ability to engage both 5T4 and PD-L1 on tumor cells, as indicated also by its reduced binding to Li-7 cells, which express lower levels of PD-L1, compared to the other cell lines.

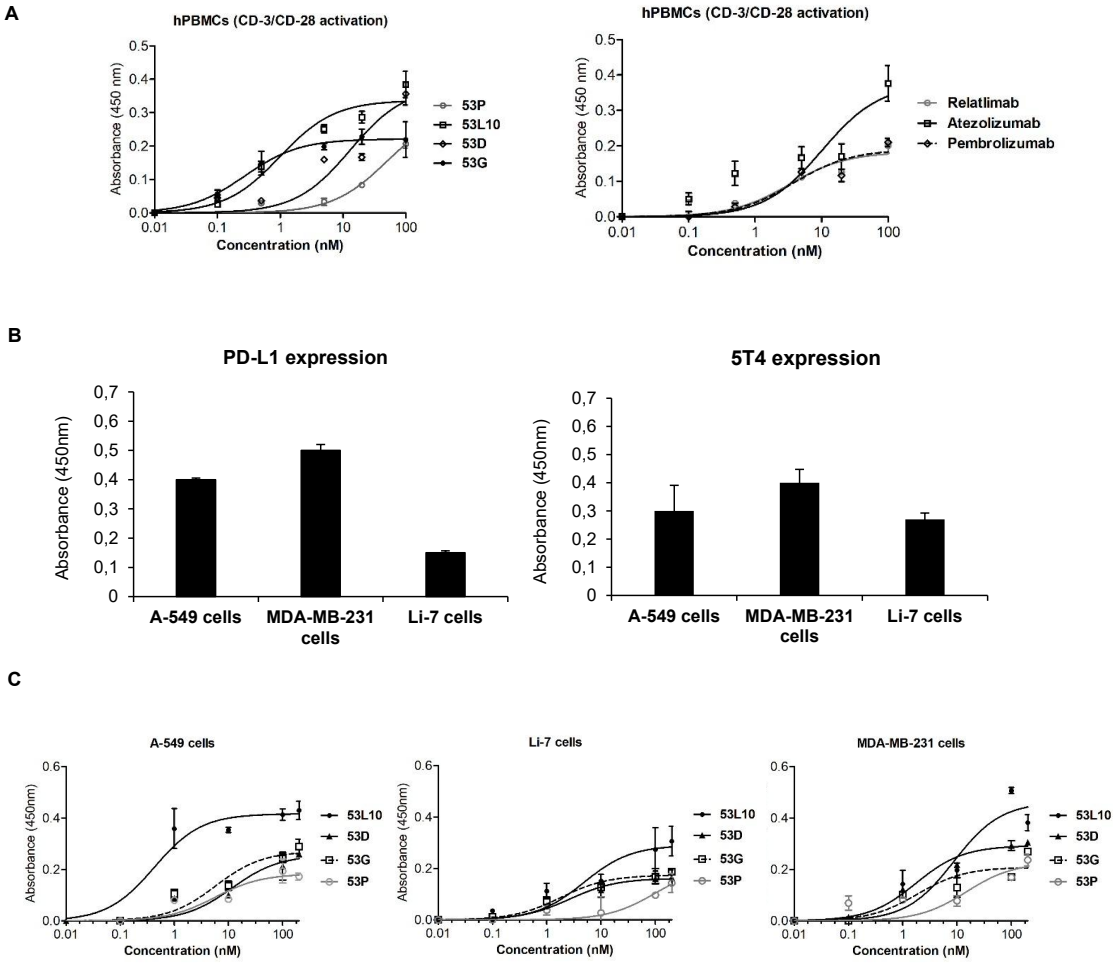

Table 4

Activated hPBMCs	53P	53L10	53D	53G	Relatlimab	Atezolizumab	Pembrolizumab
EC50 (nM)	49.8	0.99	13	0.3	3.3	10	3.8

Figure 37. Binding curves of 53X tribodies on lymphocytes and tumor cells tested in comparison with the clinically approved mAbs. (**A**) The tribodies and the FDA approved mAbs were tested at the indicated concentrations in parallel assays by cell ELISA on human lymphocytes activated with anti-CD3/CD28 beads. (**B**) Cell ELISA assays to check the expression level of 5T4 and PD-L1 on lung A-549, breast MDA-MB-231 and liver Li-7 cancer cells were performed with a commercial anti-PD-L1 or anti-5T4 antibody. (**C**) Binding curves of 53X tribodies tested at increasing concentrations (0.1–100 nM) on the indicated tumor cell lines. Binding values were reported as the mean of at least three determinations obtained in three independent experiments. Error bars depicted means ± SD.

Table 4 reports the EC50 values obtained by ELISA binding curve analyses with Prism (Graphpad) tool according to the following model: *Y = Bmax*X/(Kd +X) + NS*X + Background.*

3.2.7 Comparison of cytotoxic activity of novel immunomodulatory tribodies with that of 53P control tribody in combination with clinically validated mAbs

To evaluate the efficacy of the novel tribodies targeting PD-L1, PD-1, and LAG-3 compared to the combinations of the clinically validated mAbs, specific for the same IC target, with the control tribody (53P) lacking the immunomodulatory scFv, we set up co-cultures of tumor cells and immune cells. MDA-MB-231 and A-549 cells, both characterized by high expression of PD-L1 and 5T4, were co-cultured with hPBMCs at a 3:1 effector-to-target ratio and incubated at 37°C for 48 or 72 h in the absence or presence of the tribodies 53D, 53G, and 53L10. In parallel assays, the negative control tribody 53P was tested alone or in combination with the approved anti-PD-1 (Pembrolizumab), anti-PD-L1 (Atezolizumab), or anti-LAG-3 (Relatlimab) antibodies. Following treatment, tumor cell lysis was evaluated by measuring LDH released into the supernatants.

We found that all the novel tri-specific tribodies, with the exception of the negative control 53P, induced tumor cytotoxicity stronger than those observed with the combinations of each clinically validated mAb with 53P (**Figure 38**). Moreover, we found that the novel tribodies were able to further increase tumor cell cytotoxicity also at lower doses in prolonged treatments. Notably, treatment with 53L10 resulted in a two-fold increase in LDH release compared to the combinations of Atezolizumab plus 53P. To further confirm the specificity of the tribodies, we performed the same experiments by using Li-7 cells, which express lower levels of PD-L1 and 5T4. As expected, the cytotoxicity of TRs was reduced in co-cultures of Li-7 cells compared to the effects observed in MDA-MB-231 and A-549 co-cultures.

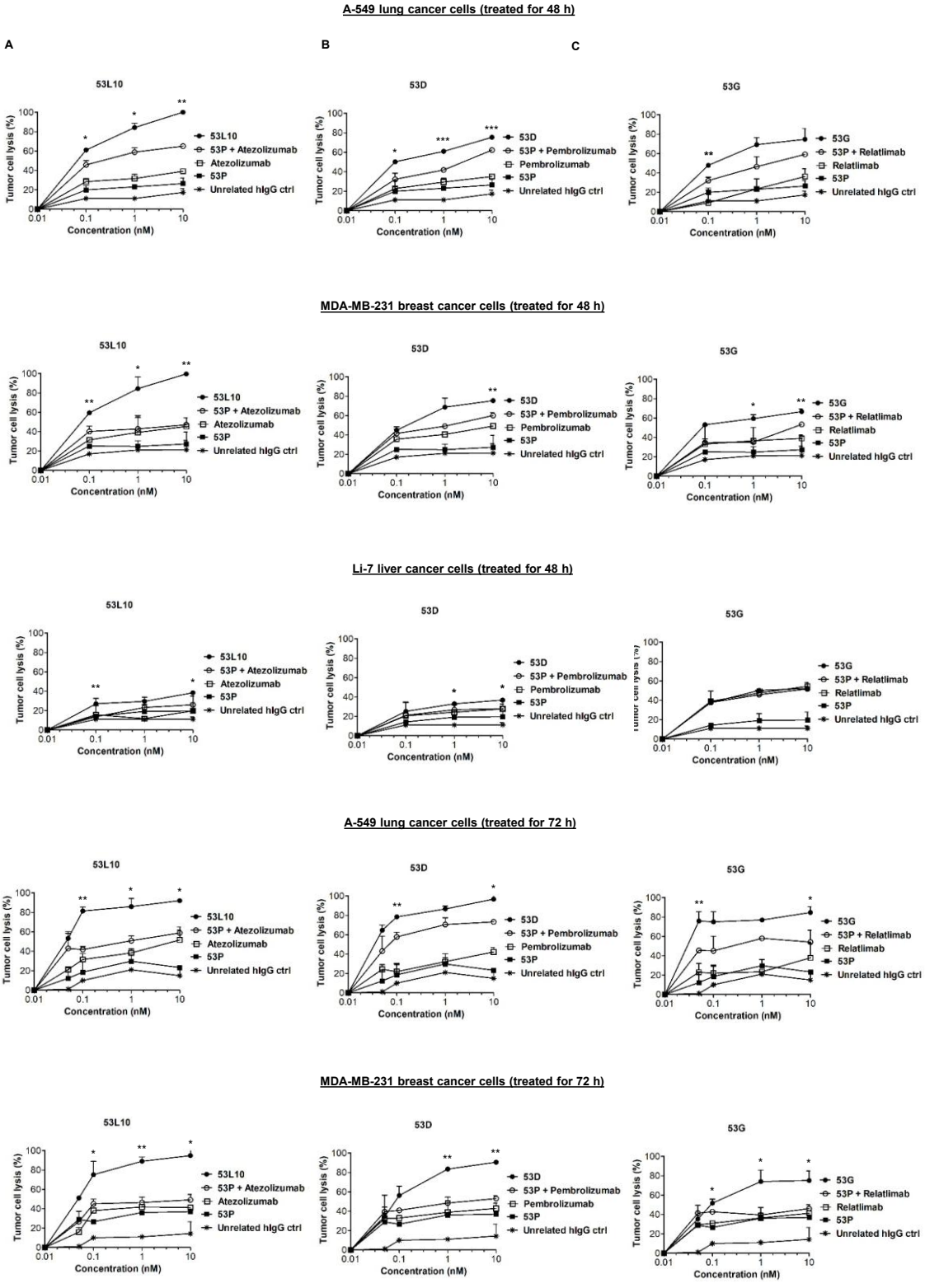

Figure 38. Cytotoxic effects of the novel tribodies in comparison with the combinations of 53 P and the clinically validated mAbs. Tumor cells (A-549, MDA-MB-231, and Li-7) were co-cultured with hPBMCs (3:1 effector/target ratio) and treated for 48 h or 72 h with the control 53P (■), 53L10 (**A**), 53D (**B**), and 53 G (**C**) tribodies (all indicated with ●). Atezolizumab, Pembrolizumab, and Relatlimab (all indicated by □), or their combinations with 53 P (○) were tested in parallel at the indicated concentrations (0.05‑10 nM). Co-cultures untreated or treated with an unrelated IgG (*) were used as negative controls. Cell lysis was measured by detecting

LDH release. The values are reported as the mean ± SD of at least three determinations obtained from three independent experiments. Error bars represent SD. Statistical significance was determined by comparing each tribody treatment with the corresponding combinatorial treatment by using Student's t-test (two-tailed). Significance levels are indicated as follows: ***$p \leq 0.001$; **$p < 0.01$; *$p < 0.05$.

To determine whether the enhanced tumor cell lysis induced by the novel tribodies was associated to increased cytokine secretion from hPBMCs, we measured the concentrations of IFNγ and IL-2 in the supernatants of treated co-cultures. The effects of the tribodies were compared with those of the control 53P tribody combined with each corresponding mAb. As shown in **Figure 39A** and **B** (IL-2 and IFNγ after 48 h of treatment) and **Figure 39C** (IL-2 after 72 h of treatment), the levels of IFNγ and IL-2 were higher in co-cultures treated with the novel tribodies than in those treated with the combinations of 53P with Pembrolizumab, Atezolizumab, or Relatlimab. Moreover, the tribodies were able to induce IL-2 and IFNγ secretion in a dose-dependent manner, leading to a 4– to 5–fold increase in cytokine levels compared to the corresponding combinatorial treatments of validated anti-IC mAbs and 53P.

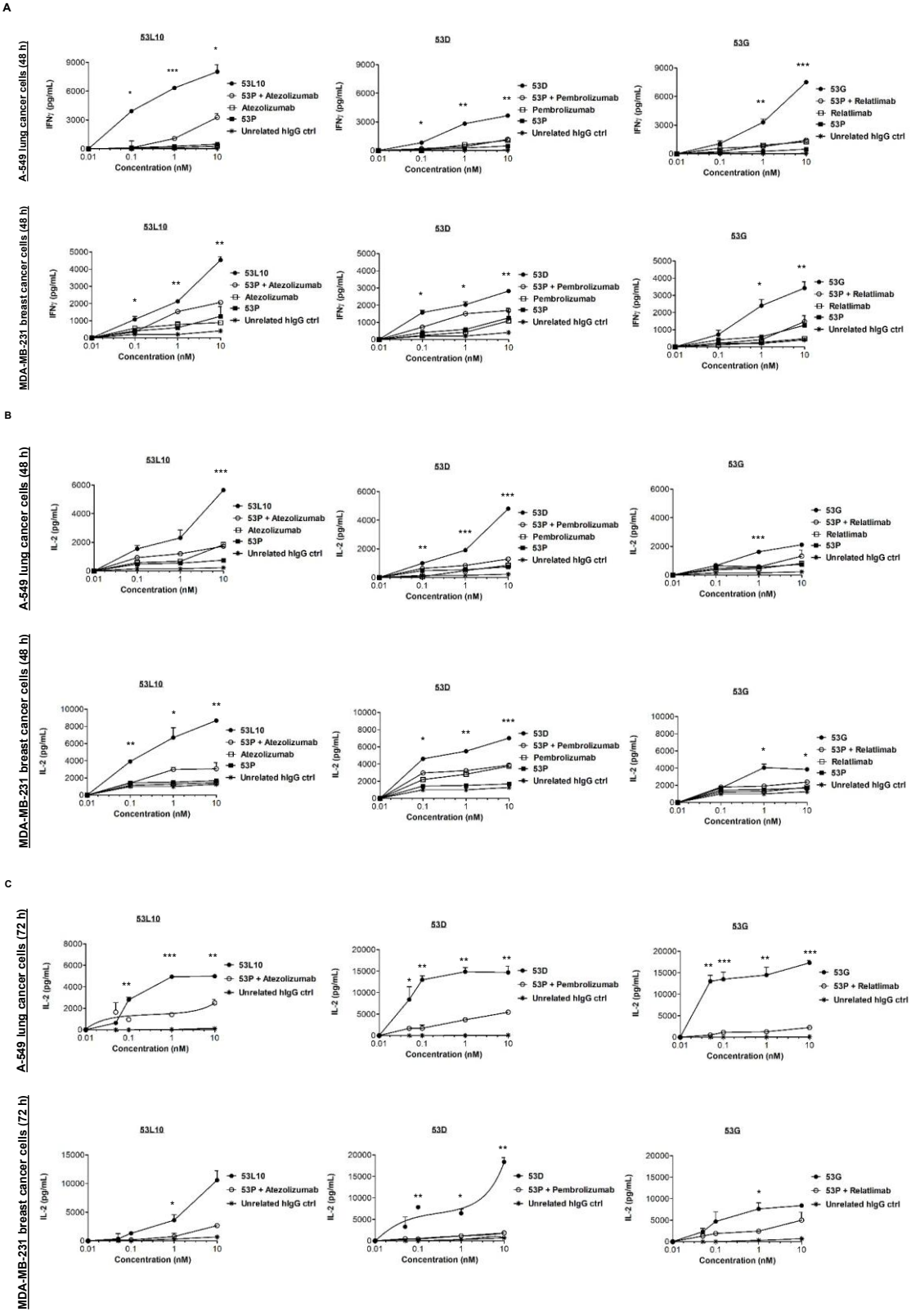

Figure 39. IFNγ and IL-2 release in co-cultures of tumor cells with hPBMCs treated with the novel tribodies. Tumor cells (A-549 and MDA-MB-231) were co-cultured with hPBMCs (3:1 effector/target ratio) and treated for 48 h or 72 h with the negative 53P (■), 53L10, 53D and 53 G tribodies (indicated with ●). The validated immunomodulatory mAbs Atezolizumab, Pembrolizumab, and Relatlimab (□), or their combinations with 53P (○) were tested in parallel assays at the indicated

concentrations (0.05‑10 nM). The levels of IFNγ (**A**) and IL-2 (**B**, **C**) released in the supernatant of co-cultures were measured by cytokine secretion kit (R&D systems). Co-cultures untreated or treated with an unrelated IgG (*) were used as negative controls. The values are reported as the mean of at least three determinations obtained from three independent experiments. Error bars represent mean ± SD. Statistical significance was determined by comparing each tribody treatment with the corresponding combinatorial treatment by using Student's t-test (two-tailed). Significance values are indicated as follows: ***$p \leq 0.001$; **$p < 0.01$; *$p < 0.05$.

3.2.8 *In vivo* anti-tumor efficacy of novel 53L10 tribody in a mouse model bearing human lung cancer

Based on the promising results of 53L10, *in vivo* studies were carried out in order to compare its anti-tumor efficacy with the control tribody 53P and the clinically validated anti-PD-L1 antibody Atezolizumab. A suspension of 5×10^6 A-549 cells mixed with an equal number of human PBMCs, activated by stimulation with Dynabeads Human T-Activator CD3/CD28 for 4 days before transplantation, was subcutaneously injected into the right flank of NOD/SCID mice (Day 0) (**Figure 40A**). Treatments with vehicle (PBS), 53P (20 μg/mouse), or 53L10 (20 μg/mouse) were administered intraperitoneally every other day for a total of six doses (Days 0, 2, 4, 6, 8, and 10). Atezolizumab (200 μg/mouse), alone or in combination with 53P, was administered intravenously 3 times (on days 0, 4, and 8).

Tumor volume was monitored starting four days post-inoculation and then twice a week until day 42, when tumors in the vehicle group reached approximately 1000 mm^3 (**Figure 40C**). Mice treated with 53L10 exhibited the highest anti-tumor activity, with a tumor growth inhibition (TGI) of 96–100% and complete tumor regression in 5 out of 8 mice by Day 42. The treatment with Atezolizumab resulted in a much lower, but still significant, reduction in tumor growth (~35% TGI) compared to the vehicle control. The control tribody 53P induced only slight anti-tumor effects (~30% TGI). The combination of Atezolizumab and 53P demonstrated improved efficacy (~50% TGI) in comparison with single-agent treatments; however, it did not achieve the complete tumor regression observed with 53L10.

A

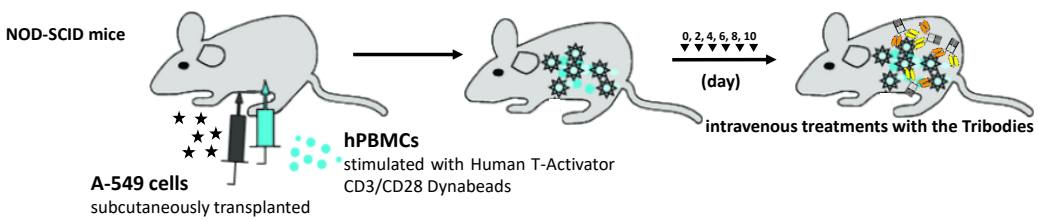

B

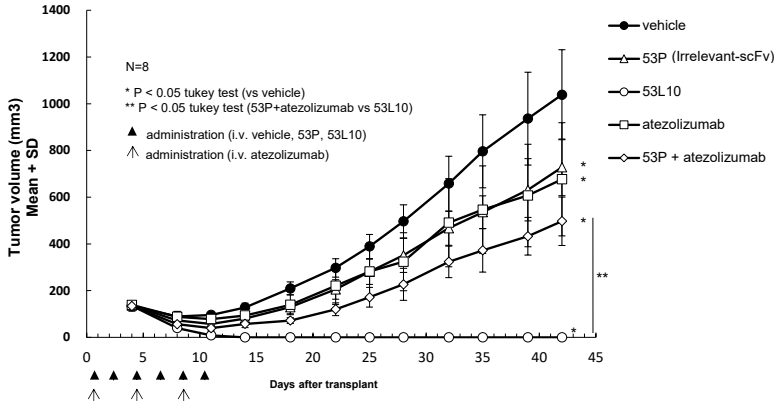

Table 5

Treatment	Dose	N	Tumor volume (mm^3) Mean ± SD	TGI (%)
Vehicle (PBS)	-	8	1038.7 ± 192.9	-
53P	20 µg/mouse	8	728.0 ± 121.3	29.9%
Atezolizumab	200 µg/mouse	8	676.8 ± 242.4	34.8%
53P + Atezolizumab	20 µg/mouse (53P) 200 µg/mouse (Atezo)	7	497.4 ± 103.8	52.1%
53L10	20 µg/mouse	8	0.0 ± 0.0	100%

Figure 40. *In vivo* anti-tumor efficacy of novel 53L10 tribody in a humanized A-549 xenograft mouse model. (**A**) Schematic representation of the *in vivo* experimental setup. (**B**) *In vivo* anti-tumor efficacy of 53L10 compared with Atezolizumab, 53P and their combination. Tumor growth curves of NOD/SCID mice subcutaneously co-inoculated with A-549 lung cancer cells and activated hPBMCs (5×10^6 cells each) and treated with Atezolizumab or the novel tribody 53L10. Intravenous administrations of vehicle (PBS; ●), 53 P (△), or 53L10 (○) on Days 0, 2, 4, 6, 8, and 10 (6 times in total) after cell transplantation were performed at the doses indicated in the figure. Intravenous administrations of Atezolizumab (□) at the dose of 200 µg were performed on Days 0, 4, and 8 (3 times in total as indicated by the arrows). The combined treatment of 53P with Atezolizumab (◇) was carried out by administering 53P on Days 0, 2, 4, 6, 8, 10 and Atezolizumab on Days 0, 4, 8. Tumor volumes are expressed as means ± standard deviations (SD). Tukey's multiple test (for all the combinations) was performed as a significance test. *$p < 0.05$ vs vehicle (PBS) group, **$p< 0.05$ (53 P + Atezolizumab vs 53L10). The table reports the tumor volume and tumor growth inhibition in each treatment group at Day 42 (final day of the study).

3.3 *Generation and characterization of novel human anti-OX-40 mAbs*

3.3.1 Phage display selection of human scFvs specific for OX-40 and screening by NGS

In order to increase the number of antibodies targeting different ICs that could be used for combinatorial treatments to increase antitumor effects, our research team previously generated a repertoire of fully human monoclonal antibodies specific for several immune checkpoints [**117**]. A novel phage display selection was carried out by direct panning on activated human lymphocytes to isolate antibodies able to bind with high affinity to ICs targets in their native conformation as presented on the cell surface.

Briefly, the first step of selection included a negative panning on untreated human lymphocytes to remove phage clones from the collection recognizing common antigens expressed on T cells, followed by a positive selection on pre-activated lymphocytes expressing high levels of immune checkpoints, thus enriching the sequences of binders specifically targeting ICs in their native conformation.

Among them, OX-40 receptor, expressed on the surface of activated T cells and involved in co-stimulatory signalling, emerged as a promising candidate due to its role in enhancing T cell proliferation and survival. To generate novel mAbs targeting OX-40 we used here the phages obtained from the first step of selection on human PBMCs that were amplified by infecting *E. coli* TG1 cells. In order to increase their specificity for OX-40, two following rounds of negative panning on immobilized Fc portion, and a positive selection on OX-40/Fc chimeric protein were carried out (**Figure 41A**). The bound phages were then eluted, amplified and digested with suitable restriction enzymes to isolate the scFv sequences for screening by Next Generation Sequencing (NGS) in collaboration with Prof. Nicosia and Dr. Sasso. To identify the most enriched sequences over the cycles of selection, the pools of sequences obtained from each cycle were analyzed in parallel. The detailed enrichment profile is reported in **Figure 41B**, and five clones were selected for the conversion into full size mAbs.

3.3.2 Production, purification and analysis of stability of the novel anti-OX-40 mAbs

The most enriched scFv sequences were converted into whole human IgG1 antibodies by cloning the corresponding VH and VL cDNAs in the pEU vectors 8.2VH and 4.2VL expressing the human heavy and light chain constant regions, respectively. Then, expression plasmids containing the sequences encoding the five newly generated anti-OX40 monoclonal antibodies, called OX-40_1, _2, _3, _5, and _8 were transfected into HEK293-EBNA cells. Briefly, for each construct, lipofectamine (20 μL) and DNA

vectors (10 µg) were diluted in serum-free medium. The HEK293-EBNA cells, seeded the previous day, were washed using the same medium and then the mixtures containing DNA-lipid complexes were added to each plate. After 5 hours of incubation at 37°C, cell culture medium was replaced with chemically defined (CD) CHO medium. Following 10 days of semi-stable production in cell culture, the novel mAbs were purified from the conditioned medium by affinity chromatography by loading the supernatant on Protein A HP SpinTrap columns.

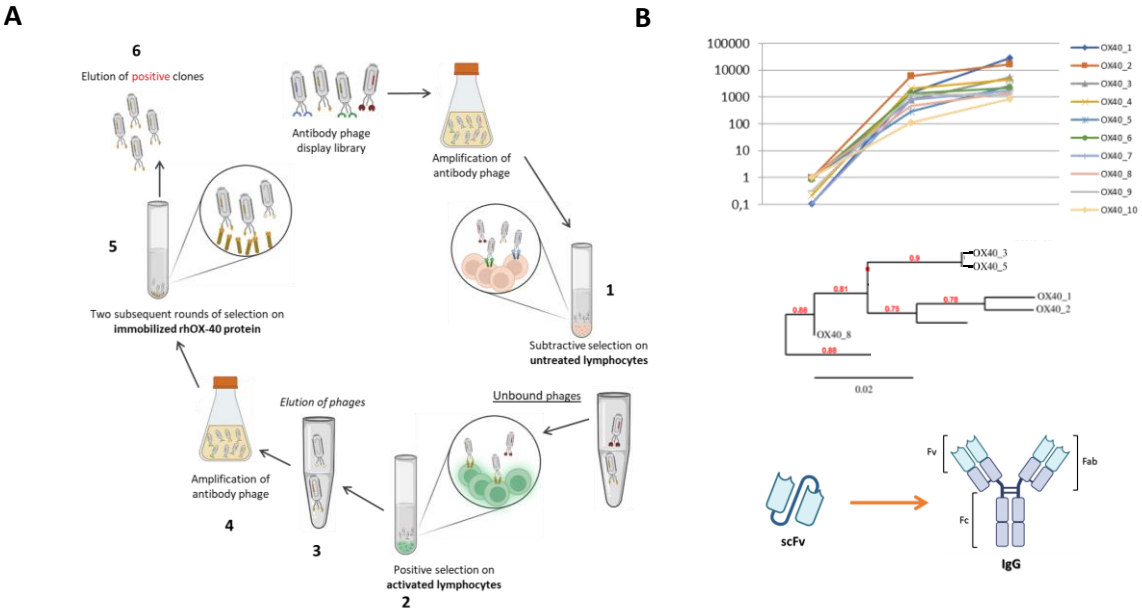

Figure 41. Graphical representation of phage display selection of anti-OX-40 positive clones. (A) Each round of selection included 4 following steps: panning, washes, elution and amplification. Phages were recovered from the antibody phage display library, amplified and used for a subtractive selection on untreated hPBMCs (1), followed by a positive selection on activated hPBMCs (2). The eluted phages (3) were amplified (4) and subjected to two subsequent rounds of selection on immobilized hrOX-40/Fc coated protein (5). The phages were then eluted (6) and the screening of positive clones performed by NGS. (**B**) Representation of enrichment trend over the three cycles of selection on OX-40 protein of the top 10 scFv binders.

The purified antibodies were eluted by using a low pH buffer, following the manufacturer's instruction, and evaluated for their purity by SDS-PAGE and Coomassie staining under reducing conditions. As shown in **Figure 42**, they showed the correct structure made up of heavy and light chains with the expected molecular weights of 50kDa and 25kDa, respectively. No signs of degradation or contaminant proteins were detected by SDS-PAGE analysis.

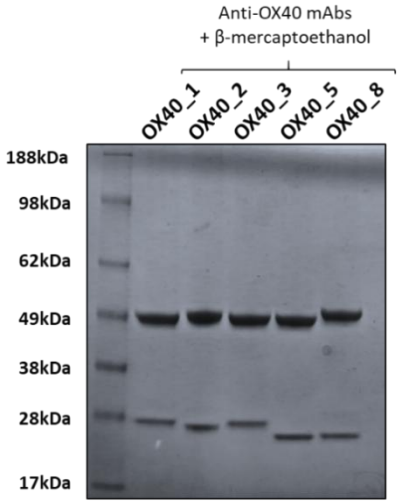

Figure 42. Analysis of purity by SDS-PAGE and Coomassie Staining of the novel purified anti-OX-40 mAbs. The novel monoclonal antibodies were generated by transfecting HEK293EBNA cells and purified by Pro-A affinity chromatography from conditioned medium, as described in methods. The analysis of purity and stability of the mAbs was performed by SDS-PAGE under reducing conditions, by adding β-mercaptoethanol.

In order to check the long-term stability of the novel anti-OX-40 mAbs, additional analyses were performed after storage under different conditions for 30 days. A Western Blotting analysis was performed under reducing conditions of samples stored for one month at 4°C or after a freezing and thawing out cycle at –80 °C. As shown in **Figure 43A**, no signs of degradation were observed, confirming the structural stability of the antibodies over time. Furthermore, to test the long-term storage, ELISA assays were carried out with aliquots of each sample at two concentrations (10 and 100 nM) on immobilized recombinant OX-40/Fc protein. We found that all the antibodies retained their binding properties in both conditions (see **Figure 43B**), thus suggesting that the storage at 4°C for 1 month or after a cycle of freezing and thawing out does not affect their functional properties.

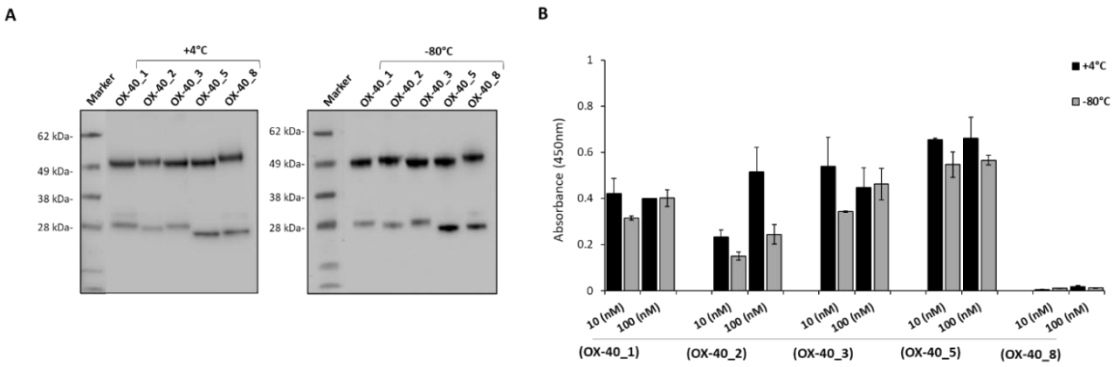

Figure 43. Analysis of stability of anti-OX-40 mAbs after storage up to 1 month in different conditions. (**A**) Western Blotting analysis under reducing conditions of

the novel anti-OX-40 mAbs tested after one month at 4°C or after one cycle of freezing and thawing out at -80°C. The signal was detected by using a mixture of HRP-conjugated anti-Fab and anti-Fc mAbs. (**B**) Binding by ELISA of novel purified mAbs tested at two concentrations (10, 100 nM) on immobilized OX-40/Fc recombinant protein after one month of storage at 4°C (black bars) or after one cycle of freezing and thawing out at -80°C (grey bars). The values are reported as the mean ± SD of at least three determinations obtained from three independent experiments. Error bars indicate SD.

3.3.3 Characterization of binding ability of the novel converted anti-OX-40 mAbs by ELISA and Biolayer Interferometry

The binding ability of the newly generated human anti-OX-40 mAbs was further evaluated by ELISA assays, by testing increasing concentrations (0.3–200 nM) of each mAb on immobilized rhOX-40 and on activated lymphocytes, expressing OX-40 on cell surface. As shown in **Figure 44A**, 4 out of 5 antibodies can bind with high affinity to OX-40/Fc in a nanomolar or subnanomolar range. No binding was detected when the same antibodies were tested on human IgG Fc portion, confirming their specificity for OX-40 receptor. In contrast, OX-40_8 mAb did not show a significant binding to OX-40 receptor and was discarded from the following analyses.

In order to evaluate the binding of OX-40_1, _2, _3 and _5 mAbs to their target also when expressed on human lymphocytes, we firstly checked the expression levels of OX-40 on hPBMCs, either untreated or stimulated with SEB, by using a commercial anti-OX-40 antibody. As shown in **Figure 44B**, a marked upregulation of OX-40 expression was observed after 72 hours of stimulation with SEB. Thus, we performed binding assays by incubating both untreated and activated hPBMCs (for 72h) with increasing concentrations (0.3–200 nM) of each mAb. As expected, a very poor binding was observed on untreated lymphocytes, while all four novel antibodies bound efficiently to SEB-activated lymphocytes, with binding affinities in the nanomolar range (**Figure 44C**). These results further support the specificity of the novel mAbs for OX-40 in its native conformation.

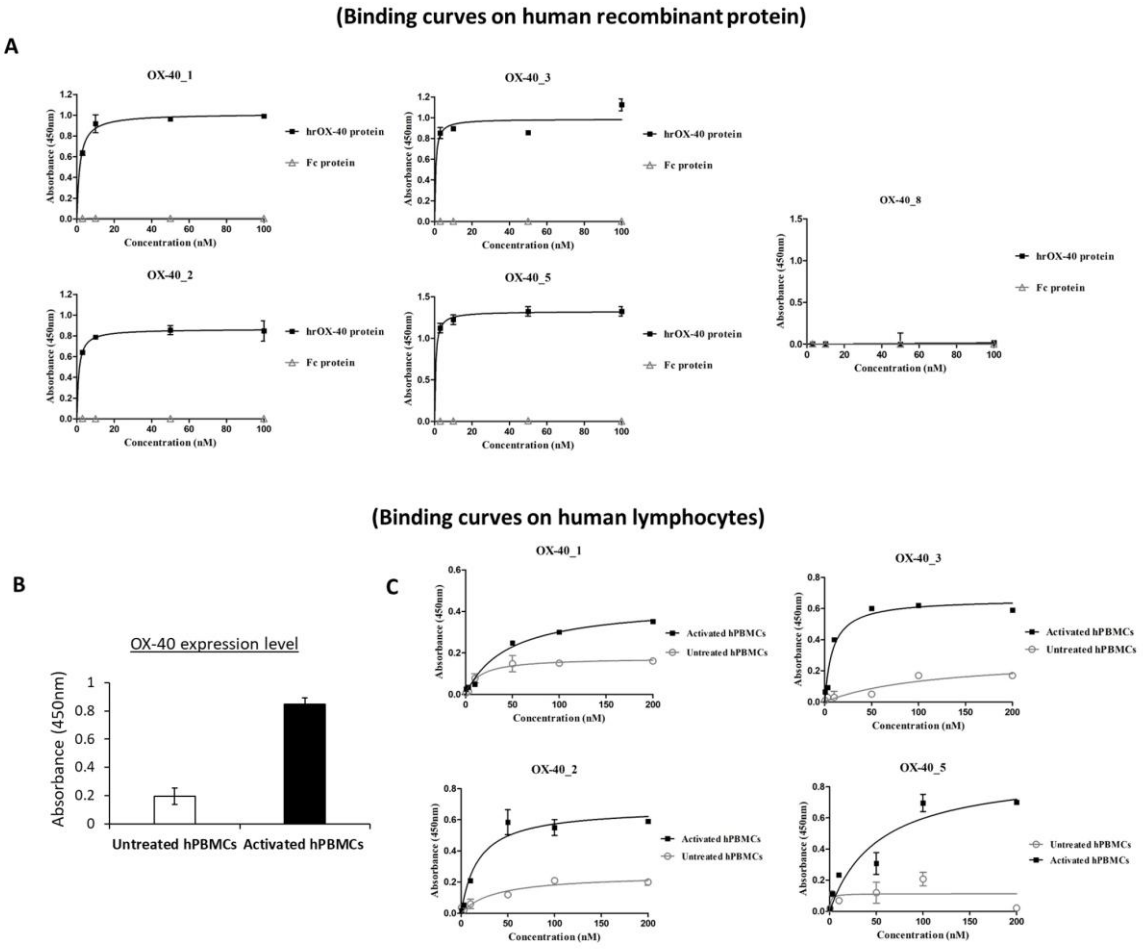

Figure 44. Binding curves by ELISA of the novel purified anti-OX-40 mAbs on immobilized OX-40/Fc recombinant protein and human lymphocytes. (**A**) Human OX-40/Fc recombinant protein or Fc domain, used in parallel as a negative control, were immobilized and then the indicated mAbs were tested at increasing concentrations (0.3–100 nM). The signal was detected by using the secondary HRP-conjugated anti-Fab antibody. OX-40_8 mAb was used as a negative control. (**B**) The expression level of OX-40 protein was determined on untreated or activated hPBMCs by using a commercial polyclonal anti-OX-40 Ab. (**C**) Binding of mAbs to untreated (grey curves) and activated (black curves) hPBMCs tested at increasing concentrations (0.3–200 nM) by cell ELISA. Concentration values were reported as the mean of at least three determinations and error bars depicted mean ± SD. The binding curves were obtained by using Prism (GraphPad Prism 5) tool.

We further analyzed the binding kinetics of the four anti-OX-40 mAbs by employing Biolayer Interferometry. To this aim, rhOX-40/Fc, used as ligand, was immobilized on protein A biosensors. To minimize any non-specific binding of the antibodies directly to the biosensor, an additional saturation step with recombinant human Fc protein was carried out before the addition of analytes. Each anti-OX-40 mAb, used as analyte, was then added at increasing concentrations (10, 50, and 100 nM). As shown

in **Figure 45**, all antibodies bound to their target in a dose-dependent fashion, with K_D values in the nanomolar range (in **Table 6** are reported kinetic parameters, including association and dissociation rate constants). Among them, OX-40_3 exhibited the slowest dissociation rate, approximately one order of magnitude lower than those observed for the other mAbs, thus suggesting an enhanced stability of the antibody–target complex. Comparable results were obtained when BLI assays were repeated by using OX-40/His immobilized on HIS1K biosensors, confirming the binding abilities of OX-40_1, _2, and _3. In particular, the affinity of OX-40_2 was slightly reduced in this system, likely due to conformational differences between the OX-40/Fc and OX-40/His chimeric proteins. By using cell ELISA, the K_D values of all the mAbs were found higher than those obtained on the purified protein, but again, OX-40_3 showed the best properties followed by OX-40_2, whereas OX-40_1 and _5 showed a lower affinity for the receptor on cell surface. In **Table 7** a comparison of the K_D values obtained by BLI or by ELISA on both purified protein or on activated hPBMCs is reported for clarity.

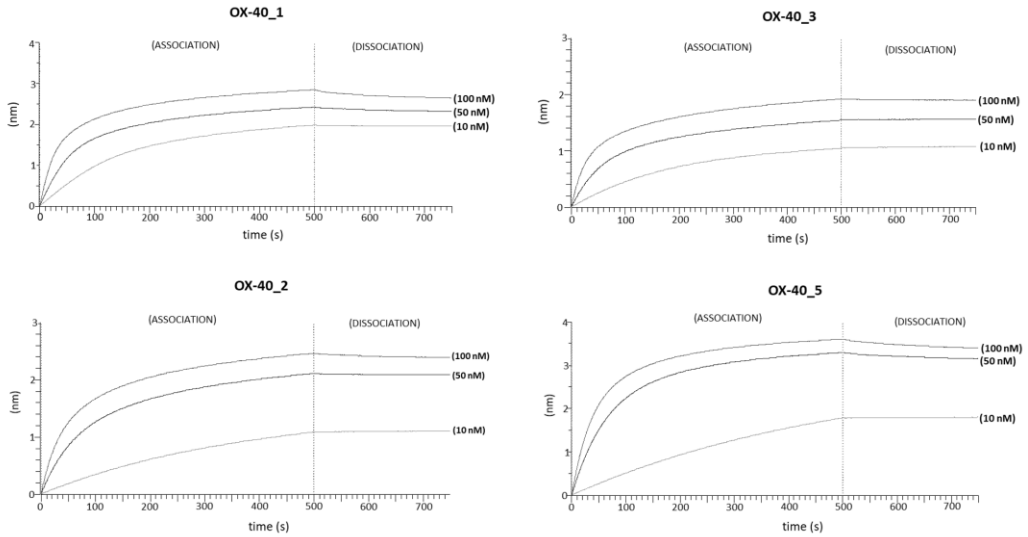

Table 6

mAb	KD (M)	KD Error	ka (1/Ms)	kdis (1/s)
OX-40_1	2.67 x10^{-9}	8.17 x10^{-11}	1.45 x10^{5}	2.93 x10^{-4}
OX-40_2	6.46 x10^{-9}	7.61 x10^{-9}	4.52 x10^{4}	1.48 x10^{-4}
OX-40_3	1.40 x10^{-9}	1.30 x10^{-9}	7.42 x10^{4}	9.07 x10^{-5}
OX-40_5	3.81 x10^{-9}	3.23 x10^{-11}	9.78 x10^{4}	2.80 x10^{-4}

Table 7

mAb	K_D (by BLI) (rOX-40/Fc)	K_D (by ELISA) on OX-40/Fc	K_D (by cell ELISA) on activated hPBMCs	K_D (by BLI) (rOX-40/his)
OX-40_1	2.67 nM	1.6 nM	45.5 nM	7.49 nM
OX-40_2	6.46 nM	**1 nM**	**18 nM**	13 nM
OX-40_3	1.40 nM	**0.56 nM**	**8.5 nM**	1.92 nM
OX-40_5	3.81 nM	0.57 nM	52 nM	4.09 nM

Figure 45. Binding kinetics of the novel anti-OX-40 mAbs on immobilized OX-40 protein via BLI analyses. The sensorgrams report the binding of novel mAbs to OX-40 measured by BLI analyses. The recombinant human OX-40/Fc protein was used as a ligand and immobilized on ProA sensor (3 µg/mL), whereas OX-40_1, OX-40_2, OX-40_3 and OX-40_5 were used as analytes and tested at increasing concentrations (10-100 nM), after saturation with Fc protein by two subsequent incubations (6 µg/mL). The sensorgrams show association and dissociation rates of the analytes.

Analysis was performed by using Octet Analysis Studio 13.0 Software (Sartorius, Fremont, CA, USA).

Table 6. The table reports K_D values (M) with association and dissociation rate constants of the novel mAbs tested by BLI analyses by using proA biosensors.

Table 7. The table reports a comparison of the K_D values (nM) of the indicated antibodies obtained by measuring the binding, via BLI analyses (both proA biosensor and HIS1K biosensors) or by ELISA assays, either on purified recombinant OX-40 or expressed on activated lymphocytes.

3.3.4 Biological properties of the novel human anti-OX-40 mAbs on lymphocytes

Based on the previous findings, we further tested the functional activity of the novel mAbs by evaluating their ability to activate immune cells by mimicking a more physiological context. To this aim, human PBMCs, previously stimulated with 50 ng/ml of SEB, were treated with increasing concentrations (0.2–10 nM) of each of the four anti-OX-40 mAbs. An unrelated human IgG1 was included in a parallel assay as a negative control. After 96 h of incubation, supernatants were collected from co-cultures and the levels of IFNγ and IL-2 secreted were evaluated by measuring cytokines released by ELISAs. As reported in **Figure 46**, all four antibodies significantly enhanced cytokines secretion, with EC50 values of about 1 nM (**Table 8**), confirming their ability to efficiently activate immune cells.

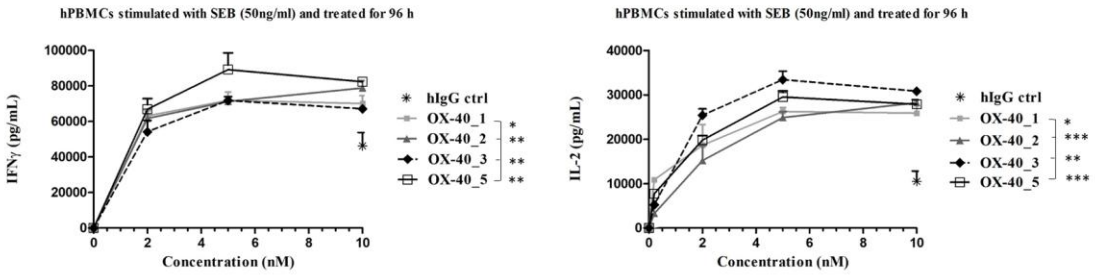

Figure 46. **Cytokines secretion in supernatants of hPBMCs stimulated with SEB and treated with anti-OX-40 mAbs.** hPBMCs were stimulated with SEB (50 ng/mL), treated with increasing concentrations (0.2–10 nM) of OX-40_1 (■), OX-40_2 (▲), OX-40_3 (♦), OX-40_5 (□) and incubated at 37°C for 96 h. Untreated cells or cells treated with the unrelated human IgG1 mAb were used as negative controls. Concentration values were reported as the mean of at least three determinations and expressed in pg/mL. Error bars depicted means ± SD and the P values reported are: *** $p < 0.001$; ** $p < 0.01$; $p^* \leq 0.05$, by student's t test (two variables), calculated by comparing each mAb with the unrelated IgG.

Table 8.

mAb	*EC50*	
	IFNγ	**IL-2**
OX-40_1	1.18 nM	0.8 nM
OX-40_2	1.25 nM	1 nM
OX-40_3	1.5 nM	1.1 nM
OX-40_5	1.2 nM	1.1 nM

Table 8. The table reports the EC50 values (nM) of the indicated mAbs obtained by ELISA cytokines secretion curve analyses with Prism (Graphpad) tool according to the following model: *Y = Bmax*X/(Kd+X) + NS*X + Background.*

3.3.5 Effects of the novel anti-OX-40 mAbs used alone or in combination with anti-PD-L1 mAbs on co-cultures hPBMCs and tumor cells

In order to evaluate potential synergistic effects of the novel isolated anti-OX-40 antibodies with those targeting different immune checkpoints useful for overcoming the limitations of monotherapy, we evaluated their biological activity when used alone or in combination with the clinically validated anti-PD-L1 mAb, Atezolizumab, in co-culture assays of hPBMCs and tumor cells.

As a first step, we analyzed the effects of the anti-OX-40 antibodies alone or in combination with Atezolizumab on the activation of human lymphocytes. For this purpose, hPBMCs were plated at a density of 1×10^5 cells/well, stimulated with SEB (50 ng/mL), and treated for 96h with either the anti-OX-40 mAbs alone or in combination with Atezolizumab (both used at a concentration of 5 μg/mL). Cytokine secretion assays were then performed on the collected supernatants to measure IL-2 release by ELISA. As shown in **Figure 47A**, combined treatments with Atezolizumab significantly enhanced IL-2 secretion for 3 of the 4 mAbs (OX-40_2, _3, and _5). In particular, the combinations of the clinically validated anti-PD-L1 mAb with OX-40_3 and OX-40_5 induced the highest levels of IL-2 secretion, which reached a concentration of 40,000 and 60,000 pg/mL, respectively. These results suggest that combinatorial strategies can potentiate lymphocyte activation and immune-mediated responses.

We further extended our investigation on co-cultures of tumor cells with hPBMCs, in order to test the anti-tumor effects of the combined treatments. To this aim e first evaluated the expression levels of OX-40 and PD-L1 on the MDA-MB-231 triple-negative breast cancer cells by performing a cell ELISA assay by using a commercial

anti-OX-40 antibody. As shown in **Figure 47B**, MDA-MB-231 cells exhibited high levels of both immune checkpoints, thereby representing a suitable model for co-culture assays. To this aim, tumor cells were plated at a density of 10^4 cells/well and co-cultured with hPBMCs previously activated with SEB (50 ng/mL) at an effector-to-target ratio of 5:1. The co-cultures were then treated with the anti-OX-40 mAbs alone or in combination with Atezolizumab, used at a concentration of 100 nM, and after 48h, the cytotoxic activity was evaluated by measuring LDH release in the supernatants. As reported in **Figure 47C**, combinations of Atezolizumab with OX-40_2, OX-40_3, or OX-40_5 resulted in a stronger cytotoxicity effect compared to single-agent treatments. These observations are in line with previous data obtained on lymphocyte cultures and further suggest that anti-OX40/ anti-PD-L1 antibody combinations can increase immune-mediated tumor cell killing.

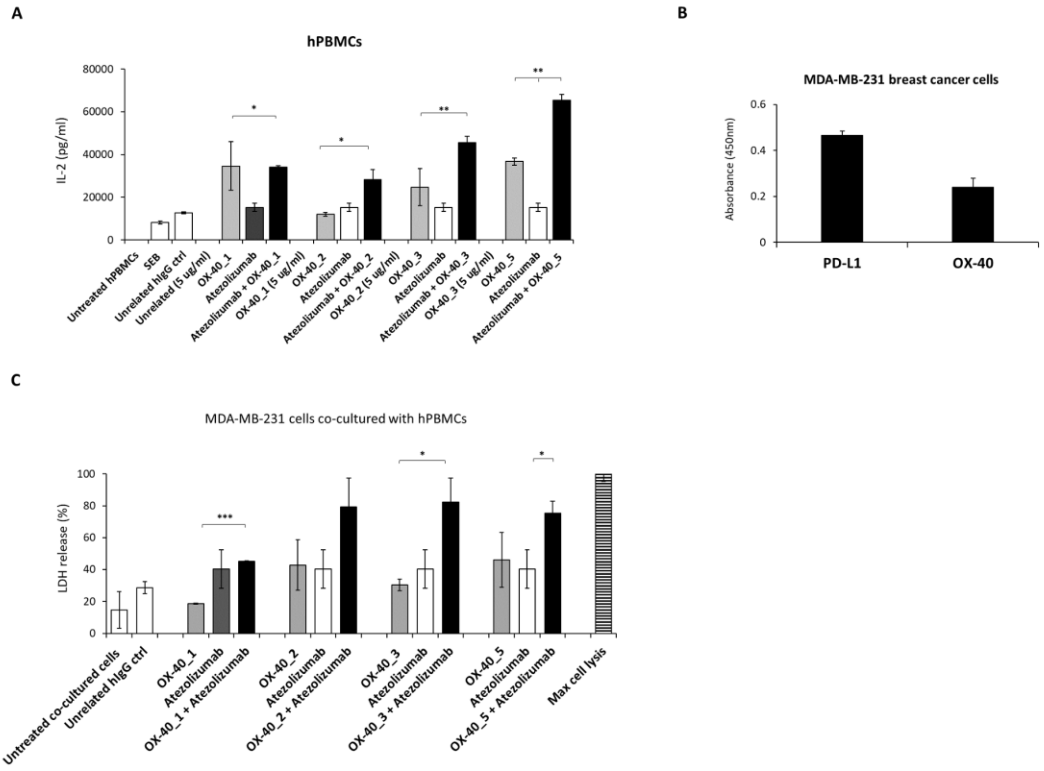

Figure 47. **Effects on co-cultures of lymphocytes and tumor cells of anti-OX-40 mAbs used alone or in combination with anti-PD-L1 mAbs.** (**A**) IL-2 secretion in supernatants of hPBMCs treated with anti-OX-40 mAbs alone or combined with anti-PD-L1 mAb. (**B**) Analysis of OX-40 and PD-L1 expression on different tumor cell lines by cell ELISA. (**C**) Tumor cell lysis induced by OX-40 mAbs alone or in combination with Atezolizumab on co-cultures of MDA-MB-231 tumor cells with hPBMCs. The values are reported as the mean of at least three determinations obtained from three independent experiments. Error bars depicted means ± SD and statistical significance was reported as: *** $p < 0.001$; ** $p < 0.01$; $p^* \leq 0.05$, by student's t test (two variables), calculated by comparing the combinations with each respective compound used as a single agent.

3.4 *Generation and characterization of a novel human anti-Factor V monoclonal antibody for diagnostic or therapeutic applications*

3.4.1 Isolation and screening of novel human scFvs specific for human Factor V of coagulation cascade

During my PhD project, we also focused our attention on the identification of novel binders targeting coagulation cascade factors for potential diagnostic and therapeutic applications [**142**]. In particular we chose as a target pro-accelerin (Factor V), a key component of both the intrinsic and extrinsic coagulation pathways, given its central role in the cascade. A monoclonal antibody specific for Factor V could be useful as a tool in the management of cardiovascular diseases associated with coagulation defects but also to detect defective levels of FV in blood of samples of patients with altered hemostasis.

To this aim, starting from a large human scFv-phage library, we performed a phage display selection strategy aimed at isolating fully human monoclonal antibodies able to recognize both the native and activated forms of Factor V (Factor V and Va, respectively). The selection strategy involved parallel panning rounds on both purified human proteins derived from plasma. Briefly, the human scFv phage library was subjected to a first panning round on immobilized native FV. The bound phages were then eluted through acidic elution and amplified in *E. coli* TG1 cells. The enriched pool was used for two consecutive parallel panning rounds on immobilized FV and FVa, to enrich the selected population with clones able to recognize common epitopes in the two forms (**Figure 48**).

The screening of the positive binders was performed by ELISA assays on both immobilized proteins. A clone, named D9, has been identified for its strong and specific binding for both FV and FVa. D9 clone, isolated after the third selection round on FVa, was tested again in triplicates by ELISA on native FV, active FVa, and on human Fc fragment used as a negative control (**Figure 49**). No significant binding was observed on Fc, whereas strong binding was detected on both FV and FVa forms, thus confirming the specificity for the targets of the phage clone.

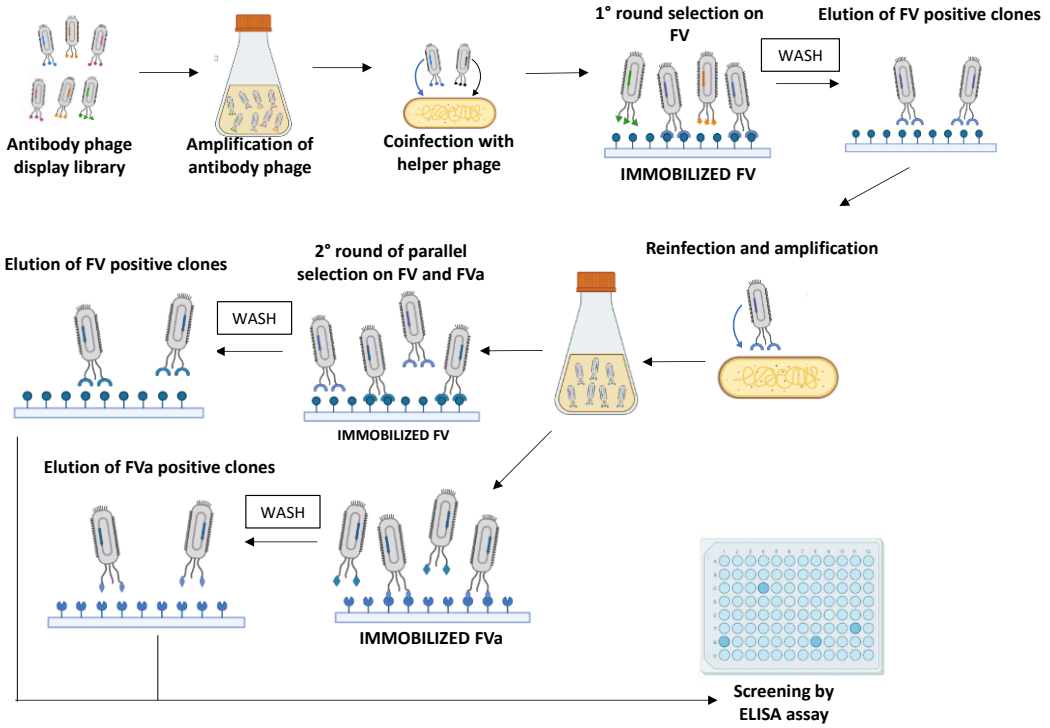

Figure 48. Phage display strategy for isolation of scFvs specific for FV and FVa. The first round of selection was performed on immobilized native FV protein, followed by washes and elution of positive clones. After amplification, the following two panning rounds were performed in parallel on immobilized FV and FVa. The identification of positive clones was carried out by screening performed by ELISA assays.

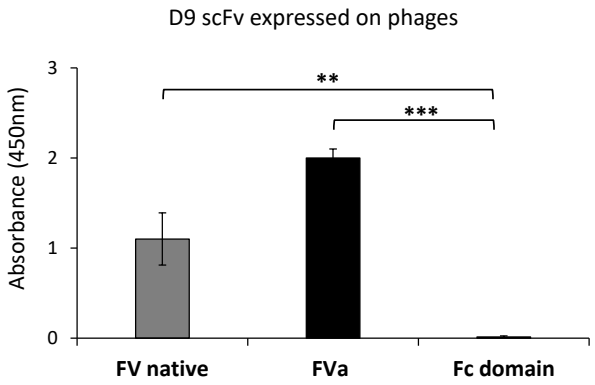

Figure 49. Binding by ELISA assays of D9 phage on FV and FVa. Binding assays of D9 positive phage-scFv clone by ELISA on human active FVa or FV, immobilized at a concentration of 5 µg/mL. In parallel assays, Fc domain was used as negative control. The signal binding was detected by an HRP-conjugated anti-M13 mAb. The data were obtained as the mean of at least three determinations and presented ± SD. *p*-values were calculated by comparing binding values of D9 phage clone on native FV or mature FVa to that observed on control Fc domain, respectively, and the values reported are *** $p \leq 0.001$; ** $p < 0.01$, obtained by two-tailed Student's *t*-test.

3.4.2 Expression of D9 clone as soluble scFv and binding to its target

To evaluate whether the newly identified scFv could be expressed in a soluble form while retaining its binding properties, the corresponding cDNA was extracted by digestion with suitable restriction enzymes (Nco*I* and Not*I*) and used to transform the *E. coli* strain, SF110. Protein expression was induced overnight at 25 °C with IPTG (Isopropyl β-d-1-thiogalactopyranoside). Periplasmic extracts from the cultures were analyzed by Western blotting and ELISA, before and after induction with IPTG, by using an anti-c-myc antibody for the detection. As shown in **Figure 50A**, D9 scFv was successfully expressed as a soluble protein with the expected molecular weight of 27 kDa. Two independent preparations of periplasmic extracts (indicated as preparation 1 and 2), collected after IPTG induction, were then tested for binding to immobilized human purified FV and FVa proteins by ELISA, by using a commercial anti-FV mAb at the concentration of 200 nM, as a positive control (**Figure 50B**). D9, expressed as a soluble scFv, retained its ability to specifically recognize both forms of the target. As a negative control, no binding signal was detected in extracts not induced with IPTG.

The higher signal observed on FV compared to FVa likely reflects a higher concentration of the scFv in preparation 1 compared to preparation 2 used in that assay.

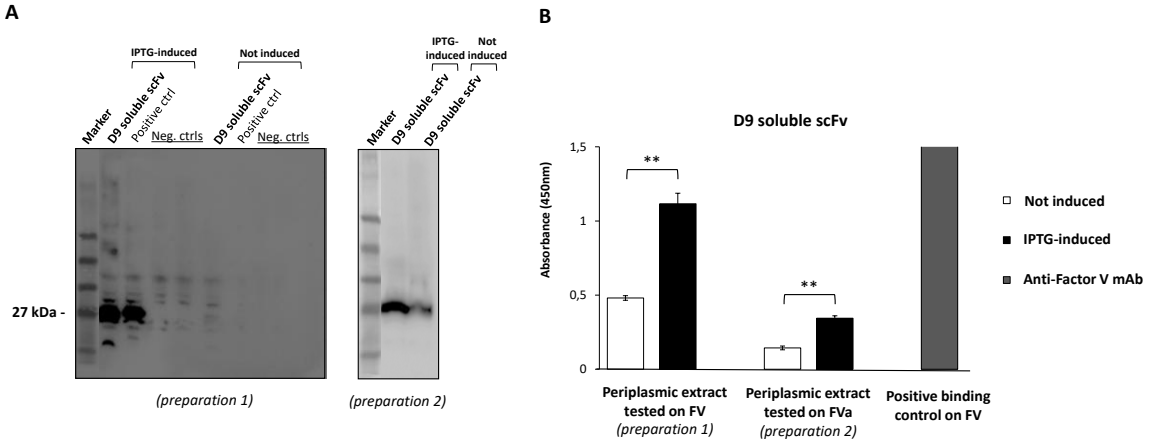

Figure 50. Analysis of D9 expression and binding as soluble scFv. (**A**) Western blotting analyses of two different periplasmic exctracts (preparation 1 and preparation 2) of bacterial cells transformed with D9 clone, expressed in the absence (not induced) or presence (induced) of IPTG, used O.N. at 25°C. The signal was detected by using the HRP-conjugated anti-cmyc antibody. The blot images were acquired by using the ChemiDoc Imaging System and optimized by Image Lab software. (**B**) In parallel, the periplasmic extracts (preparations 1 and 2) were tested on immobilized human FV or FVa purified protein by ELISA assays and the binding detected by using the HRP-conjugated anti-cmyc antibody. Data were obtained by two determinations and presented as mean ± SD. *p*-values were calculated by comparing the binding to FV or FVa immobilized protein of IPTG-induced D9 soluble scFv to that of not induced

culture for each preparation. Statistical significance was determined by using a two-tailed Student's t-test, with results reported as follows: ** $p < 0.01$.

In silico approaches were employed, in collaboration with Prof. Merlino of Department of Biology, to investigate the interaction between the D9 scFv and Factor V. As shown in **Figure 51**, D9 scFv structure is made up of a canonical β-sandwich immunoglobulin fold, while the FV structure, resolved at 3.3 Å by cryo-EM [**138**], includes the A1-A2-B-A3-C1-C2 domains, with an unresolved B domain. The A1 domain (residues 1–316) is connected to A2 (residues 317–709) by a short basic segment (residues 304–316), while A2 is linked to B2 (residues 710–1545) through the acidic segment constituted by residues 657–709. B2 is connected to A3 (residues 1546–1877), which, together with C1 (residues 1878–2036) and C2 (residues 2037–2196), is part of the light chain of FV that is generated after the removal of the B2 domain by proteolysis. [**140**]. Docking simulations revealed that A2 domain is likely the binding site for D9 (**Figure 51B**) which overlaps with regions involved in prothrombin binding. A comparison with the prothrombin–prothrombinase complex (**Figure 51C**) indeed suggests a potential competitive interaction between D9 and prothrombin, although further experimental validation is required.

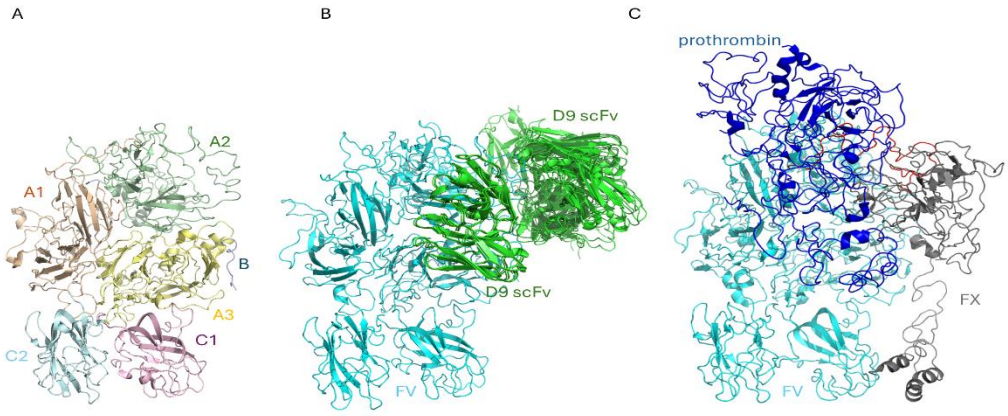

Figure 51. *In Silico* binding of D9 scFv to FV. Overall structures of FV (PDB code 7KVE, panel A), of the complex between FV and D9 scFv from docking calculations (panel B), and of the complex of FV with FX and prothrombin (PDB code 7TPP, panel C). In panel A, the A1, A2, A3, B, C1 and C2 domains are in wheat, pale green, light blue, pale yellow, light pink and pale cyan, respectively. In panel B, FV is in cyan, eight out of the ten poses with highest scores in the docking calculation are shown. In this panel, docked structures of D9 scFv are in green, the acidic region of FV is in red. In panel C, FX is in grey, and prothrombin is in blue.

3.4.3 Generation and characterization of the novel human full-size anti-FVa D9 mAb

In order to obtain a bivalent full-length antibody format, the isolated D9 scFv was converted into a more stable human IgG1 by subcloning its variable domains into mammalian expression vectors containing the sequences encoding the constant heavy and light regions of IgG1 Fc region in collaboration with Prof. Leonardi. The recombinant antibody was then expressed in CHO cells and purified from the conditioned medium by protein G affinity chromatography. Following purification, the binding activity of the full-size D9 mAb was tested by ELISA assays on both native FV and activated FVa at increasing concentrations (1-20 nM) at RT. As shown in **Figure 52A**, D9 mAb retained its ability to recognize both forms of the coagulation factor with high affinity (K_D values of 3–4 nM). To evaluate its specificity, D9 was also tested at a saturating concentration (20 nM) on other immobilized coagulation factors, such as FXa, FVIIIc, and FXIIIa. Even though a slight reactivity was observed with FXa, no significant binding was detected to FVIIIc or FXIIIa (**Figure 52B**), confirming the specificity of D9 for Factor V and its activated form.

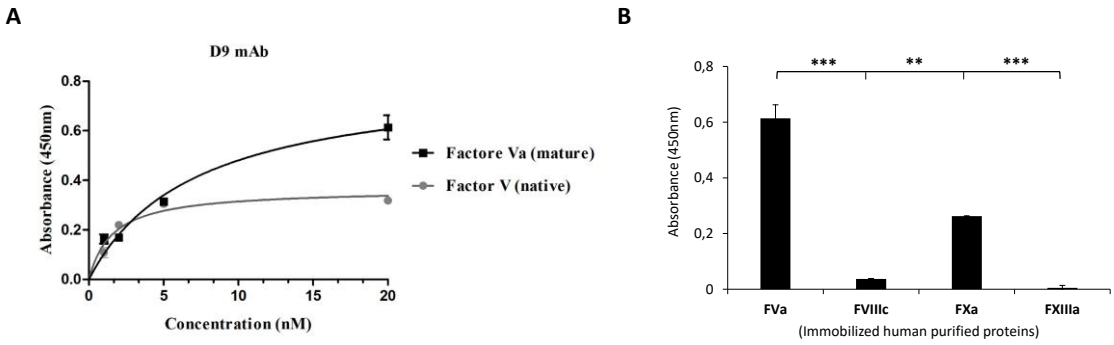

Figure 52. Binding of D9 mAb to FV and its cross-reactivity for other coagulation factors. (**A**) Binding curves of D9 mAb (1-20 nM) on immobilized coagulation native Factor V (grey circles) and matured Factor Va (black squares) by ELISA assays. **(B)** Evaluation of the cross-reactivity, by ELISA assays, of D9 mAb, at a fixed concentration of 20 nM, for different coagulation factors, coated on the plate at a concentration of 5 µg/mL. D9 was detected by using an anti-Fab HRP-conjugated antibody. Binding values were reported as the mean of two or three determinations. Data are presented as mean ± SD. *p*-values were calculated by comparing binding values of D9 mAb to immobilized FVa protein to that observed on FVIIIc, FXa or FXIIIa protein, respectively. The values reported are: *** $p \leq 0.001$; ** $p < 0.01$, obtained by Student's *t*-test (two-tailed)

3.4.4 Effects of the D9 mAb on the coagulation cascade in plasma samples

After evaluating the binding properties of D9 mAb, in collaboration with Dr. Miele of Laboratory of Medicine of Hematology and Hemostasis, we tested its effects on the coagulation cascade in a functional assay. To this aim, D9 was incubated with different samples of human plasma at increasing concentrations for 1h at RT, and clotting parameters were then evaluated. As reported in **Table 9A**, treatment with D9 led to a marked prolongation of activated partial thromboplastin time (aPTT), while prothrombin time (PT) remained unaffected. These findings led us to further explore its potential interference with the other factors involved in intrinsic coagulation pathway. As shown in **Table 9B**, D9 induced a dose-dependent reduction of Factor V levels and, at higher concentrations (1–2 μM), was able to reduce the levels of the other key components of the intrinsic pathway, including FVIII and FIX. Altogether, these results suggest that D9 mAb affects the intrinsic pathway of the coagulation cascade.

(A) D9 mAb effects on the coagulation time		
Sample	PT (v.r. 0.8-1.20 Ratio)	PTT (v.r. 0.8-1.20 Ratio)
NORMAL POOL PLASMA (untreated)	1.01	1.01
NORMAL POOL PLASMA (+100nM D9 mAb)	0.97	1.08
NORMAL POOL PLASMA (+ 1μM D9 mAb)	0.96	**1.46**
NORMAL POOL PLASMA (+2μM D9 mAb)	0.95	**1.95**

(B) D9 mAb effects on the coagulation factors					
NORMAL POOL PLASMA	FII (v.r. 60%-120%)	FV (v.r. 60%-120%)	FVIII (v.r. 50%-130%)	FIX (v.r. 50%-120%)	FX (v.r. 60%-120%)
(untreated)		102			
(+100nM D9 mAb)		97			
(+ 1μM D9 mAb)	101	82	54	67	97
(+2μM D9 mAb)		73	41	45	
p-value	ns	**	**	**	ns

Tables 9. **Effects of D9 on blood coagulation**. Functional assays on plasma samples to measure the effects of the D9 mAb on the coagulation cascade. Plasma samples of 0.5mL were pre-incubated for 1 h at R.T. with increasing doses of D9 (100 nM, 1 μM and 2 μM). (**A**) The prothrombin time and the partial thromboplastin time or (**B**) different coagulation factors levels were measured and expressed as percentages with respect to untreated normal pool plasma, used as a negative control. Statistical analyses were carried out using both Student's *t*-test and Kruskal–Wallis by comparing the samples treated with 1 and 2 μM concentrations of D9 with the untreated one. *p*-values are $p < 0.01$ ** which were considered statistically significant. ns means not significant.

4. DISCUSSION

4.1 Novel immunomodulatory antibodies and identification of effective and safe combinatorial strategies

Over the past decade, immune checkpoint inhibitors (ICIs) have significantly changed the therapeutic landscape of oncology, providing durable clinical responses in multiple types of cancer [**12**, **23**]. The use of ICIs increases the immune neutralization of tumor cells through the selective inhibition of peripheral immune tolerance [**150**]. Nevertheless, their clinical benefits remain limited by the emergence of primary or acquired resistance and by the occurrence of immune-related adverse events [**70-74**, **143-145**].

In this context, my research project was aimed at identifying combinatorial strategies based on novel fully human immunomodulatory monoclonal antibodies with improved efficacy and safety profiles, and at combining them in multi-specific compounds able to overcome some of the current limitations of immunotherapy.

In the first part of this thesis, novel anti-CTLA-4 (ID-1), anti-PD-L1 (PD-L1_1) and anti-LAG-3 (LAG-3_1) antibodies, previously generated in our laboratory [**117, 118, 120**], were tested as single agents or in combinatorial treatments and showed more potent antitumor effects than their clinically validated counterparts [**146**]. In particular, ID-1 and PD-L1_1 induced a stronger activation of hPBMCs, with higher secretion of IL-2 and IFNγ cytokines compared with Atezolizumab and Ipilimumab, either when used as single agents or in combination. In order to identify the combinatorial treatments endowed with the strongest anti-tumor efficacy and the lowest cardiotoxic side effects, we then tested these mAbs on *in vitro* models based on parallel co-cultures of hPBMCs with either tumor cells or human cardiomyocytes. Interestingly, the combination of PD-L1_1 and ID-1 mAbs induced total cell lysis of TNBC cells and lower cytotoxicity on cardiomyocytes, when co-cultured with hPBMCs, compared with the treatments of Ipilimumab or Atezolizumab, or their combination. This result was associated with a decrease in IL-6 secretion, a pro-inflammatory cytokine implicated in cardiovascular diseases, and with lower levels of granzyme B, usually released by either cytotoxic CD8+ T cells or by NK cells [**144**, **145**].

We further explored novel combinatorial regimens involving anti-LAG-3 antibodies, in light of the recent FDA approval of the anti-LAG-3 Relatlimab used in combination with the anti-PD-1 Nivolumab [**65**]. Interestingly, the novel LAG-3_1 combined with PD-

L1_1 showed low cytotoxic effects on HFC and significant anti-tumor activity also on T cell lymphoma-derived cells.

The differences in antitumor activity and cardiac side effects observed after treatments with the combinations of the novel mAbs compared to the clinically validated ICIs could be explained by the distinct epitopes recognized, as previously reported [**117, 146**]. Another explanation could be associated with the different modulation of downstream signalling pathways (such as Erk, Akt) and consequent effects, as previously reported, in the treatments of TNBC cells with the novel anti-PD-L1 mAbs and Atezolizumab or the novel CTLA-4 mAbs and Ipilimumab [**118**, **120**].

Another combinatorial treatment under clinical evaluation for metastatic or advanced non-small cell lung cancer is the association of anti-PD-L1 with anti-CTLA-4 mAbs, which showed significant increases in survival compared to monotherapy in early-phase trials [**151**]. For this reason, in collaboration with the group of Dr. Maurea of the Pascale Foundation, another part of my work was aimed at evaluating the pro-inflammatory effects of combinatorial treatments of ICIs (anti-PD-L1 plus anti-CTLA-4 mAbs or anti-PD-1 plus anti-LAG-3 mAbs) approved by FDA, in co-cultures of hPBMCs and human cardiomyocytes. Our findings highlight that combinations of immune checkpoint inhibitors, and in particular regimens including anti-LAG-3 Relatlimab, promoted an inflammatory response, with higher levels of cytokines secretion, such as IL-6, IL-1β, TNF-α, IFNγ, and increased granzyme B secretion (4–8-fold increase compared to single-agent treatments). The study also suggested the involvement of NLRP3 inflammasome, previously associated with myocarditis and heart failure [**145, 147**].

These findings are of particular relevance since cardiotoxic side effects of ICIs, leading to myocarditis and pericarditis, are among the most severe immune-related adverse events reported in patients treated with ICIs [**145**, **147, 152**]. Further validation will be necessary in *in vivo* models to confirm the efficacy and safety of the novel constructs. Despite the limitations of an *in vitro* system, we think that this model could represent a useful tool to early evaluate the combinations of mAbs endowed with higher anti-tumor efficacy and cardiac safety.

4.2 Development and preclinical evaluation of multi-specific tribodies

We found that the combinations of the anti-LAG-3 antibody with either anti-PD-1 or anti-PD-L1 mAbs, generated in our laboratory, achieved a more efficient tumor cell

killing at lower doses and reduced cardiotoxicity than the combinations based on clinically validated mAbs. On the basis of these results, we selected the best combinations of the novel antibodies that showed the most favorable profile (potent antitumor efficacy combined with reduced cardiotoxicity), in order to develop multi-specific constructs designed to combine the effects of different IC inhibitors into a single molecule.

We generated four novel human bi-specific tribodies- TR0102, TR0304, TR0506 and TR0708- each made up of two scFvs recognizing one of these ICs and a Fab recognizing a different IC, all derived from the parental LAG-3_1, PD-1_1 or PD-L1_1 mAbs. These novel constructs showed high affinity, with K_D values in the low nanomolar or sub-nanomolar range for their targets, either used as purified proteins or in their native conformation on activated hPBMCs. Moreover, the novel bi-specific compounds were found able to interfere in the interactions between their targets and their respective ligands.

Two of the novel TRs (TR0304 and TR0506) showed binding affinities to their targets comparable to validated mAbs (Atezolizumab, Pembrolizumab or Relatlimab), even though they recognized distinct or only partially overlapping epitopes in BLI analyses. When tested for their functional properties, they induced stronger lymphocyte activation in comparison with the corresponding parental mAbs used in combination and more potent *in vitro* cytotoxicity against TNBC cells, also compared to combinatorial treatments based on clinically validated mAbs targeting the same ICs, even when tested at lower concentrations than the combined antibodies. Notably, the novel TR0304 was found to induce a more efficient activation of hPBMCs in co-cultures with tumor cells, achieving a 2-fold increase in IL-2 secretion and a 7-fold increase in IFNγ release compared to combinations of Relatlimab with either Atezolizumab or Pembrolizumab. Interestingly, the bi-specifics TR0304 and TR0506 showed a more favorable *in vitro* cardiotoxicity profile, likely due to the absence of Fc-mediated effector functions.
These results indicate the advantage of fusing two moieties targeting different ICs into a single tribody to achieve more potent activation of immune cells, with the practical benefit of producing a single therapeutic molecule with reduced manufacturing costs. The simultaneous blockade of LAG-3 and PD-1/PD-L1 pathways could re-activate T-cell functions in TME more extensively than targeting each axis separately, overcoming adaptive resistance mechanisms commonly observed during ICI monotherapies, such as the compensatory expression of other ICs [**84**].

In addition, compared with BiTEs, the novel tribodies may offer further advantages, such as the capacity to simultaneously bind to two different targets, a higher molecular weight (100 kDa) that can prolong their half-life in circulation [**80**, **81**], but lower than that of conventional mAbs, which could improve their tumor penetration. Moreover, the Fc-free format reduces the risk of nonspecific cytokine storms, that have been associated with older bispecific molecules such as Catumaxomab, an anti-CD3/EpCAM used for the treatment of malignant ascites [**82, 153**].

With the aim of generating stronger antitumor tribodies, we also generated tri-specific T-cell engager tribodies (53D, 53L10, 53G), able to simultaneously bind to 5T4, an oncofetal antigen expressed on many tumor cells, CD3 on T cells, and an immune checkpoint, by using the scFvs derived from the mentioned novel mAbs. They were found to promote stronger T-cell activation and more marked antitumor responses compared with the parental compounds [**102**]. In this study, we evaluated the binding kinetics of the novel T cell engagers to the purified targets in comparison with clinically validated Relatlimab, Atezolizumab, and Pembrolizumab targeting the same ICs and tested their binding also on hPBMCs. The tribodies showed comparable or even superior affinity than conventional mAbs for activated immune cells, likely due to the presence of the anti-CD3 scFv within their structure, which can be exploited to achieve more effective engagement of immune cells *in vivo*. In addition, the novel tribodies also bound to their targets on tumor cells with nanomolar affinity, especially in TNBC and NSCLC where PD-L1 and 5T4 targets are highly expressed.

More interestingly, the novel tribodies activated hPBMCs more efficiently than clinically approved ICIs, whether used alone or in combination with the control parental bi-specific construct 53P, which lacks the immunomodulatory moieties. Moreover, these trispecific constructs markedly enhanced tumor cytotoxicity, promoted cytokines release by hPBMCs, with a strong secretion of IL-2 and IFNγ. In particular, one of them, 53L10, appears to be the most effective at inducing tumor cell lysis, likely due to its dual binding to 5T4 and PD-L1 on tumor cells, as confirmed by binding assays. Therefore, 53L10 was selected for *in vivo* studies, where it induced complete tumor regression in a mouse model bearing lung cancer even at very low concentrations, whereas Atezolizumab, either used alone or in combination with bi-specific 53P, achieved only a partial tumor growth inhibition at a much higher dose.

Thus, the tri-specific constructs could represent promising tools for cancer therapies, as no similar constructs have yet been approved by FDA, even though some are in clinical

trials with a different TAA/CD3/CD28 formats. Indeed, the novel tri-specifics contain different ICIs from anti-CD28 binding domains, which have previously been associated with the risk of severe cytokine release [**96**, **97**]. Moreover, the inclusion of an anti-PD-L1 moiety, as in 53L10, allow to preferentially act on exhausted T cells, improving both efficacy and safety, overcoming the immunosuppressive tumor microenvironment.

Taken together, our data validate the rationale of incorporating immunomodulatory moieties within multi-specific scaffolds and support the extension of this strategy to other T-cell engager formats, targeting a large variety of TAAs. Nevertheless, further *in vivo* investigations are required to determine whether this approach could be translated into a safe and effective therapeutic platform for clinical applications.

4.3 Generation and characterization of novel anti-OX-40 mAbs

In parallel, to increase the collection of anti-IC mAbs, our study also focused on the generation of novel anti-OX-40 antibodies, since this co-stimulatory receptor has a relevant role in sustaining T-cell proliferation and memory [**41**, **42, 154**]. By phage display selection on OX-40 (used both in its native conformation on immune cells and as recombinant purified protein) combined with a NGS–based high-throughput screening strategy, four distinct human antibody fragments were identified as potential binders [**117**]. These scFvs were subsequently converted into full-length IgG1 antibodies, and as part of my thesis work, they were tested for their stability and then fully characterized for their biological properties [**155**].

All four anti-OX-40 novel antibodies showed nanomolar binding affinities in either BLI or ELISA assays on both purified protein and on hPBMCs, with high specificity for activated lymphocytes. They induced T-cell activation by enhancing cytokines secretion, also at the lowest doses, with EC50 values of about 1 nM. When tested in combination with the clinically validated anti-PD-L1, Atezolizumab, both for the activation of immune cells and in co-culture assays of TNBC cells with hPBMCs, the novel anti-OX-40 antibodies displayed additive effects, enhancing both cytokine release and tumor cell killing.

These results suggest that these novel anti-OX-40 mAbs could become potential tools for therapeutic applications and underscore the relevance of simultaneously targeting co-inhibitory and co-stimulatory immune pathways to achieve more potent antitumor responses.

However, further studies on the mechanisms of action will be useful in order to fully elucidate the emerging role of this co-stimulatory receptor. In particular, it would be interesting to investigate whether the different antibodies, by recognizing distinct or partially overlapping epitopes [**155**], can differentially modulate receptor clustering or downstream signalling pathways. Moreover, the evaluation of the synergistic effects of novel anti-OX40 mAbs with other targeting different ICs or TAA could be useful in order to set up novel more potent combinatorial treatments. Finally, *in vivo* studies will be essential to determine the efficacy and safety of targeting OX40, especially in combinatorial regimens.

4.4 A Novel Monoclonal Antibody-based Approach to Target the Coagulation Cascade

Cardiovascular diseases remain the leading cause of mortality worldwide, with thrombosis representing a major cause of acute events such as myocardial infarction and ischemic strokes [**122, 123**].

The main goal of anticoagulant therapy is to prevent pathological clot formation while minimizing the risk of bleeding. Conventional agents such as heparins and vitamin K antagonists, although effective, are limited by unpredictable pharmacokinetics and the need for constant monitoring. More recently, direct oral anticoagulants (DOACs) have improved treatment by offering greater specificity and fewer interactions; however, bleeding remain a significant concern [**131**, **132**]. In this context, monoclonal antibodies targeting specific coagulation factors represent a promising tool to achieve safer and more targeted anticoagulant therapies.

Factor V is an attractive candidate of common pathway, as it is a key cofactor of the prothrombinase complex and plays an essential role in the conversion of prothrombin to thrombin [**138-140**].

In our laboratory, we employed a phage display strategy involving parallel selections on both native Factor V and its active form, Factor Va, in order to isolate a novel scFv able to recognize both forms. After conversion into a fully human IgG1, this novel antibody, named D9, showed high specificity for both FV and FVa, with a K_D of 3–4 nM, and no significant binding to other coagulation factors. Functional studies revealed that D9 interfered with FV activation by thrombin and affected the intrinsic pathway by reducing the levels of FV and other coagulation factors (FVIII, FIX, and FXI), and by prolonging coagulation time in plasma samples (aPTT). These data are in line with *in silico* docking predictions suggesting its binding to the A2 domain of FV, that is also

recognized by prothrombin. Thus, its effects on coagulation could be likely due to a competitive binding or protection exerted by D9 against thrombin-mediated FV activation.

Although the functional data are encouraging, further studies will be needed to validate these findings *in vivo,* evaluate its pharmacokinetic properties and eventual side effects.

Altogether, these findings indicate that D9 could be employed both as an anticoagulant therapeutic and a diagnostic tool for FV detection in biological samples, to highlight FV deficit in patients with haematological diseases.

5. REFERENCES

1. World Health Organization. *Cancer*. World Health Organization, 2022, https://www.who.int/news-room/fact-sheets/detail/cancer. Accessed 14 Aug. 2025.
2. Li Z, Li J, Bai X, Huang X, Wang Q. Tumor microenvironment as a complex milieu driving cancer progression: a mini review. *Clin Transl Oncol*. 2025;27(5):1943-1952.
3. Hanahan D, Weinberg RA. Hallmarks of cancer: the next generation. *Cell*. 2011;144(5):646-674.
4. Sonkin D, Thomas A, Teicher BA. Cancer treatments: Past, present, and future. *Cancer Genet*. 2024;286-287:18-24.
5. Dracham CB, Shankar A, Madan R. Radiation induced secondary malignancies: a review article. *Radiat Oncol J*. 2018;36(2):85-94.
6. Habeck M. FDA licences imatinib mesylate for CML. *Lancet Oncol*. 2002;3(1):6.
7. Khozin S, Blumenthal GM, Jiang X, et al. U.S. Food and Drug Administration approval summary: Erlotinib for the first-line treatment of metastatic non-small cell lung cancer with epidermal growth factor receptor exon 19 deletions or exon 21 (L858R) substitution mutations. *Oncologist*. 2014;19(7):774-779.
8. Cohen MH, Williams GA, Sridhara R, Chen G, Pazdur R. FDA drug approval summary: gefitinib (ZD1839) (Iressa) tablets. *Oncologist*. 2003;8(4):303-306.
9. Zhang H. Three generations of epidermal growth factor receptor tyrosine kinase inhibitors developed to revolutionize the therapy of lung cancer. *Drug Des Devel Ther*. 2016;10:3867-3872.
10. Schumacher TN, Schreiber RD. Neoantigens in cancer immunotherapy. *Science*. 2015;348(6230):69-74.
11. Rodríguez-Nava C, Ortuño-Pineda C, Illades-Aguiar B, et al. Mechanisms of Action and Limitations of Monoclonal Antibodies and Single Chain Fragment Variable (scFv) in the Treatment of Cancer. *Biomedicines*. 2023;11(6):1610.
12. Goydel RS, Rader C. Antibody-based cancer therapy. *Oncogene*. 2021;40(21):3655-3664.
13. Wittrup KD. Antitumor Antibodies Can Drive Therapeutic T Cell Responses. *Trends Cancer*. 2017;3(9):615-620.
14. Jeyakumar A, Younis T. Trastuzumab for HER2-Positive Metastatic Breast Cancer: Clinical and Economic Considerations. *Clin Med Insights Oncol*. 2012;6:179-187.
15. Leget GA, Czuczman MS. Use of rituximab, the new FDA-approved antibody. *Curr Opin Oncol*. 1998 Nov;10(6):548-51. doi: 10.1097/00001622-199811000-00012.

16. Salles G, Barrett M, Foà R, et al. Rituximab in B-Cell Hematologic Malignancies: A Review of 20 Years of Clinical Experience. *Adv Ther*. 2017;34(10):2232-2273.
17. *Herceptin: Metastatic Breast Cancer – Side Effects Summary.* Genentech, www.herceptin.com/patient/metastatic-breast-cancer/side-effects/summary.html. Accessed 16 Aug. 2025.
18. *Rituxan.* Genentech, www.rituxan.com. Accessed 16 Aug. 2025.
19. Cruz E, Kayser V. Monoclonal antibody therapy of solid tumors: clinical limitations and novel strategies to enhance treatment efficacy. *Biologics*. 2019;13:33-51.
20. Pardoll DM. The blockade of immune checkpoints in cancer immunotherapy. *Nat Rev Cancer*. 2012;12(4):252-264.
21. Ribas A, Wolchok JD. Cancer immunotherapy using checkpoint blockade. *Science*. 2018;359(6382):1350-1355.
22. Mayes PA, Hance KW, Hoos A. The promise and challenges of immune agonist antibody development in cancer. *Nat Rev Drug Discov*. 2018;17(7):509-527.
23. Scott AM, Wolchok JD, Old LJ. Antibody therapy of cancer. *Nat Rev Cancer*. 2012;12(4):278-287.
24. Dunn GP, Bruce AT, Ikeda H, Old LJ, Schreiber RD. Cancer immunoediting: from immunosurveillance to tumor escape. *Nat Immunol*. 2002;3(11):991-998.
25. Chen DS, Mellman I. Oncology meets immunology: the cancer-immunity cycle. *Immunity*. 2013;39(1):1-10.
26. Mellman I, Chen DS, Powles T, Turley SJ. The cancer-immunity cycle: Indication, genotype, and immunotype. *Immunity*. 2023;56(10):2188-2205.
27. Qureshi OS, Zheng Y, Nakamura K, et al. Trans-endocytosis of CD80 and CD86: a molecular basis for the cell-extrinsic function of CTLA-4. *Science*. 2011;332(6029):600-603.
28. Fu J, Mao L, Jiao Y, Mei D, Chen Y. Elucidating CTLA-4's role in tumor immunity: a comprehensive overview of targeted antibody therapies and clinical developments. *Mol Divers*. 2025;29(5):5075-5084.
29. Rowshanravan B, Halliday N, Sansom DM. CTLA-4: a moving target in immunotherapy. *Blood*. 2018;131(1):58-67.
30. Parvez A, Choudhary F, Mudgal P, et al. PD-1 and PD-L1: architects of immune symphony and immunotherapy breakthroughs in cancer treatment. *Front Immunol*. 2023;14:1296341.
31. Lin X, Kang K, Chen P, et al. Regulatory mechanisms of PD-1/PD-L1 in cancers. *Mol Cancer*. 2024;23(1):108.

32. Zhulai G, Oleinik E. Targeting regulatory T cells in anti-PD-1/PD-L1 cancer immunotherapy. *Scand J Immunol*. 2022;95(3):e13129.
33. Leitner J, Aigner-Radakovics K, Steinberger P. LAG-3-An incompletely understood target in cancer therapy. *FASEB J*. 2024;38(22):e70190.
34. Maruhashi T, Sugiura D, Okazaki IM, et al. Binding of LAG-3 to stable peptide-MHC class II limits T cell function and suppresses autoimmunity and anti-cancer immunity. *Immunity*. 2022;55(5):912-924.e8.
35. Chavanton A, Mialhe F, Abrey J, Baeza Garcia A, Garrido C. LAG-3 : recent developments in combinational therapies in cancer. *Cancer Sci*. 2024;115(8):2494-2505.
36. Joller N, Anderson AC, Kuchroo VK. LAG-3, TIM-3, and TIGIT: Distinct functions in immune regulation. *Immunity*. 2024;57(2):206-222.
37. Woo SR, Turnis ME, Goldberg MV, et al. Immune inhibitory molecules LAG-3 and PD-1 synergistically regulate T-cell function to promote tumoral immune escape. *Cancer Res*. 2012;72(4):917-927.
38. Andrews LP, Butler SC, Cui J, et al. LAG-3 and PD-1 synergize on $CD8^+$ T cells to drive T cell exhaustion and hinder autocrine IFN-γ-dependent anti-tumor immunity. *Cell*. 2024;187(16):4355-4372.e22.
39. Mejía-Guarnizo LV, Monroy-Camacho PS, Turizo-Smith AD, Rodríguez-García JA. The role of immune checkpoints in antitumor response: a potential antitumor immunotherapy. *Front Immunol*. 2023;14:1298571.
40. Willoughby J, Griffiths J, Tews I, Cragg MS. OX40: Structure and function - What questions remain?. *Mol Immunol*. 2017;83:13-22.
41. Linch SN, McNamara MJ, Redmond WL. OX40 Agonists and Combination Immunotherapy: Putting the Pedal to the Metal. *Front Oncol*. 2015;5:34.
42. Vu MD, Xiao X, Gao W, et al. OX40 costimulation turns off Foxp3+ Tregs. *Blood*. 2007;110(7):2501-2510.
43. Rojas-Diaz JM, Solorzano-Ibarra F, Garcia-Barrientos NT, et al. Uncovering the Expression Pattern of the Costimulatory Receptors ICOS, 4-1BB, and OX-40 in Exhausted Peripheral and Tumor-Infiltrating Natural Killer Cells from Patients with Cervical Cancer. *Int J Mol Sci*. 2024;25(16):8775.
44. Weinberg AD, Rivera MM, Prell R, et al. Engagement of the OX-40 receptor in vivo enhances antitumor immunity. *J Immunol*. 2000;164(4):2160-2169.
45. Sadrolashrafi K, Guo L, Kikuchi R, et al. An OX-Tra'Ordinary Tale: The Role of OX40 and OX40L in Atopic Dermatitis. *Cells*. 2024;13(7):587.

46. Sun Q, Hong Z, Zhang C, Wang L, Han Z, Ma D. Immune checkpoint therapy for solid tumours: clinical dilemmas and future trends. *Signal Transduct Target Ther*. 2023;8(1):320.
47. Hellmann MD, Paz-Ares L, Bernabe Caro R, et al. Nivolumab plus Ipilimumab in Advanced Non-Small-Cell Lung Cancer. *N Engl J Med*. 2019;381(21):2020-2031.
48. Baas P, Scherpereel A, Nowak AK, et al. First-line nivolumab plus ipilimumab in unresectable malignant pleural mesothelioma (CheckMate 743): a multicentre, randomised, open-label, phase 3 trial. *Lancet*. 2021;397(10272):375-386.
49. Janjigian YY, Bendell J, Calvo E, et al. CheckMate-032 Study: Efficacy and Safety of Nivolumab and Nivolumab Plus Ipilimumab in Patients With Metastatic Esophagogastric Cancer. *J Clin Oncol*. 2018;36(28):2836-2844.
50. Lau G, Sangro B, Cheng AL, et al. Immune-mediated adverse events and overall survival with tremelimumab plus durvalumab and durvalumab monotherapy in unresectable HCC: HIMALAYA phase III randomized clinical trial. *Hepatology*. 2025.
51. Ouyang T, Cao Y, Kan X, et al. Treatment-Related Serious Adverse Events of Immune Checkpoint Inhibitors in Clinical Trials: A Systematic Review. *Front Oncol*. 2021;11:621639.
52. Wolchok JD, Chiarion-Sileni V, Rutkowski P, et al. Final, 10-Year Outcomes with Nivolumab plus Ipilimumab in Advanced Melanoma. *N Engl J Med*. 2025;392(1):11-22.
53. Brahmer JR, Lee JS, Ciuleanu TE, et al. Five-Year Survival Outcomes With Nivolumab Plus Ipilimumab Versus Chemotherapy as First-Line Treatment for Metastatic Non-Small-Cell Lung Cancer in CheckMate 227. *J Clin Oncol*. 2023;41(6):1200-1212.
54. Macioch T, Krzakowski M, Gołębiewska K, Dobek M, Warchałowska N, Niewada M. Pembrolizumab monotherapy survival benefits in metastatic non-small-cell lung cancer: a systematic review of real-world data. *Discov Oncol*. 2024;15(1):303.
55. Bagegni NA, Davis AA, Clifton KK, Ademuyiwa FO. Targeted Treatment for High-Risk Early-Stage Triple-Negative Breast Cancer: Spotlight on Pembrolizumab. *Breast Cancer (Dove Med Press)*. 2022;14:113-123.
56. Shalata W, Weissmann S, Itzhaki Gabay S, et al. A Retrospective, Single-Institution Experience of Bullous Pemphigoid as an Adverse Effect of Immune Checkpoint Inhibitors. *Cancers (Basel)*. 2022;14(21):5451.
57. Almutairi AR, McBride A, Slack M, Erstad BL, Abraham I. Potential Immune-Related Adverse Events Associated With Monotherapy and Combination Therapy of

Ipilimumab, Nivolumab, and Pembrolizumab for Advanced Melanoma: A Systematic Review and Meta-Analysis. *Front Oncol.* 2020;10:91.

58. West H, McCleod M, Hussein M, et al. Atezolizumab in combination with carboplatin plus nab-paclitaxel chemotherapy compared with chemotherapy alone as first-line treatment for metastatic non-squamous non-small-cell lung cancer (IMpower130): a multicentre, randomised, open-label, phase 3 trial. *Lancet Oncol*. 2019;20(7):924-937.
59. Reck M, Dziadziuszko R, Sugawara S, et al. Five-year survival in patients with extensive-stage small cell lung cancer treated with atezolizumab in the Phase III IMpower133 study and the Phase III IMbrella A extension study. *Lung Cancer*. 2024;196:107924.
60. Kagihara JA, Andress M, Diamond JR. Nab-paclitaxel and atezolizumab for the treatment of PD-L1-positive, metastatic triple-negative breast cancer: review and future directions. *Expert Rev Precis Med Drug Dev*. 2020;5(2):59-65.
61. "FDA Approves Neoadjuvant/Adjuvant Durvalumab for Resectable Non-Small Cell Lung Cancer." *U.S. Food and Drug Administration*, https://www.fda.gov/drugs/resources-information-approved-drugs/fda-approves-neoadjuvantadjuvant-durvalumab-resectable-non-small-cell-lung-cancer. Accessed 19 Aug. 2025.
62. "FDA Approves Durvalumab for Limited-Stage Small Cell Lung Cancer." *U.S. Food and Drug Administration*, www.fda.gov/drugs/resources-information-approved-drugs/fda-approves-durvalumab-limited-stage-small-cell-lung-cancer. Accessed 19 Aug. 2025.
63. "FDA Approves Durvalumab for Muscle Invasive Bladder Cancer." *U.S. Food and Drug Administration*, www.fda.gov/drugs/resources-information-approved-drugs/fda-approves-durvalumab-muscle-invasive-bladder-cancer. Accessed 19 Aug. 2025.
64. Grivas P, Park SH, Voog E, et al. Avelumab First-line Maintenance Therapy for Advanced Urothelial Carcinoma: Comprehensive Clinical Subgroup Analyses from the JAVELIN Bladder 100 Phase 3 Trial. *Eur Urol*. 2023;84(1):95-108.
65. "FDA Approves Opdualag for Unresectable or Metastatic Melanoma." *U.S. Food and Drug Administration*, www.fda.gov/drugs/resources-information-approved-drugs/fda-approves-opdualag-unresectable-or-metastatic-melanoma. Accessed 19 Aug. 2025.
66. Davar D, Anderson AC, Diaz-Padilla I. Therapeutic potential of targeting LAG-3 in cancer. *J Immunother Cancer*. 2025;13(7):e011652.
67. Lé AM, Torres T. OX40-OX40L Inhibition for the Treatment of Atopic Dermatitis-Focus on Rocatinlimab and Amlitelimab. *Pharmaceutics*. 2022;14(12):2753.

68. Kraehenbuehl L, Weng CH, Eghbali S, Wolchok JD, Merghoub T. Enhancing immunotherapy in cancer by targeting emerging immunomodulatory pathways. *Nat Rev Clin Oncol*. 2022;19(1):37-50.
69. Holay N, Yadav R, Ahn SJ, et al. INBRX-106: a hexavalent OX40 agonist that drives superior antitumor responses via optimized receptor clustering. *J Immunother Cancer*. 2025;13(5):e011524.
70. Cozma A, Sporis ND, Lazar AL, et al. Cardiac Toxicity Associated with Immune Checkpoint Inhibitors: A Systematic Review. *Int J Mol Sci*. 2022;23(18):10948.
71. Gan L, Liu D, Ma Y, et al. Cardiotoxicity associated with immune checkpoint inhibitors: Current status and future challenges. *Front Pharmacol*. 2022;13:962596.
72. Ascierto PA, Del Vecchio M, Robert C, et al. Ipilimumab 10 mg/kg versus ipilimumab 3 mg/kg in patients with unresectable or metastatic melanoma: a randomised, double-blind, multicentre, phase 3 trial. *Lancet Oncol*. 2017;18(5):611-622.
73. Cone EB, Haeuser L, Reese SW, et al. Immune checkpoint inhibitor monotherapy is associated with less cardiac toxicity than combination therapy. *PLoS One*. 2022;17(11):e0272022.
74. Makunts T, Saunders IM, Cohen IV, et al. Myocarditis occurrence with cancer immunotherapy across indications in clinical trial and post-marketing data. *Sci Rep*. 2021;11(1):17324.
75. Ayoub NM, Al-Shami KM, Yaghan RJ. Immunotherapy for HER2-positive breast cancer: recent advances and combination therapeutic approaches. *Breast Cancer (Dove Med Press)*. 2019;11:53-69.
76. Guo X, Wu Y, Xue Y, Xie N, Shen G. Revolutionizing cancer immunotherapy: unleashing the potential of bispecific antibodies for targeted treatment. *Front Immunol*. 2023;14:1291836.
77. Bergamaschi C, Gaspar M, Ciucci T, et al. Innovative strategies for T cell engagers for cancer immunotherapy. *MAbs*. 2025;17(1):2531223.
78. NISONOFF A, WISSLER FC, LIPMAN LN. Properties of the major component of a peptic digest of rabbit antibody. *Science*. 1960;132(3441):1770-1771.
79. NISONOFF A, WISSLER FC, LIPMAN LN. Properties of the major component of a peptic digest of rabbit antibody. *Science*. 1960;132(3441):1770-1771.
80. Surowka M, Klein C. A pivotal decade for bispecific antibodies? *MAbs*. 2024;16(1):2321635. Erratum in: *MAbs*. 2024;16(1):2335597.
81. Klein C, Brinkmann U, Reichert JM, Kontermann RE. The present and future of bispecific antibodies for cancer therapy. *Nat Rev Drug Discov*. 2024;23(4):301-319.

82. Seimetz D, Lindhofer H, Bokemeyer C. Development and approval of the trifunctional antibody catumaxomab (anti-EpCAM x anti-CD3) as a targeted cancer immunotherapy. *Cancer Treat Rev*. 2010;36(6):458-467.
83. Zhao J, Song Y, Liu D. Recent advances on blinatumomab for acute lymphoblastic leukemia. *Exp Hematol Oncol*. 2019;8:28.
84. Huang RY, Francois A, McGray AR, Miliotto A, Odunsi K. Compensatory upregulation of PD-1, LAG-3, and CTLA-4 limits the efficacy of single-agent checkpoint blockade in metastatic ovarian cancer. *Oncoimmunology*. 2016;6(1):e1249561.
85. Frentzas S, Gan HK, Cosman R, et al. A phase 1a/1b first-in-human study (COMPASSION-01) evaluating cadonilimab in patients with advanced solid tumors. *Cell Rep Med*. 2023;4(11):101242.
86. Passariello M, Yoshioka A, Takahashi K, et al. Novel Bi-Specific Immuno-Modulatory Tribodies Potentiate T Cell Activation and Increase Anti-Tumor Efficacy. *Int J Mol Sci*. 2022;23(7):3466.
87. First-in-class T cell engager approved for lung cancer. *Nat Biotechnol*. 2024;42(6):824.
88. Zhou C, Tang KJ, Cho BC, et al. Amivantamab plus Chemotherapy in NSCLC with *EGFR* Exon 20 Insertions. *N Engl J Med*. 2023;389(22):2039-2051.
89. Yoon J, Oh DY. An evaluation of zanidatamab, a novel, anti-HER2 biparatopic antibody, for the treatment of biliary tract cancer. *Expert Opin Biol Ther*. 2025;25(9):935-946.
90. Hegde PS, Chen DS. Top 10 Challenges in Cancer Immunotherapy. *Immunity*. 2020;52(1):17-35.
91. Sun Y, Zhou L, Gu X, Zhao J, Bi J, Pan L. Leveraging T cell co-stimulation for enhanced therapeutic efficacy of trispecific antibodies targeting prostate cancer. *J Immunother Cancer*. 2025;13(3):e010140.
92. Amoozgar B, Bangolo A, Habibi M, Cho C, Goy A. From Molecular Precision to Clinical Practice: A Comprehensive Review of Bispecific and Trispecific Antibodies in Hematologic Malignancies. *Int J Mol Sci*. 2025;26(11):5319.
93. Lancman G, Richter J, Chari A. Bispecifics, trispecifics, and other novel immune treatments in myeloma. *Hematology Am Soc Hematol Educ Program*. 2020;2020(1):264-271.
94. Yao Y, Hu Y, Wang F. Trispecific antibodies for cancer immunotherapy. *Immunology*. 2023;169(4):389-399.

95. Gauthier L, Morel A, Anceriz N, et al. Multifunctional Natural Killer Cell Engagers Targeting NKp46 Trigger Protective Tumor Immunity. *Cell*. 2019;177(7):1701-1713.e16.
96. Tapia-Galisteo A, Álvarez-Vallina L, Sanz L. Bi- and trispecific immune cell engagers for immunotherapy of hematological malignancies. *J Hematol Oncol*. 2023;16(1):83.
97. Tapia-Galisteo A, Compte M, Álvarez-Vallina L, Sanz L. When three is not a crowd: trispecific antibodies for enhanced cancer immunotherapy. *Theranostics*. 2023;13(3):1028-1041.
98. Riccio G, Ricardo AR, Passariello M, et al. T-cell Activating Tribodies as a Novel Approach for Efficient Killing of ErbB2-positive Cancer Cells. *J Immunother*. 2019;42(1):1-10.
99. "A Phase I, First in Human Study of CBA-1535, T Cell Engager (5T4/CD3/5T4) in Patients With Advanced Solid Tumors." *ClinicalTrials.gov*, National Library of Medicine, 5 Jan. 2024, https://clinicaltrials.gov/study/NCT07016997. Accessed 20 Aug. 2025.
100. Stern PL. Immunotherapies targeting a tumor-associated antigen, 5T4 oncofetal glycoprotein. Chapter in: *Cancer Immunology: Bench to Bedside Immunotherapy of Cancers*. 2015; pp. 409–425.
101. Stern PL, Harrop R. 5T4 oncofoetal antigen: an attractive target for immune intervention in cancer. *Cancer Immunol Immunother*. 2017;66(4):415-426.
102. Passariello M, Yoshioka A, Takahashi K, et al. Novel tri-specific tribodies induce strong T cell activation and anti-tumor effects in vitro and in vivo. *J Exp Clin Cancer Res*. 2022;41(1):269.
103. Köhler G, Milstein C. Continuous cultures of fused cells secreting antibody of predefined specificity. *Nature*. 1975;256(5517):495-497.
104. Freysd'ottir J. Production of monoclonal antibodies. *Methods Mol Med*. 2000;40:267-279.
105. Garcia-Calvo E, García-García A, Madrid R, Martin R, García T. From Polyclonal Sera to Recombinant Antibodies: A Review of Immunological Detection of Gluten in Foodstuff. *Foods*. 2020;10(1):66.
106. Alejandra WP, Miriam Irene JP, Fabio Antonio GS, et al. Production of monoclonal antibodies for therapeutic purposes: A review. *Int Immunopharmacol*. 2023;120:110376.
107. Smith GP. Filamentous fusion phage: novel expression vectors that display cloned antigens on the virion surface. *Science*. 1985;228(4705):1315-1317.

108. Hoogenboom HR. Selecting and screening recombinant antibody libraries. *Nat Biotechnol*. 2005;23(9):1105-1116.
109. Jaroszewicz W, Morcinek-Orłowska J, Pierzynowska K, Gaffke L, Węgrzyn G. Phage display and other peptide display technologies. *FEMS Microbiol Rev*. 2022;46(2):fuab052.
110. Sasso E, Latino D, Froechlich G, et al. A long non-coding SINEUP RNA boosts semi-stable production of fully human monoclonal antibodies in HEK293E cells. *MAbs*. 2018;10(5):730-737.
111. De Lorenzo C, Tedesco A, Terrazzano G, et al. A human, compact, fully functional anti-ErbB2 antibody as a novel antitumour agent. *Br J Cancer*. 2004;91(6):1200-1204.
112. Palmieri D, Richmond T, Piovan C, et al. Human anti-nucleolin recombinant immunoagent for cancer therapy. *Proc Natl Acad Sci U S A*. 2015;112(30):9418-9423.
113. Paciello R, Urbanowicz RA, Riccio G, et al. Novel human anti-claudin 1 mAbs inhibit hepatitis C virus infection and may synergize with anti-SRB1 mAb. *J Gen Virol*. 2016;97(1):82-94.
114. Passariello M, Gentile C, Ferrucci V, et al. Novel human neutralizing mAbs specific for Spike-RBD of SARS-CoV-2. *Sci Rep*. 2021;11(1):11046.
115. Passariello M, Ferrucci V, Sasso E, et al. A Novel Human Neutralizing mAb Recognizes Delta, Gamma and Omicron Variants of SARS-CoV-2 and Can Be Used in Combination with Sotrovimab. *Int J Mol Sci*. 2022;23(10):5556.
116. Passariello M, Esposito S, Manna L, et al. Comparative Analysis of a Human Neutralizing mAb Specific for SARS-CoV-2 Spike-RBD with Cilgavimab and Tixagevimab for the Efficacy on the Omicron Variant in Neutralizing and Detection Assays. *Int J Mol Sci*. 2023;24(12):10053..
117. Sasso E, D'Avino C, Passariello M, et al. Massive parallel screening of phage libraries for the generation of repertoires of human immunomodulatory monoclonal antibodies. *MAbs*. 2018;10(7):1060-1072.
118. Passariello M, D'Alise AM, Esposito A, et al. Novel Human Anti-PD-L1 mAbs Inhibit Immune-Independent Tumor Cell Growth and PD-L1 Associated Intracellular Signalling. *Sci Rep*. 2019;9(1):13125.
119. Vetrei C, Passariello M, Froechlich G, Rapuano Lembo R, Zambrano N, De Lorenzo C. Immunomodulatory mAbs as Tools to Investigate on Cis-Interaction of PD-1/PD-L1 on Tumor Cells and to Set Up Methods for Early Screening of Safe and Potent Combinatorial Treatments. *Cancers (Basel)*. 2021;13(12):2858.

120. Passariello M, Vetrei C, Sasso E, et al. Isolation of Two Novel Human Anti-CTLA-4 mAbs with Intriguing Biological Properties on Tumor and NK Cells. *Cancers (Basel)*. 2020;12(8):2204.
121. So WV, Dejardin D, Rossmann E, Charo J. Predictive biomarkers for PD-1/PD-L1 checkpoint inhibitor response in NSCLC: an analysis of clinical trial and real-world data. *J Immunother Cancer*. 2023;11(2):e006464.
122. Ashorobi D, Ameer MA, Fernandez R. Thrombosis. In: *StatPearls*. Treasure Island (FL): StatPearls Publishing; February 12, 2024.
123. Senst B, Tadi P, Basit H, Jan A. Hypercoagulability. In: *StatPearls*. Treasure Island (FL): StatPearls Publishing; August 22, 2023.
124. del Zoppo GJ. Virchow's triad: the vascular basis of cerebral injury. Rev Neurol Dis. 2008;5 Suppl 1(Suppl 1):S12-S21.
125. Morange, P.E.; Suchon, P.; Trégouët, D.A. Genetics of Venous Thrombosis: Update in 2015. *Thromb. Haemost*. 2015, 114, 910–919.
126. Morange PE, Suchon P, Trégouët DA. Genetics of Venous Thrombosis: update in 2015. *Thromb Haemost*. 2015;114(5):910-919.
127. Chaudhry R, Killeen RB, Babiker HM. Physiology, Coagulation Pathways. In: *StatPearls*. Treasure Island (FL): StatPearls Publishing; June 2, 2025.
128. Franchini M, Mannucci PM. Direct oral anticoagulants and venous thromboembolism. *Eur Respir Rev*. 2016;25(141):295-302.
129. Linkins LA, Dans AL, Moores LK, et al. Treatment and prevention of heparin-induced thrombocytopenia: Antithrombotic Therapy and Prevention of Thrombosis, 9th ed: American College of Chest Physicians Evidence-Based Clinical Practice Guidelines. *Chest*. 2012;141(2 Suppl):e495S-e530S.
130. Patel, P., and M. A. Varacallo. “Low-Molecular-Weight Heparin (LMWH).” *StatPearls*, updated 28 Mar. 2025, StatPearls Publishing, Treasure Island (FL), 2025 Jan–. Available at: https://www.ncbi.nlm.nih.gov/books/NBK525957/. Accessed 19 Aug. 2025
131. Zirlik A, Bode C. Vitamin K antagonists: relative strengths and weaknesses vs. direct oral anticoagulants for stroke prevention in patients with atrial fibrillation. *J Thromb Thrombolysis*. 2017;43(3):365-379.
132. Chai-Adisaksopha C, Hillis C, Isayama T, Lim W, Iorio A, Crowther M. Mortality outcomes in patients receiving direct oral anticoagulants: a systematic review and meta-analysis of randomized controlled trials. *J Thromb Haemost*. 2015;13(11):2012-2020.

133. Liu M, Zaman K, Fortenberry YM. Overview of the Therapeutic Potential of Aptamers Targeting Coagulation Factors. *Int J Mol Sci*. 2021;22(8):3897.
134. Derszniak K, Przyborowski K, Matyjaszczyk K, et al. Comparison of Effects of Anti-thrombin Aptamers HD1 and HD22 on Aggregation of Human Platelets, Thrombin Generation, Fibrin Formation, and Thrombus Formation Under Flow Conditions. *Front Pharmacol*. 2019;10:68.
135. Badreldin HA, Alsuhebany N, Alzahrani M, et al. Abelacimab: A leap forward in anticoagulation with FXI and FXIa Inhibition. *Curr Res Pharmacol Drug Discov*. 2024;6:100179.
136. Samaha E, Schwameis M, Schranz S, et al. The factor XIa antibody osocimab strongly inhibits clotting in extracorporeal circuits with human blood and in baboons. *Res Pract Thromb Haemost*. 2025;9(4):102932.
137. Lam, W., and L. Moosavi. "Physiology, Factor V." *StatPearls*, updated 17 Jul. 2023, StatPearls Publishing, Treasure Island (FL), 2025 Jan–. Available at: https://www.ncbi.nlm.nih.gov/books/NBK544237/. Accessed 19 Aug. 2025.
138. Ruben EA, Rau MJ, Fitzpatrick JAJ, Di Cera E. Cryo-EM structures of human coagulation factors V and Va. *Blood*. 2021;137(22):3137-3144.
139. Dahlbäck B. Novel insights into the regulation of coagulation by factor V isoforms, tissue factor pathway inhibitorα, and protein S. *J Thromb Haemost*. 2017;15(7):1241-1250.
140. Schreuder M, Reitsma PH, Bos MHA. Blood coagulation factor Va's key interactive residues and regions for prothrombinase assembly and prothrombin binding. *J Thromb Haemost*. 2019;17(8):1229-1239.
141. Ayombil, F, Quinn SM, Cid EA, Bunce MW, and Camire RM. "A Monoclonal Antibody against Human Factor V Impairs Its Activation and Procoagulant Function." *ISTH 2023 Congress*, Montreal, June 2023.
142. Passariello M, Rapuano Lembo R, Manna L, et al. A Novel Human Anti-FV mAb as a Potential Tool for Diagnostic and Coagulation Inhibitory Approaches. *Int J Mol Sci*. 2025;26(6):2721.
143. Quagliariello V, Passariello M, Coppola C, et al. Cardiotoxicity and pro-inflammatory effects of the immune checkpoint inhibitor Pembrolizumab associated to Trastuzumab. *Int J Cardiol*. 2019;292:171-179.
144. Quagliariello V, Passariello M, Rea D, et al. Evidences of CTLA-4 and PD-1 Blocking Agents-Induced Cardiotoxicity in Cellular and Preclinical Models. *J Pers Med*. 2020;10(4):179.

145. Quagliariello V, Passariello M, Bisceglia I, et al. Combinatorial immune checkpoint blockade increases myocardial expression of NLRP-3 and secretion of H-FABP, NT-Pro-BNP, intrleukin-1β and interleukin-6: biochemical implications in cardio-immuno-oncology. *Front Cardiovasc Med*. 2024;11:1232269.
146. Vetrei C, Passariello M, Froechlich G, et al. Novel Combinations of Human Immunomodulatory mAbs Lacking Cardiotoxic Effects for Therapy of TNBC. *Cancers (Basel)*. 2021;14(1):121.
147. Kinoshita T, Imamura R, Kushiyama H, Suda T. NLRP3 mediates NF-κB activation and cytokine induction in microbially induced and sterile inflammation. *PLoS One*. 2015;10(3):e0119179.
148. Manna L, Rapuano Lembo R, Yoshioka A, Nakamura K, Passariello M, De Lorenzo C. A Comparison of the Antitumor Efficacy of Novel Multi-Specific Tribodies with Combinations of Approved Immunomodulatory Antibodies. *Cancers (Basel)*. 2023;15(22):5345.
149. Passariello M, Manna L, Rapuano Lembo R, et al. Tri-specific tribodies targeting 5T4, CD3, and immune checkpoint drive stronger functional T-cell responses than combinations of antibody therapeutics. *Cell Death Discov*. 2025;11(1):58.
150. Chen H, Yang H, Guo L, Sun Q. The Role of Immune Checkpoint Inhibitors in Cancer Therapy: Mechanism and Therapeutic Advances. *MedComm*. 2025;6(10):e70412.
151. Wong DJ, Bauer TM, Gordon MS, et al. Safety and Clinical Activity of Atezolizumab Plus Ipilimumab in Locally Advanced or Metastatic Non-Small Cell Lung Cancer: Results From a Phase 1b Trial. *Clin Lung Cancer*. 2022;23(3):273-281.
152. Sharma A, Alexander G, Chu JH, et al. Immune Checkpoint Inhibitors and Cardiotoxicity: A Comparative Meta-Analysis of Observational Studies and Randomized Controlled Trials. *J Am Heart Assoc*. 2024;13(10):e032620.
153. Shah D, Soper B, Shopland L. Cytokine release syndrome and cancer immunotherapies - historical challenges and promising futures. *Front Immunol*. 2023;14:1190379.
154. Thapa B, Kato S, Nishizaki D, et al. OX40/OX40 ligand and its role in precision immune oncology. *Cancer Metastasis Rev*. 2024;43(3):1001-1013.
155. Rapuano Lembo R, Passariello M, Manna L, et al. Generation of novel human anti-OX-40 mAbs endowed with different biological properties as tools for cancer therapy. *Front Immunol*. 2025;16:1644391.